Processing of Polymer-based Systems for Improved Performance and Controlled Release

A THESIS SUBMITTED TO THE UNIVERSITY OF LONDON

FOR THE DEGREE OF DOCTOR OF PHILOSOPHY

October 2011

By

Jia Ma

School of Engineering and Materials Science

Queen Mary, University of London

Mile End Road, London, E1 4NS

Declaration

I declare that the work performed is entirely by myself during the course of my Ph.D. studies at the Queen Mary, University of London and has not been submitted for a degree at this or any other university.

Jia Ma

Acknowledgements

I would like to thank all the people that helped me throughout my Ph.D. study. First of all, I would like to express my deep and sincere gratitude to my supervisor, Prof. Ton Peijs, Prof. Gleb Sukhorukov for their detailed guidance, constructive comment and encouraging support throughout this work. I would also like to express my sincere thanks to Dr. Jawwad A Darr in Chemistry department at University College London and Dr. Natalie Stingelin in Materials department at Imperial College London for their essential assistance and valuable advice.

I would like to thank the support staff for their kind assistance, which has been of great value for my work. I wish to acknowledge Dr. Zofia Luklinska and Mr Mick Willis for helpful advice on SEM and TEM imaging, Dr. Monisha Phillips for DSC measurements, Dr. Rory Wilson for XRD analysis and Dr. Andrei Sapelkin in the physics department for fluorescence microscopy analysis.

During this work, I have collaborated with many colleagues for whom I have great regard, and I would like to thank Dr. Emiliano Bilotti, Dr. Hua Deng, Dr. Denys Usov, Mr. Marc Simonet and Dr. Anil Shiva Ramlogan for their valuable discussions.

My special thanks are given to my husband Wei Tu, my baby girl Jiayi Tu, my parents and my friend Derek Patterson who have always been there for me. Without their encouragement and understanding it would have been impossible for me to finish this work.

Abstract

This thesis focuses on improved processing methods for enhanced mechanical properties in polymer nanocomposites, and controlled drug release in polymer based delivery systems. Supercritical carbon dioxide assisted mixing was successfully used in preparation of polypropylene/sepiolite and polypropylene/multiwall carbon nanotube nanocomposites. Relatively homogeneous dispersed and well separated nanofillers were obtained throughout the PP matrix. A better preservation of nanofiller lengths was observed in the $scCO_2$ assisted mixing. Mechanical property studies showed a marked increase in Young's modulus and tensile strength with the addition of nanofillers. More interestingly, techniques usually designed to achieve high quality PP nanocomposites, such as the use of masterbatches, maleic anhydride grafted polypropylene compatibilizers or polymer coated MWNTs are not needed to achieve equivalent mechanical properties with $scCO_2$ assisted mixing. $ScCO_2$ was also used as a foaming technique to modify the traditional cured poly(ethyl methacrylate/tetrahydrofurfuryl methacrylate) system for a controlled release of chlorhexidine. Highly porous structures were produced and chlorhexidine released from $scCO_2$ foamed samples was more than 3 times higher than traditionally cured samples. By altering the processing conditions, such as CO_2 saturation time and depressurization time the CX release rate was altered. Finally, the electrospinning method was combined with the layering encapsulation technique in order to enable the incorporation of water-soluble drugs in poly(lactic-co-glycolic acid) fibres for biomedical applications. Water-soluble drug, Rhodamine 6G or protein bovine serum albumin, loaded calcium carbonate microparticles were successfully incorporated in PLGA fibres and a bead and string structured composite fibres.

Table of Contents

Chapter 6. Drug Release from Poly(ethyl methacrylate/tetrahydrofurfuryl methacrylate) Systems

Chapter 7. Drug Release from Multilayer Capsules in Biodegradable Poly(lactic-co-glycolic acid) Fibres

List of Tables

List of Figures

List of Abbreviations

BSA	Bovine serum albumin
$CaCO_3$	calcium carbonate
CMCs	ceramic matrix composites
CNT	carbon nanotube
CX	chlorhexidine
DDS	drug delivery system
DSC	Differential scanning calorimetry
Eq	Equation
Fig.	Figure
FITC-BSA	fluorescein isothiocyanate labelled bovine serum albumin
FTIR	Fourier transform infrared spectroscopy
HPMC	hydroxypropyl methylcellulose
LbL	Layer-by-Layer
MMCs	metal matrix composites
MWNTs	multiwall carbon nanotubes
O/W	oil-in-water
PAH/PSS	poly (allylamine hydrochloride)/poly (sodium 4-styrenesulfonate)
PEM/THFM	polyethylmethacrylate / tetrahydrofurfurylmethacrylate
PGA	polyglycolides
PLA	polylactides
PLGA	poly (lactic-co-glycolic acid)
PMCs	polymer matrix composites
PP	polypropylene

PP-g-MA	Maleic anhydride grafted polypropylene
psi	pounds per square inch
R6G	Rhodamine 6G
RBITC	Rhodamine B isothiocyanate
$scCO_2$	Supercritical carbon dioxide
SEM	Scanning electron microscopy
SWNTs	single wall carbon nanotubes
TEM	Transmission electron microscopy
TGA	thermogravimetric analysis
UV	Ultraviolet
W/O	water-in-oil
XRD	X-ray diffraction

Chapter 1

Introduction

1.1 Background Information for Polymer Matrix Composites

Composites refer to materials composed of two or more distinct phases (matrix phase and dispersed phase) each having significantly different physical or chemical properties[1]. Composites are around us everywhere. A tree is a good example of a natural composite, consisting of cellulose (the fibrous material) and a matrix of lignin (a natural polymer). A pavement is a man-made composite formed with steel and aggregate reinforced asphalt concrete. Composites started attracting more and more attention since their successful development for aerospace use in the 1960s. Since then, further exploration on composites has led to their use in the automotive, biomedical, and sporting goods markets. In addition, more recently, increased usage

of composite materials can be seen in the rehabilitation, repair, and retrofit of civil infrastructure--including, for example, as replacement bridge decks and as wrapping of concrete columns.

Depending on the nature of the matrix, composites can be classified into metal matrix composites (MMCs), ceramic matrix composites (CMCs) and polymer matrix composites (PMCs)[1]. Among them, PMCs are most common and widely applied in commercial applications. A wide range of fillers have been employed as the dispersed phases in the polymer matrix for enhanced performance with regard to the mechanical, thermal and electrical properties[2]. In addition, PMCs are also the preferred materials in bioengineering and biomedical research as witnessed by their use in tissue engineering and advanced drug delivery systems. This is because they can be designed to be non-toxic, biocompatible and biodegradable[2].

1.1.1 Polymer Composites for Improved Mechanical Properties

There has been intensive research carried out for enhanced mechanical properties - for example, higher strength and higher modulus[1]. Conventional composites are normally filled with micro-scale fillers including metals, ceramics and high modulus fillers. However, enhanced mechanical properties are often compromised in terms of embrittlement of the polymer due to stress concentrations[1]. By comparison with conventional micro-scale fillers, nano-scale fillers give rise to significant improvements in the toughness of the composites along with other properties including thermal stability, flame retardancy, chemical resistance, electrical conductivity and optical clarity[3]. The differences should be related to the extremely small size of the fillers giving them unique properties, and a better interaction with the polymer matrix.

The most promising nanofillers are those such as carbon nanotubes (CNTs) or nanoclays, due to their high aspect ratios, since only a small amount of them is needed to reinforce the polymer matrix. Mechanical reinforcement by CNTs or clays in polymer composites has been extensively investigated[4-9]. However, the effective use of these nanofillers is far from perfect since they have extremely large surface area which causes agglomerates. The major challenge is in the breaking down of bundles of aggregated nanofillers and in reaching a fine dispersion in the selected polymer matrix. In particular, the most common composite processing method, melt compounding, is less effective at dispersing nanofillers such as CNTs and clays. Moreover, the high viscosity of the composite caused by the addition of nanofillers limits the nanofiller loadings and the high shear rates and high temperatures involved cause the thermal instability of the polymers[4,9].

1.1.2 Polymer Systems for Controlled Release in Drug Delivery

In addition to the enhanced mechanical properties, polymer systems are widely applied in advanced drug delivery systems. Normally, a therapeutic agent is administered in a high dose at a given time and repeated later. This sometimes results in undesirable (e.g. toxic) side-effects. It is inconvenient and patient compliance is often poor[10]. For these reasons, interest has focused on developing sustained-release devices to deliver a drug for prolonged time periods and in a controlled manner. The sustained-release of drugs can be achieved by the polymer delivery systems in which the polymer acts as a drug carrier. Also, polymer delivery systems can be designed for drug targeting, which is to deliver drugs to a specific tissue or organ using polymer carriers[11].

Polymer delivery systems can be classified into non-biodegradable and

biodegradable delivery systems. The first polymer drug release system was based on non-biodegradable polymers designed by Folkman and Long in 1964[12]. They reported the use of silicone for sustained release. Since then, many non-biodegradable polymers have been studied and used for controlled drug delivery[13]. On the other hand, biodegradable delivery systems have attracted more and more attention. Biodegradable delivery systems can be metabolised and excreted by natural pathways, so there is no need for surgical removal. The polymer is used as protection for the drug during its transfer through the body until it is released, or used to control the release rate of the drug. The polymers such as polycaprolactone, polylactides (PLA), polyglycolides (PGA), and copolymers poly(lactide-co-glycolides) (PLGA)[14-16] have been actively studied.

1.2 Objectives

This thesis focuses on improved processing methods for polymer-based systems. Attention is paid on improved mechanical properties for polymer nanocomposites and controlled drug release for polymer based delivery systems. Particularly in melt compounding nanocomposite processes, the achievement of well dispersed nanofillers in the polymer matrix is a major challenge. Supercritical carbon dioxide ($scCO_2$) processing offer an interesting alternative to overcome some of the challenges in traditional melt compounding such as the occurrence of high viscosities, high temperatures and high shear stress. The plasticization of $scCO_2$ could reduce the polymer viscosity, decrease the melting temperature, and hence increase the processiblity of nanocomposites and lead to a better dispersion of nanofillers[17]. In drug delivery, the sustained release is essential and is the ultimate goal for both nonbio- and biodegradable polymer systems. Changing the morphology of the polymer matrix, porosity for example, is believed to have a great impact on the drug

release profile. It is expected that the porous structures created by the $scCO_2$ foaming process should enhance the release of the drug. On the other hand, a second barrier around the drug, created by layer-by-layer (LbL) encapsulation, could give better protection to it and may establish a new method for delivering water soluble drugs. Hence, the main objectives of this thesis are:

- To investigate the potential benefits of using $scCO_2$ for a better dispersion of nanofillers in nanocomposites
- To study the foaming of traditional cured polymer systems by $scCO_2$ techniques and its impact on the drug release profile
- To fabricate a drug release device for water soluble drugs by a combined encapsulation and electrospinning technique

1.3 Outline of the Thesis

There are two major parts in this thesis. ***Part A*** concentrates on the processing of polypropylene (PP) nanocomposites with $scCO_2$ assisted mixing. The nanofillers studied are multiwall carbon nanotubes (MWNTs) and sepiolite clays. ***Chapter 2*** will introduce the materials used in this study. An introduction in polymer nanocomposites including their properties, the processing methods and the effective properties of nanofillers in the composites will be presented. ***Chapter 3*** will describe the preparation of PP/sepiolite nanocomposites using $scCO_2$ assisted mixing. The resulting properties of the nanocomposites will be compared with those from traditional melt compounding methods. In ***Chapter 4***, preparation of PP/CNT nanocomposites using $scCO_2$ assisted mixing will be discussed in detail. The potential benefits of using $scCO_2$ in this system will be investigated. Micromechanical modelling will be used to analyse the effective properties of the

MWNTs in the nanocomposites.

Part B investigates the processing of polymer delivery systems for the controlled release of drugs. ***Chapter 5*** will give an overview of drug delivery systems. The designs and types of drug delivery systems will be introduced. Theoretical analysis using kinetic equations to analyse the drug release mechanism will be described as well. ***Chapter 6*** will present the preparation of a foamed poly(ethyl methacrylate/tetrahydrofurfuryl methacrylate) (PEM/THFM) polymer system by $scCO_2$ foaming processing. Chlorhexidine (CX) will be used as the dispersed drug. The $scCO_2$ foaming condition processed on the traditional cured CX-PEM/THFM polymeric system will be investigated for the optimum release of CX from the PEM/THFM matrix. The kinetics of the drug release will also be studied. In ***Chapter 7***, a biodegradable polymer, PLGA, will be chosen for the drug release device. Water soluble drug loaded calcium carbonate ($CaCO_3$) microparticles incorporated in PLGA fibres will be prepared by a combined layering encapsulation and electrospinning technique. The morphology of the fibres will be studied. The drug release behavior, the degradation of the fibre and the bioactivity of the drug will be investigated in detail. Finally, ***Chapter 8*** will summarize the main conclusions and will address possible research directions for the future.

1.4 References

1. Hull D and Clyne TW. An Introduction to Composite Materials. 2nd ed. Cambridge: Cambridge University Press; 1996
2. Pillai O and Panchagnula R. Polymers in Drug delivery. Curr. Opin. Chem. Biol. 2001, 4, 447
3. Ajayan PM, Schadler LS and Braun PV. Nanocomposite Science and Technology.

Wiley-VCH GmbH & Co. KgaA; 2004

4. Coleman JN, Khan U, Blau WJ and Gun'ko YK. Small but Strong: A review of the Mechanical Properties of Carbon Nanotube-Polymer Composites. Carbon. 2006, 44, 1624
5. Moniruzzaman M and Winey KI. Polymer Nanocomposites Containing Carbon Nanotubes. Macromol. 2006, 39, 5194
6. Ahir SV. Polymer Containing Carbon Nanotubes: Active Composite Materials. In: Nalwa SH, editor. Polymeric Nanostructures and Their Applications. California: American Scientific Publishers; 2005
7. Hasegawa N, Okamoto H, Kato M and Usuki A. Preparation and Mechanical Properties of Polypropylene-Clay Hybrids Based on Modified Polypropylene and Organophilic Clay. J. Appl. Polym. Sci. 2000, 78, 1918
8. Garcia-Lopez D, Picazo O, Merino JC and Pastor JM. Polypropylene Clay Nanocomposites: Effect of Compatibilizing Agents on Clay Dispersion. Eur. Polym. J. 2003, 39, 945
9. Alexander M, Doubis P. Polymer-Layered Silicate Nanocomposites, Properties and Uses of a New Class of Materials. Mater. Sci. Eng. R. 2000, 28, 1
10. Roseman TJ and Yalkowsky SH. Importance of Solute Partitioning on the Kinetics of Drug Release from Matrix Systems. In: D. R. Paul DR and Harris FW, editors. Controlled Release Polymeric Formulations. Washington DC: American Chemical Society; 1976
11. Mathiowitz E, Kreitz MR, Brannon-Peppas L. Microencapsulation. In: Mathiowitz E, editor. Encyclopedia of Controlled Drug Delivery. New York, NY: John Wiley & Sons, Inc; 1999
12. Folkman J and Long DM. The Use of Silicone Rubber as a Carrier for Prolonged Drug Therapy. J. Surg. Res. 1964, 4, 139

13. Bajpai AK, Shukla SK, Bhanu S and Kankane S. Responsive Polymers in Controlled Drug Delivery. Prog. Polym. Sci. 2008, 11, 1088
14. Luten J, van Nostrum CF, De Smedt SC and Hennink WE. Biodegradable Polymers as Non-viral Carriers for Plasmid DNA Delivery. J. Controlled Release. 2008, 2, 97
15. Pitt CG. Poly-$^{\varepsilon}$Caprolactone and Its Copolymers. In: Chasin M and Langer R, editors. Biodegradable Polymers as Drug Delivery Systems. New York: Marcel Dekker; 1990
16. Willerth SM and Sakiyama-Elbert SE. Approaches to Neural Tissue Engineering using Scaffolds for Drug Delivery. Adv. Drug Delivery Rev. 2007,4, 325
17. Tomasko DL, Li H, Liu D, Han X, Wingert MJ, Lee LJ and Koelling KW. A Review of CO_2 Applications in the Processing of Polymers. Ind. Eng. Chem. Res. 2003, 42, 6431

Part A:

Processing Polymer Nanocomposites by Supercritical CO_2 Assisted Mixing

Chapter 2

Polymer Nanocomposites and $ScCO_2$

2.1 Introduction

In recent years polymer nanocomposites have attracted great interest in academia[1].The attractiveness of this new class of material lies in the large improvements in both mechanical and thermal properties, as well as in gas barrier and fire resistance. First, the nanofillers and polymer matrices used in this study are introduced. Then polymer nanocomposites and the processing methods used are overviewed.

2.2 Nanofillers

The term 'nanofillers' is vague and no precise definition exists. Nanofillers are understood, in essence, to be additives in solid form, which differ from the polymer matrix in terms of their composition and structure. Nanofillers are of the order of 100 nm or less in at least one dimension Fig. 2.1 shows the nanometre domain in the context of some common microscopic objects.

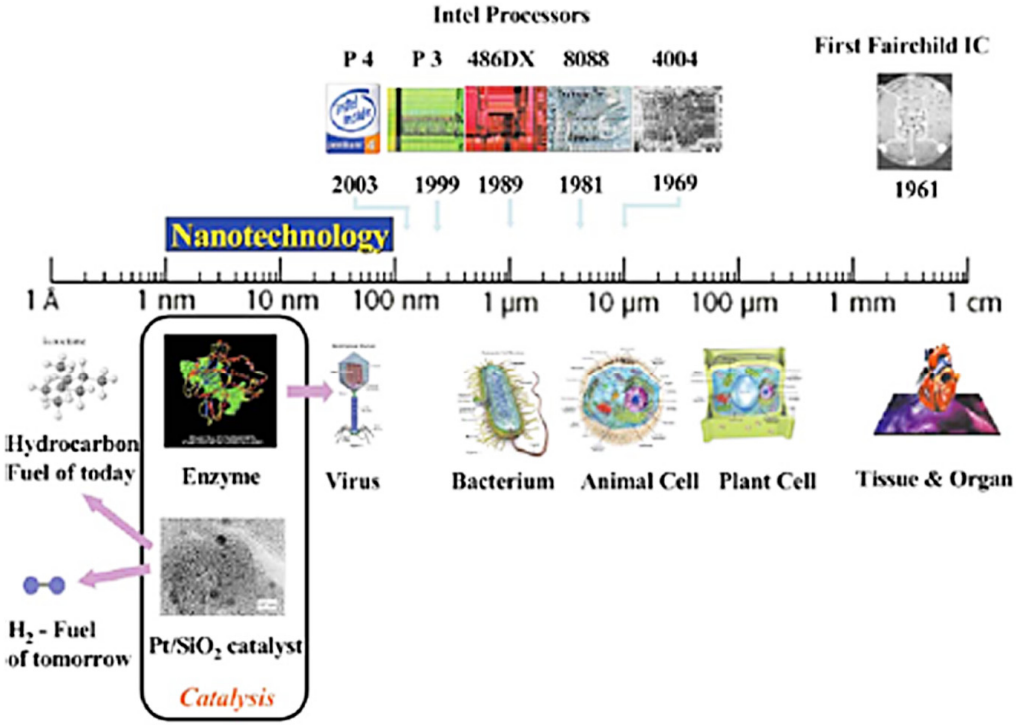

Fig. 2.1 *The nanometre domain relative to some common architectures*[1]

Nanofillers are often added to enhance one or more of the properties of the polymer. Inactive fillers or extenders raise the quantity and lower the prices, while active fillers bring about targeted improvements in certain mechanical or physical properties. Common nanofillers include calcium carbonate, ceramic nanofillers, carbon black, CNTs, carbon nanofibres, cellulose nanowhiskers, nanoclays, gold particles, kaolin, mica, silica, silver nanoparticles, titanium dioxide, etc. Because of

their impressive intrinsic mechanical properties, nanoscale dimensions and high aspect-ratio, nanofillers such as CNTs or nanoclays are the most promising due to the fact that small amounts (less than 5 %) of them can provide the resulting nanocomposite material with significant property improvements.

2.2.1 Carbon Nanotubes (CNTs)

CNTs are considered to be ideal candidates for a wide range of applications in materials science because of their exceptional mechanical, thermal, and electronic properties[2]. Carbon nanotubes exist as two types of structures: singlewall carbon nanotubes (SWNTs) and multiwall carbon nanotubes (MWNTs). Fig. 2.2 shows the schematic pictures of different types of carbon nanotubes. SWNT can be considered as graphene sheet rolled cylinders of covalently bonded carbon atoms with very high aspect ratios of 1000 or more. MWNTs consist of a number of graphene cylinders concentrically nested like rings in a tree trunk with an interlayer distance of ~0.34 nm.

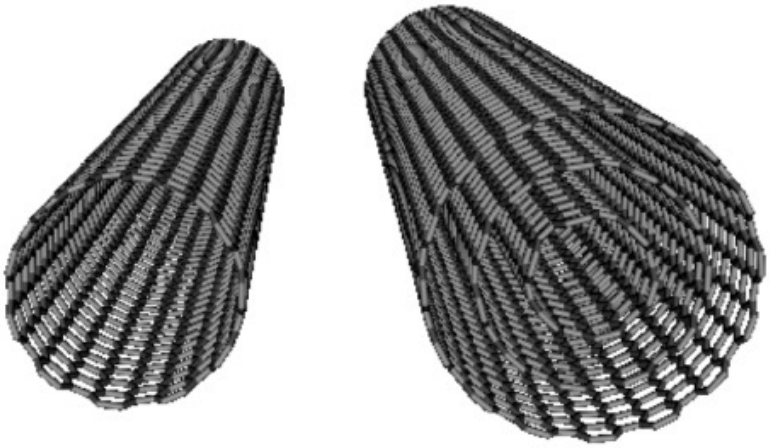

(a) (b)

Fig. 2.2 *A schematic illustration of different types of carbon nanotubes. (a) single-walled carbon nanotubes and (b) multi-walled carbon nanotubes*[3]

2.2.1.1 The Structure of Carbon Nanotubes

Based on the geometry of the carbon bonds around the circumference of the carbon nanotube, CNTs are divided into zig-zag, armchair and chiral nanotubes[4]. As illustrated in Fig. 2.3, 'zig-zag' and 'armchair' are the only two cases of achiral nanotubes. Most nanotubes do not have these highly symmetric forms but have structures in which the hexagons are arranged helically around the tube axis. In general, these structures are known as chiral.

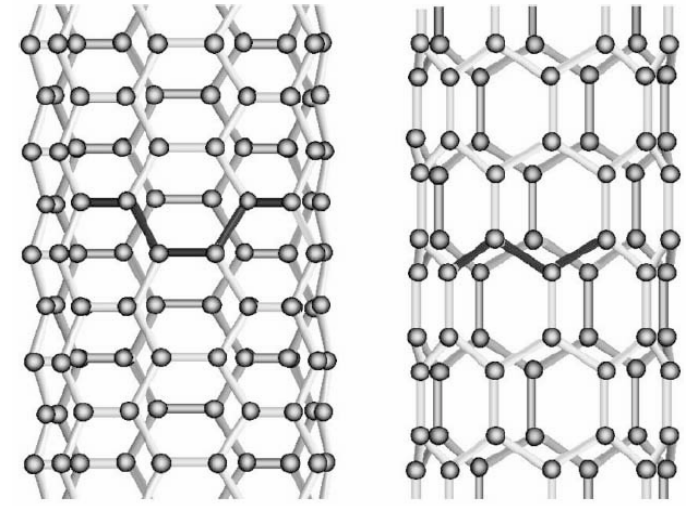

(a) (b)

Fig. 2.3 *A schematic illustration of carbon nanotube structure of (a) armchair and (b) zig-zag*[4]

2.2.1.2 The Properties of Carbon Nanotubes

The carbon-carbon covalent bond in graphite and carbon nanotubes is considered to be one of the strongest atomic bonds in nature. The mechanical properties of CNTs have been extensively studied, both experimentally and theoretically[5-8]. CNTs possess tensile moduli and strengths as high as 1 TPa and 150 GPa respectively. This

is an order of magnitude stronger than high strength carbon fibres. Their density can be as low as 1.3 gcm^{-3}, which is lower than commercial carbon fibres at 1.8-1.9 gcm^{-3}. CNTs are thermally stable at up to 2800 ^{o}C in a vacuum. Their thermal conductivity is about twice as high as that of diamonds. Their electric-current-carrying capacity is 1000 times higher than that of copper wires[4].

Since the first CNTs and polymer composites were made in 1994[9], large amounts of work have been done on Polymer/CNT composites. Incorporating nanotubes into plastics can potentially provide structural materials with a dramatic increase in both stiffness and strength. Extensive studies have been carried out producing strong Polymer/CNT composites[11-13]. The effective use of CNTs as reinforcements still presents some major difficulties. The key challenge still remains in breaking down bundles of aggregated CNTs and reaching a fine dispersion in the selected polymer matrix. Much work needs to be done to optimise the conditions required for the potential dispersion of nanotubes as well as a good interfacial interaction[12].

2.2.2 Nanoclays

Clay is a natural, earthy, fine-grained material and is the main constituent of the sedimentary rocks in marine sediments and in soils. Clay minerals belong to the family of phyllosilicates (or layered silicate) and have particles less than 2 μm in size as stated in ISO 14688[14]. There are three main groups of clays: kaolinite, montmorillonite-smectite and illite, and most clays are a mixture of these different types.

In this work, sepiolite was chosen as the nanofiller. Sepiolite is a needle-like shaped nanoclay composed with elemental particles of lengths of 0.2-4 μm, widths of 10-30

nm and thicknesses of 5-10 nm. Sepiolite can have a surface area as high as 200-300 m^2g^{-1} and normally it is found stuck together as bundles of fibres which can form micro-agglomerates (Fig. 2.4a). Sepiolite is a hydrous magnesium silicate with $[Si_{12}O_{30}Mg_8(OH)_4(H_2O)_4 \cdot 8H_2O]$ as the unit cell formula. The structure of sepiolite can be described as consisting of narrow strips which are formed by two sheets of tetrahedral silica units bonded to a central sheet of magnesium atoms. The strips link to each other by an inversion of the direction of the apical O of SiO_4 tetrahedrons (Fig. 2.4b). Therefore, rectangular channels occur in the longitudinal direction of the strips[14].

Sepiolite provides a pseudoplastic and thixotropic behaviour which make it a valuable material in multiple applications to improve the processability, application or handling of the final product. Sepiolite has recently gained increasing attention as a reinforcement for polymeric matrices[15,16]. Montmorillonite is the most popular clay used for polymer nanocomposites. Compared with montmorillonite, the morphology of sepiolite provides a lower specific surface area and smaller contact surface between the nanoclay fibres. Therefore, polymer chains have a better chance not only of interacting with the external surface of the sepiolite, but also of penetrating into the structure, which facilitates a more even dispersion of the clays in the polymer matrix. Sepiolite has been successfully used to reinforce different polymers, such as poly (hydroxyethyl acrylate)[15], chitosan[17], epoxy[16], etc.

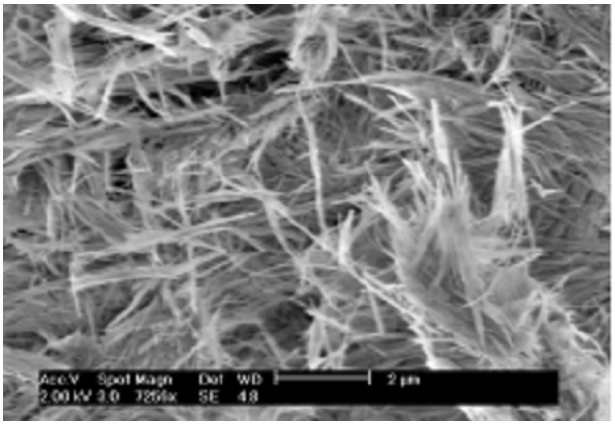

(a)

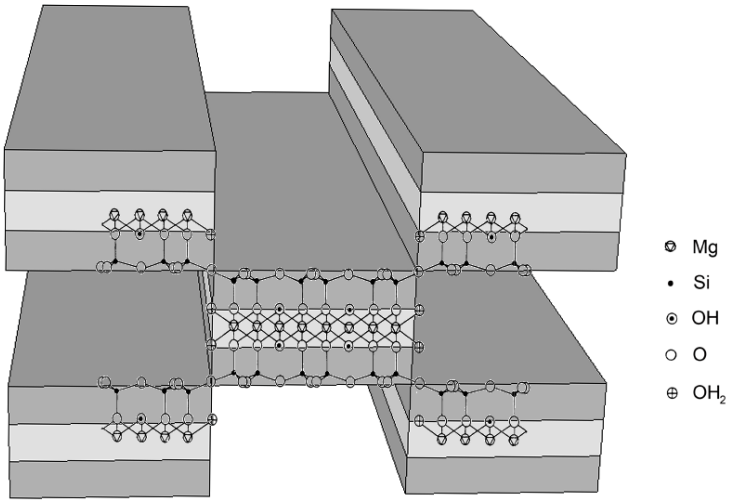

(b)

Fig. 2.4 *The structure of sepiolite fibre*

2.3 Polymer Nanocomposites

For decades we have been dealing with polymer microcomposites, where the length scale of the fillers is in micrometres. In the case of polymer nanocomposites, nano-fillers, being additives of nanometre scale, are dispersed in a polymer matrix, offering multifunctional, high-performance polymer characteristics beyond those possessed by traditional filled polymeric materials. Improvements in physical and mechanical properties have been well documented in the literature[4,10,18]. Apart from

mechanical enhancements, the value of polymer nanocomposites comes from providing value-added properties not present in the polymer matrix, without sacrificing the inherent processability and mechanical properties of the matrix. The multifunctional features consist of improved thermal, fire, and moisture resistance, decreased permeability, charge dissipation, and chemical resistance[12,15,18].

The properties of nanocomposites can be greatly affected by the dispersion of the nanofillers in the polymer matrix[19]. Generally, the better the dispersion, the better the properties of the final nanocomposites. However, nanofillers are, in essence, agglomerates due to their high surface energy, and it is very difficult to disperse them in most polymers. The achievement of well-dispersed sepiolites or carbon nanotubes in polymer matrices is the most investigated research topic worldwide[10,18,19].

2.3.1 Polymer/CNT Nanocomposites

Much effort has been expended in order to achieve good CNT dispersion and efficient stress transfer from the matrix to the tubes. Because of Van der Waals forces between individual CNTs, they tend to form bundles. The de-agglomeration of CNTs is necessary for dispersing individual nanotubes before mixing them with the polymer matrix.

The ultrasonication process is the most common method, but severe sonication may make the tubes shorter[20]. Milling and grinding is considered to be a cheap and fast method for industrial processes although it is the most destructive method for CNTs[21]. Non-covalent functionalizations, such as surfactants, are often utilised to overcome carbon nanotube entanglement resulting from Van der Waals forces[22]. Covalent functionalization of CNTs helps to break up the CNT bundles and improves the

polymer/CNT interface adhesion[23]. Polymer wrapping has been proposed as an alternative method to achieve a good dispersion of the carbon nanotubes without destroying their electrical properties[24]. Dissociated CNTs were produced by grafting polymer chains directly onto the CNTs to achieve a homogeneous polymer coating on the CNT surface[24-26]. Enhanced dispersion and improved properties, compared with the direct incorporation of CNTs in polymer melts, has been reported for high-density polyethylene coated MWNTs in thermoplastic matrices such as ethylene-vinyl acetate, polycarbonate, polyamide and polypropylene (PP)[24-29]. Fig. 2.5 illustrates four common types of functionalization of CNTs.

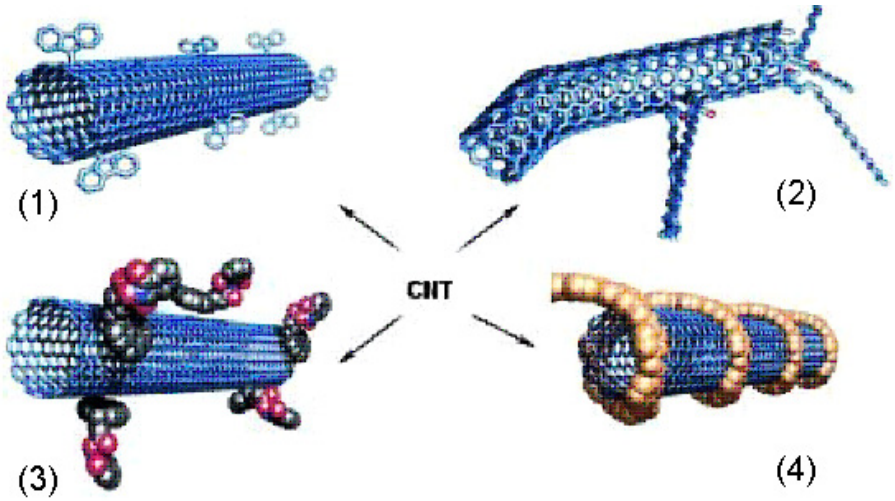

Fig. 2.5 *The functionalization of carbon nanotubes (1) oxidation (2) polymer grafted (3) surfactant-assisted and (4) polymer wrapped*[29]

2.3.2 Polymer/Clay Nanocomposites

There are two ways to modify the surface of hydrophilic clays in order to improve their dispersion in the polymer matrix. The first one is to modify the surface with cationic surfactants to make the silicate surface organophilic via ion exchange

reactions[30,31]. The second method is based on grafting polymeric molecules through covalent bonding to the hydroxyl groups existing on the particles. However, for polyolefin polymers such as PP and PE, they are non-polar and incompatible with silicate surfaces even after modifying them with non-polar long alkyl groups. Therefore, a compatibilizer is needed to facilitate the interaction between the polymer and the clays[32,33]. Compatibilizers are usually polar functional oligomers providing both a hydrophobic part (which can be easily mixed with a polymer) and a hydrophilic part (which is compatible with clay). Maleic anhydride grafted polypropylene (PP-g-MA) is a commonly used compatibilizer to aid the dispersion of clay.

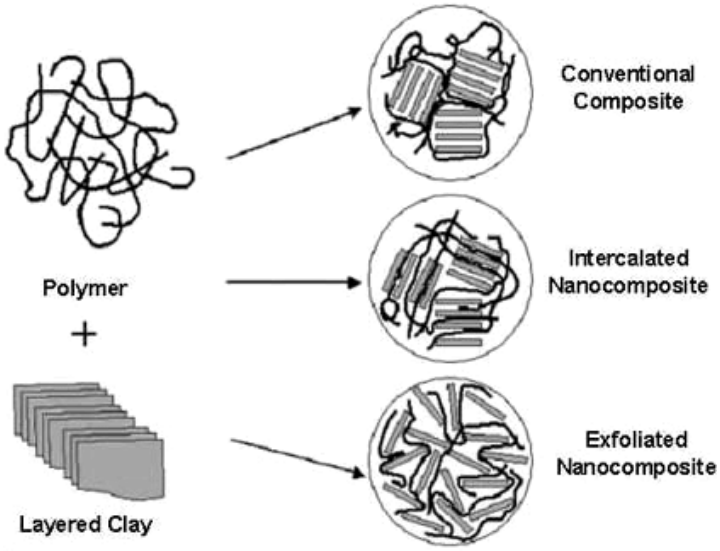

Fig. 2.6 *A possible morphology from the interaction of clays and polymer*

Depending on the degree of intercalation of matrix polymer chains into the galleries of the clays, intercalated or exfoliated nanocomposites can be obtained, and huge amounts of surface area can be created between the matrix polymer and the clay in the nanocomposites (Fig. 2.6). Intercalation results from a limited insertion of polymer chains into the interlayer region and an interlayer expansion. In contrast,

extensive polymer penetration and delamination of clay crystallites leads to exfoliated nanocomposites, in which the nanometer-thick silicate platelets are homogeneously dispersed throughout the whole polymer matrix. Exfoliated nanocomposites usually provide the best property enhancement due to the large aspect ratio and surface area of the clay[34].

2.4 Processing Methods for Polymer Nanocomposites

2.4.1 Traditional Processing Methods

Nanocomposites can be prepared by different methods such as solution intercalation, in-situ polymerisation or melt compounding.

Solution intercalation has been known for over a century and has proved to be one of the most successful methods for incorporating nanofillers into polymers. Nanocomposites with water-soluble polymers such as poly(ethylene oxide) and poly(vinyl alcohol)[35,36] and organic solvent-soluble polymers such as HDPE[37], have been successfully prepared via this method. However, their application on an industrial scale is still hindered by two major problems:

1. The involvement of large quantities of aqueous/organic solvent
2. A limited number of solvent/polymer pairs available for polymer dissolution

In-situ polymerisation has been intensively investigated in recent years. The advantage of this process is that the polymer chain can be grafted onto the nanofillers on a molecular scale. This gives excellent dispersion and the potential for good interfacial strength between the nanofillers and the polymer matrix. A relatively good

dispersion can be maintained even with high nanotube loading in the matrix. Successful investigations have been reported in the literature from different groups[38,39]. The uniform dispersions of CNTs or clays were obtained and improved properties were observed. However, the molecular weight of the polymer is often significantly lower with a wide distribution by comparison with other methods.

Melt compounding is the most common method used to process thermoplastic polymer nanocomposites because it is a cost-effective technology for polyolefin-based systems and is compatible with current industrial practices, such as extrusion, injection moulding, etc[40]. However, melt compounding, especially in the case of polyolefin matrices, is generally less effective at dispersing nanofillers such as CNTs and clays, and is limited to low nanofiller loadings due to the high viscosity of the composite systems caused by the addition of nanofillers[40]. Moreover, the high shear rates and high temperatures utilised can also cause thermal instability of the molten polymers[41]. One approach to promote compatibilization includes the use of polymer-coated nanofillers instead of pristine CNTs or clays into polymer melts. Alternatively, one can use the masterbatch process, where a pre-mixed highly loaded nanofiller composite is diluted with a fresh polymer melt[42].

2.4.2 The Supercritical Fluid Technique

In recent years, supercritical technology, especially supercritical carbon dioxide ($scCO_2$), has been widely applied in polymer processing. A supercritical fluid is defined as "any substance, the temperature and pressure of which are higher than their critical values, and which has a density close to, or higher than, its critical density"[43]. Fig. 2.7 shows a schematic representation of the density and organization of molecules of a pure fluid in solid state, gas state, liquid state and the supercritical

domain. No phase separation occurs for any substance at pressures or temperatures above its critical values. In other words, the critical point represents the highest temperature and pressure at which gas and liquid can coexist in equilibrium.

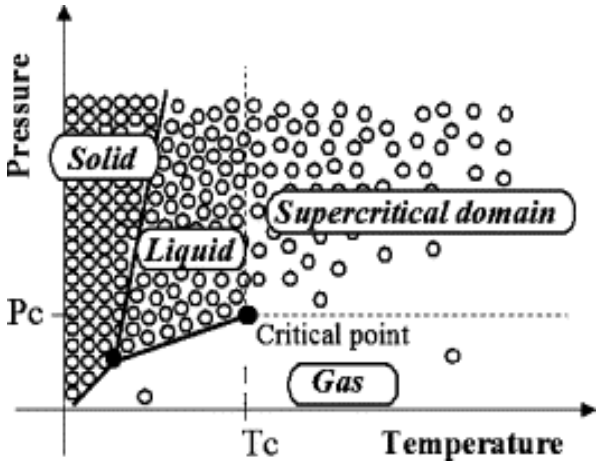

Fig. 2.7 *A schematic representation of the microscopic behaviour of a pure fluid in the P-T plane phase diagram*[44]

Supercritical fluids are unique solvents with a wide range of interesting properties. Supercritical fluids have high diffusivities, similar to gas which allows them to effuse through solids, while also having liquid-like densities that allow them to act as effective solvents for many compounds. In addition, small changes in pressure and temperature greatly affect the density of a supercritical fluid and therefore many properties of SCF can be 'fine-tuned'. The unique properties of supercritical fluids allow them to be widely exploited in the materials processing. The most promising developments are the processing of fine powders, core-shell particles, the processing and/or impregnation of aerogels, surface modifications and the processing of polymers[44].

2.4.2.1 Supercritical Carbon Dioxide

Among all the supercritical fluids, the use of supercritical carbon dioxide ($scCO_2$) is the most desirable for polymer processing because of its environmental compatibility as well as the following properties:

- CO_2 has relatively easily accessible critical points of 31.06 °C and 1070 psi (7.38 MPa) [45].
- The density of $scCO_2$ is easily tunable (Fig. 2.8). Therefore, the solvent strength and processes can be easily controlled.
- CO_2 is non-combustible and non-toxic in contrast to most of the organic solvents suitable for supercritical applications.
- It is also easily available because it occurs naturally as well as being the by-product of many industrial processes; therefore CO_2 is relatively inexpensive.
- As CO_2 is a gas at ambient temperatures and pressures it can be easily removed, leaving no solvent residues in the processed material[46].

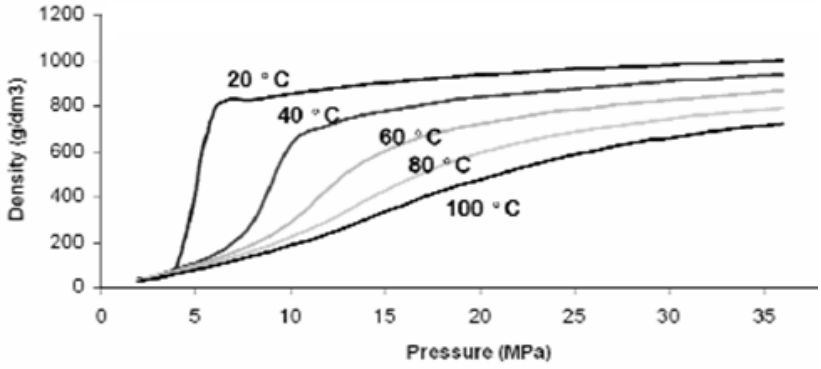

Fig. 2.8 *The density of CO_2 as a function of pressure for a range of temperatures*

$ScCO_2$ has found widespread application in industrial processes, including the extraction of metals or organic material, the decaffeination of green coffee beans, dry cleaning and de-greasing, nano and micro particle formation, impregnation and dyeing, the processing and synthesis of polymers and composites, tissue engineering scaffolds, drug delivery, etc[47-49]. The important fields most relevant to this thesis are in the $scCO_2$ processing of polymers and composites which will be discussed in greater detail below.

$ScCO_2$ processing, as one of the new and cleaner processing methods for polymer nanocomposites, has recently received increasing attention. The solubility of polymers in $scCO_2$ is poor for many high molecular weight polymers. Table 2.1 gives a representative sample of the available literature data for the solubility of CO_2 in a variety of polymers. The low solubility is a result of the lower density of $scCO_2$ and the weak interaction between the CO_2 molecules and the non-polar groups of many polymers[44]. However, even for polymers which are not soluble in $scCO_2$, the CO_2 is still able to permeate resulting in substantial and sometimes dramatic changes in the properties of these polymers. The permeation of $scCO_2$ into a polymer causes it to swell. Aided by their zero surface tension, the addition of $scCO_2$ into the polymer phase gives the chains a greater mobility. The CO_2 molecules act as lubricants, which reduces the chain-chain interactions as it increases the inter-chain distance and free volume of the polymer. This is called plasticization. The physical properties of the polymer are changed dramatically, including the depression of the glass transition temperature (T_g), the lowering of interfacial tension and a reduction of the viscosity of the polymer melt. $ScCO_2$ may increase the crystallinity of the polymers because the polymer chains are given more freedom to align themselves into a more favourable order.

Table 2.1 *The solubility of CO_2 in polymers*[50]

Polymer	Method[a]	Pressure [atm]	Temp. [°C]	Solubility
poly(methyl methacrylate)	GM-M	50	65	46 SCC/cm^3
	GM-D	204	70	10.5 wt.%
polystyrene	GM-M	13.2	25	14.5 SCC/cm^3
high-impact polystyrene	GM-D	204	70	0.5 wt.%
polycarbonate	GM-M	13.2	25	24 SCC/cm^3
	GM-D	68	25	13 g/100g
poly(ethylene terephthalate)	GM-D	136	40	1.5 wt.%
poly(vinyl chloride)	GM-D	68	25	8 g/100g
	GM-D	136	40	0.1 wt.%
poly(vinyl acetate)	GM-D	54.4	25	29 g/100g
low density polyethylene	GM-D	68	40	0.2 wt.%
high density polyethylene	GM-D	68	40	0.1 wt.%
polypropylene	GM-D	68	40	0.1 wt.%
	GM-D	204	25	0.1 wt.%
	BM	73	160	1.59 g/100g
	BM	61.2	200	1.09 g/100g
Nylon 66	GM-D	68	40	1.8 wt.%
polyurethane	BM	136	40	2.2 wt.%
Teflon	GM-D	68	40	0.0 wt.%

[a]*Method: GM-M, gravimetric method (microbalance); GM-D, gravimetric method (desorption); BM, barometric method. Units: SCC/cm^3, cm^3(STP)/cm^3 of polymer; g/100g, g of CO_2/100g of polymer.*

A wide range of opportunities have opened up for $scCO_2$ that have an impact on the plastics industry[50]. These include usages for extraction, foaming and impregnation. Extraction occurs merely by removing the soluble extractant material, such as any unreacted monomer, while leaving the insoluble substrate. Foaming occurs when rapid decompression forms gaseous CO_2 inside the polymer, leaving the polymer in the form of a porous (micro) material. This is very important in supporting the growth of blood vessels and collagen fibres in the matrix of biodegradable polymers or when the final product is intended to be used as a catalyst. As for impregnation, CO_2 can act as a transport medium facilitating the diffusion of monomers, initiators and molecules to impregnate a polymer, while the CO_2 can be cleanly removed afterwards. A better dispersion of the molecules has been provided within the polymer matrix. Substances impregnated into polymers have included dyes, fragrances, drugs for controlled release, anti-microbial and anti-fungal agents, and nanoparticles[51].

2.4.2.2 The Influence of $ScCO_2$ on the T_g of Polymers

T_g is the critical temperature that separates the glassy and rubbery behaviours of the polymers[52]. When a polymer at a temperature below its T_g, it is hard and brittle and its molecular chains are essentially frozen. If it is at a temperature above its T_g, its molecular chains can slide past each other, allowing it to be soft or rubbery.

The introduction of $scCO_2$ causes the plasticization of the polymer, which will increase the inter-chain distance and allow the chains to move past each other at lower temperature, hence decrease T_g[53]. The glass transition is a transition which happens to the amorphous phase of polymers. Therefore, for semi-crystalline polymers, the decrease of T_g from the $scCO_2$ is less significant compared with

amorphous polymers. Condo *et al*.[54] has proposed a thermodynamic model of T_g behaviour versus CO_2 solubility in the polymer. (Fig.2.9) According to Fig. 2.9, a higher CO_2 sorption is needed to achieve a further decrease of T_g This near-linear prediction of the model has been backed up experimentally by many authors[54-58]. Table 2.2 lists the T_g depression of common polymers under CO_2.

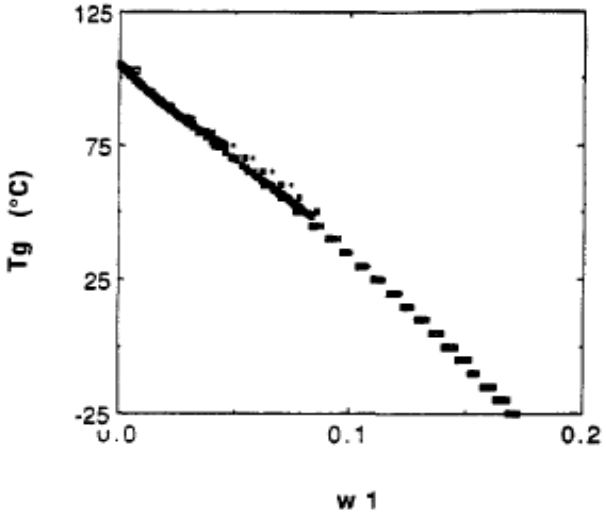

Fig.2.9 *T_g behaviour as a function of solubility (weight fraction units) of the compressed fluid in the polymer*[54]

Table 2.2 *T_g depression of Polymers under CO_2*[50]

Polymer	Pressure range investigated	T_g depression $-dT_g/dP$ (°C/atm)
poly(methyl methacrylate)	0-37 atm	1.2
polystyrene	0-60 atm	1.08
poly(vinyl chloride)	0-42 atm	1.45
polycarbonate	0-56 atm	0.73
poly(ethylene terephthalate)	0-20 atm	1.1

2.4.2.3 The Influence of $ScCO_2$ on the T_m of Polymers

The reduction of T_g by plasticization has been well established in the literature, while the influence of $scCO_2$ on the melting temperature of semicrystalline polymers has interested many researchers. Handa *et al.*[59] reported at 72 bar of CO_2, the T_m of syndiotactic PS (270 °C) is lowered by about 12 °C. Varma-Nair *et al.*[60] reported that $T_{m(\text{onset})}$ of isotactic polypropylene decreased from 147 °C at ambient pressure to ca. 141 °C at 650 psi. As shown in the paper of Garcia-Leiner *et al.*[61], HDPE can be continuously processed at temperatures below its melting point (127 °C) when CO_2 is introduced into the system. In semicrystalline polymers, the solubility of CO_2 occurs predominantly in amorphous regions. Varma-Nair *et al.* suggested that CO_2 absorbed in the amorphous regions will dilate the overall polymer matrix, which will lead to a lowering of the energy barriers. Some authors relate the decrease in T_m to an increase in the specific surface free energy caused by the dissolved CO_2. The decrease in T_m benefits the moulding process greatly, in terms of energy saving, since the process can be operated at a lower temperature.

2.4.2.4 The Influence of $ScCO_2$ on the Crystallization of Polymers

The effect of CO_2 on the crystallization of a polymer is related to the temperature of maximum crystallization rate ($T_{\max}$). The crystallization rate changes with temperature and reaches its maximum at $T_{\max,}$ which is close to the mean of T_g and the equilibrium melt temperature T_m^0: $T_{\max} \approx (T_g+T_m^0)/2$. Above $T_{\max}$ the overall crystallization rate is controlled by the nucleation rate, and the temperature region between $T_{\max}$ and T_m^0 is called the nucleation-controlled region. Below $T_{\max}$ the overall rate is controlled by the crystal-growth rate. Fig. 2.10 shows the temperature dependence of the crystallization rate in the presence of CO_2 and atmospheric air.

The dissolved CO_2 will depress T_m^0, and hence reduce T_{max} to T'_{max}. This means that the dissolved CO_2 accelerates the crystallization rate of an isothermally crystallized semicrystalline polymer within the crystallization growth region and reduces the rate within the nucleation controlled region[62].

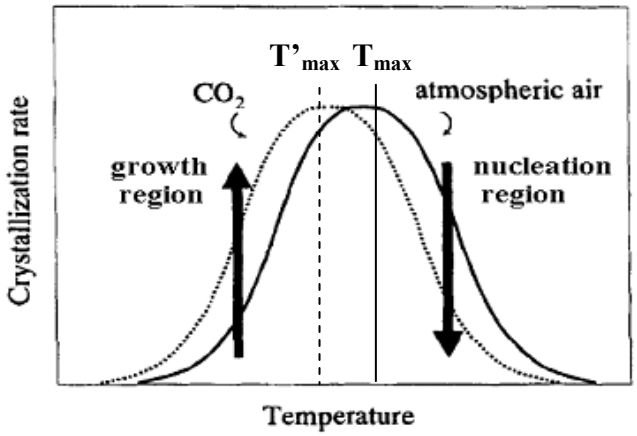

Fig. 2.10 *The temperature dependence of the crystallization rate in the presence of CO_2 and atmospheric air*

2.4.2.5 Polymer Nanocomposite Processing in $ScCO_2$

The effective dispersion of the fillers in the polymer matrix and the improvement of polymer-filler interactions are two key challenges in the field of polymer nanocomposites. The development of polymer processing technologies in $scCO_2$ has enabled the synthesis of very complex polymer nanocomposites. $ScCO_2$ can be used as the reaction medium allowing a homogeneous dispersion of the monomer, the initiator and the subsequent polymerisation under lower viscosity[63]. Green *et al.*[64] developed a poly(methyl methacrylate)/silicate nanocomposite in $scCO_2$ exhibiting a significant improvement in physical properties. Poly(methyl methacrylate)/clay and polystyrene/clay have been produced via in-situ polymerisation with $scCO_2$ acting as both a plasticizer for the polymer matrix and a carrier of the monomer[63,65]. Studies in

PP have indicated improvements in the dispersion of nanofillers in the matrix via melt compounding in $scCO_2$[66].

2.5 Polypropylene Nanocomposites

PP underwent a dramatic growth in production and use throughout the latter half of the 20th century[67]. PP is a thermoplastic polymer of the chemical designation C_3H_6. The main types of PP produced are isotactic PP and syndiotactic PP (Fig. 2.11). The position of the large methyl side group determines the tacticity of the PP molecule, which affects the ability of the molecules to crystallize. In isotactic PP, all the methyl groups are on the same side of the polymer chain, which allows a high degree of crystallisation. In contrast, atactic PP does not have the methyl groups on the same side of the polymer chain, which directly makes it non-crystallizable[61]. PP has been used in a wide variety of applications including packaging, fibres, textiles, stationary, pastic parts and reusable containers, automotive components, etc[68].

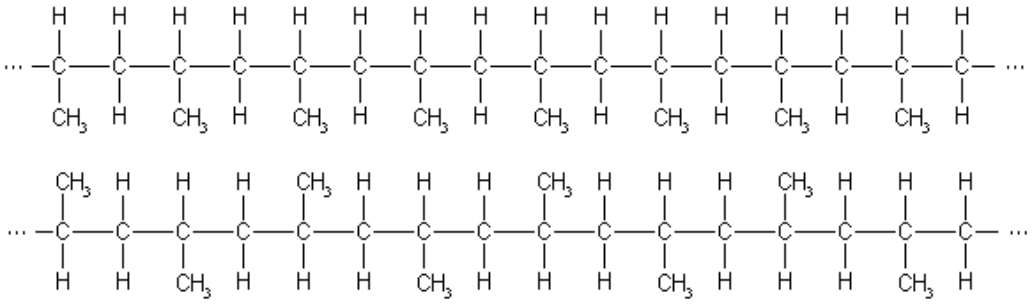

Fig. 2.11 *Polypropylene (a) Isotactic and (b) syndiotactic*

Because of PP's good balance between properties and cost and its wide usage in industry, PP nanocomposites have been extensively studied in recent years[28,40,69,70]. Due to the lack of polar groups in PP, many efforts have been attempted to improve the dispersion of inorganic fillers such as clay and CNTs into a PP matrix for the

preparation of effective PP nanocomposites and enhanced mechanical properties. Andrews *et al*.[40] fabricated PP/MWNT composites by a shear mixer and found a modulus increase from 1.0 GPa to 2.4 GPa with a relatively high nanotube content of 12.5 wt.%. However, this was at the expense of a reduction in yield stress from 30 MPa to 18 MPa. Deng *et al*.[28] investigated the effects of a high density polyethylene (HDPE) coating onto MWNTs on the mechanical properties of PP/MWNT composites produced by melt compounding. A property increase from 1.42 GPa to 1.79 GPa for Young's modulus and from 34.5 MPa to 37.9 MPa for tensile strength, was achieved at relatively low loadings (0.5 wt.%) of coated MWNTs. Liu and Wu[70] reported the preparation of PP/montmorillonite nanocomposites with the aid of a compatibiliser (maleic anhydride). Although the mechanical properties were improved in all cases, the lack of polar groups in the PP macromolecules makes it difficult to obtain well exfoliated nanocomposites and is limited to low nanofiller loadings. Moreover, due to the high temperatures and high shear rates involved in the melt compounding method, many problems may occur including the thermal instability of PP and the reduction of filler length, etc.

By treating the PP with CO_2, PP will become plasticized. CO_2 can be absorbed only in the amorphous phase of the material and not in the crystalline phase. Narma-Nair *et al.*[60] have suggested that 1% CO_2 could be dissolved in PP at 50 °C at 180 psi. Both decreases in T_m and T_c of PP in presence of CO_2 have been reported in the literature[60,71]. It has also been reported that a decrease in weight for PP under some $scCO_2$ conditions, which suggested the extraction of some agents, such as monomers, oligomers, additives, or plasticizers from the polymer during the process[72]. Little difference has been found with the $scCO_2$ plasticized PP compared with untreated one in both yield strength and modulus[73].

2.6 Effective Mechanical Properties of Fillers in Polymer Composites

The reinforcing efficiency of fillers in the polymer matrices has been extensively studied since 1950s. One of most common models is the rule of mixtures, which enables the comparison of literature results by the calculation of the effective contribution of the fillers to the composite properties. For composites in which discontinuous fibres are not perfectly aligned, the Young's modulus of the composite (E_c) can be written as[74]:

$$E_c = \eta_o \eta_L V_f E_f + (1 - V_f) E_m \qquad 2\text{-}1$$

where η_L is the length efficiency factor, η_o is the orientation factor, E_m and E_f are the Young's modulus of the matrix and the fibre respectively, and V_f is the volume fraction of the fibre. η_L can vary between 0 and 1. η_o is equal to 1 for fully aligned fibres, 3/8 for random (in-plane) 2D orientation and 1/5 for random 3D orientation. A similar equation can be formulated for the strength:

$$\sigma_c = \eta_L \eta_o V_f \sigma_f + (1\text{-}V_f)\, \sigma_m \qquad 2\text{-}2$$

Therefore, equations 2-1 and 2-2 can be used to evaluate the effective mechanical properties of CNTs in the composites. In the calculation, η_o was chosen to be the random 3D orientation value of 1/5, η_L equals 1 for high fibre aspect ratios (1/d > 100). The volume fractions were deduced from the weight fractions and densities of the materials.

2.7 Objectives for Part 1

The achievement of well dispersed nanofillers in the polymer matrix is one of the most essential topics in the processing of polymer nanocomposites, particularly in melt compounding processes. Considering the high viscosities, high temperatures and high shear stresses involved in common melt compounding processes, $scCO_2$ processing can be an interesting alternative to produce PP nanocomposites as it should overcome some of these issues. The plasticization of $scCO_2$ could reduce the PP viscosity, decrease the T_m of the PP, and hence increase the processablity of nanocomposites and improve the dispersion of nanofillers.

The main objectives of this part are:

1. To prepare PP/MWNT and PP/sepiolite nanocomposites using $scCO_2$ assisted processing
2. To study the properties of nanocomposites obtained using $scCO_2$ processing by comparison with those of traditional melt compounded samples and to investigate the potential benefits of using $scCO_2$
3. To analyze the effective properties of the nanofillers in the nanocomposites using a simple micromechanical model

2.8 References

1. Grunes J, Zhu J and Somorjai GA. Catalysis and Nanoscience. Chem. Commun. 2003, 7, 2257
2. Baughman AA and Zakhidov WA deHeer. Carbon Nanotubes - The Route Toward Applications. Science. 2002, 297, 787

3. Dresselhaus MS, Lin YM, Rabin O, Jorio A, Souza Filho AG, Pimenta MA, Saito R, Samsonidze Ge G and Dresselhaus G. Nanowires and nanotubes. Mater. Sci. Eng. 2003, 23, 129
4. Thostenson ET, Ren Z and Chou TW. Advances in the Science and Technology of Carbon Nanotubes and Their Composites: a Review. Compos. Sci. Technol. 2001, 61, 1899
5. Yakobson BI, Brabec CJ and Bernholc J. Nanomechanics of Carbon Tubes: Instabilities beyond Linear Response. Phys. Rev. Lett. 1996, 76, 2511
6. Lu JP. Elastic Properties of Carbon Nanotubes and Nanoropes. Phys. Rev. Lett. 1997, 79, 1297
7. Nardelli MB, Yakobson BI and Bernholc J. Mechanism of Strain Release in Carbon Nanotubes. Phys. Rev. B. 1998, 57, 4277
8. Yakobson BI. Mechanical Relaxation and ‘‘Intramolecular Plasticity’’ in Carbon Nanotubes. Appl. Phys. Lett. 1998, 72, 918
9. Ajayan PM. Stephan O, Colliex C and Trauth D. Aligned Carbon Nanotube Arrays Formed by Cutting a Polymer Resin-Nanotube Composite. Science. 1994, 265, 1212
10. Coleman JN, Khan U and Gun'ko Y.K. Mechanical Reinforcement of Polymers Using Carbon Nanotubes. Adv. Mater. 2006, 18, 689
11. Coleman JN, Khan U and Blau WJ and Gun'ko YK. Small but Strong: A Review of the Mechanical Properties of Carbon-Nanotube-Polymer Composites. Carbon. 2006, 44, 1624
12. Moniruzzaman M. WK. Polymer Nanocomposites Containing Carbon Nanotubes. Macromol. 2006, 39, 5194
13. Ahir SV. Polymer Containing Carbon Nanotubes: Active Composite Materials. In: Nalwa SH, editor. Polymeric Nanostructures and Their Applications. California: American Scientific Publishers; 2005

14. Moore DM and Reynolds RC. X-Ray Diffraction and the Identification and Analysis of Clay Minerals. 2nd Ed. New York: Oxford University Press; 1997
15. Bokobza L, Burr A, Garnaud G, Perrin MY and Pagnotta S. Fibre Reinforcement of Elastomers: Nanocomposites Based on Sepiolite and Poly(hydroxyethyl acrylate). Polym. Int. 2004, 8, 1060
16. Zheng Y and Zheng Y. Study on Sepiolite-Reinforced Polymeric Nanocomposites. J. App Polym Sci. 2006, 5, 2163
17. Darder M, Lopez-Blanco M, Aranda P, Aznar AJ, Bravo J and Ruiz-Hitzky E. Microfibrous Chitosan-Sepiolite Nanocomposites. Chem. Mater. 2006, 6, 1602
18. Koo JH. Polymer Nanocomposites: Processing, Characterization, and Applications. New York: McGraw-Hill; 2006
19. Ray SS and Okamoto M., Polymer/Layered Silicate Nanocomposites: A review from Preparation to Processing. Prog. Polym. Sci. 2003, 28, 1539
20. Saito T, Matsushige K and Tanaka K. Chemical Treatment and Modification of Multi-Walled Carbon Nanotubes. Physica B. 2002, 323, 280
21. Pierard N, Fonseca A, Konya Z, Willems I, Van Tendeloo G and Nagy JB. Production of short carbon nanotubes with open tips by ball milling. Chem. Phys. Lett. 2001, 335, 1
22. Bonduel D, Mainil M, Alexandre M, Monteverde F, and Dubois P. Supported Coordination Polymerisation: A Unique Way to Potent Polyolefin Carbon Nanotube Nanocomposites. Chem. Commun. 2004, 781
23. Liu L, Barber AH, Nuriel S and Wagner HD. Mechanical Properties of Functionalized Single-Walled Carbon-Nanotube/Poly(vinyl alcohol) Nanocomposites. Adv. Funct. Mater. 2005, 15, 975
24. Star A., Stoddart JF, Steuerman D, Diehl M, Boukai A, Wong EW, Yang X, Chung SW, Choi H and Heath JR. Preparation and Properties of Polymer-Wrapped Single-Walled Carbon Nanotubes. Angew. Chem. Int. Ed. 2001, 40, 1721
25. Peeterbroeck S, Laoutid F, Taulemesse JM, Monteverde F, Lopez-Cuesta JM, Nagy JB,

Alexandre M and Dubois P. Mechanical Properties and Flame-Retardant Behavior of Ethylene Vinyl Acetate/High-Density Polyethylene Coated Carbon Nanotube Nanocomposites. Adv. Funct. Mater. 2007, 15, 2787

26. Dubois P and Alexandre M. Performant Clay/Carbon Nanotube Polymer Nanocomposites. Adv. Eng. Mater. 2006, 8, 147
27. Pötschke P, Pegel S, Claes M and Bonduel D. A Novel Strategy to Incorporate Carbon Nanotubes into Thermoplastic Matrices. Macromol. Rapid Commun. 2008, 3, 244
28. Deng H, Bilotti E, Zhang R and Peijs T. Effective Reinforcement of Carbon Nanotubes in Polypropylene Matrices. J. Appl. Poly. Sci. 2010, 1, 30.
29. Ciselli P. the Potential of Carbon Nantoubes in Polymer Composites. PhD thesis, The Eindhoven University of Technology; 2007
30. Lan T and Pinnavaia TJ. Clay-Reinforced Epoxy nanocomposites. Chem. Mater. 1994, 6, 2216
31. Shi H, Lan T and Pinnavaia TJ. Interfacial Effects on the Reinforcement Properties of Polymer-Organoclay Nanocomposites. Chem. Mater. 1996, 8, 1584
32. Hasegawa N, Okamoto H, Kato M and Usuki A. Preparation and Mechanical Properties of Polypropylene-Clay Hybrids based on Modified Polypropylene and Organophilic Clay. J. Appl. Polym. Sci. 2000, 78, 1918
33. Garcia-Lopez D, Picazo O, Merino JC and Pastor JM. Polypropylene Clay Nanocomposites: Effect of Compatibilizing Agents on Clay Dispersion. Eur. Polym. J. 2003, 39, 945
34. Alexander M and Doubis PH. Polymer-Layered Silicate Nanocomposites: Preparation, Properties and Uses of a New Class of Materals. Mater. Sci. Eng. R. 2000, 28, 1
35. Wu JH and Lerner MM. Structural, Thermal, and Electrical Characterization of Layered Nanocomposites Derived from Sodium-Montmorillonite and Polyethers. Chem. Mater. 1993, 5, 835

36. Ogata N, Kaawakage S and Ogihara T. Poly(vinyl alcohol)-Clay and Poly(ethylene oxide)-Clay Blends Prepared Using Water as Solvent. J. Appl. Polym. Sci. 1997, 66, 573
37. Joen HG, Jung HT, Lee SW and Hudson SD. Morphology of polymer/Silicate Nanocomposites High Density Polyethylene and a Nitrile Copolymer. Polym. Bull. 1998, 41, 107
38. Park C, Ounaies Z, Watson KA, Crooks RE, Smith J, Lowther SE, Connell JW, Siochi EJ, Harrison JS and Clair TLS. Dispersion of Single Wall Carbon Nanotubes by in situ Polymerisation under Sonication. Chem. Phys. Lett. 2002, 364, 303
39. Ozdilek C, Kazimierczak K and Picken SJ. Preparation and Characterization of Titanate-Modified Boehmite-Polyamide-6 Nanocomposites. Polym. 2005, 16, 6025
40. Andrews R, Jacques D, Minot M and Rantell T. Fabrication of Carbon Multiwall Nanotube/Polymer Composites by Shear Mixing. Mater. Eng. 2002, 287, 395
41. Potschke P, Bhattacharyya AR, Janke A and Goering H. Melt Mixing of Polycarbonate/Multi-wall Carbon Nanotube Composites. Compos. Interfaces. 2003, 10, 389
42. Prashantha K, Soulestin J, Lacrampe MF, Krawczak P, Dupin G and Claes M. Masterbatch-Based Multi-Walled Carbon Nanotube Filled Polypropylene Nanocomposites: Assessment of Rheological and Mechanical Properties. Compos. Sci. Technol. 2009, 11, 1756
43. Darr JA and Poliakoff M. New Directions in Inorganic and Metal-Organic Coordination Chemistry in Supercritical Fluids. Chem. Rev. 1999, 99, 495
44. Cansell F, Aymonier C and Loppinet-Serani A. Review on Materials Science and Supercritical Fluids. Curr. Opin. Solid State Mater. Sci. 2003, 7, 331
45. Hyatt JA. Liquid and Supercritical Carbon Dioxide as Organic Solvents. J. Org. Chem. 1984, 49, 5097

46. Behles JA and DeSimone JM. Developments in CO_2 Research. Pure Appl. Chem. 2001, 73, 1281

47. Taylor DK, Carbonell R and DeSimone JM. Opportunities for Pollution Prevention and Energy Efficiency Enabled by the Carbon Dioxide Technology Platform. Annu. Rev. Energy Env. 2000, 25, 115

48. Quirk RA, France RM, Shakesheff KM and Howdle SM. Supercritical Fluid Technologies and Tissue Engineering Scaffolds. Curr. Opin. Solid State Mater. Sci. 2004, 8, 313

49. Hyde JR, Licence P, Carter D and Poliakoff M. Continuous Catalytic Reactions in Supercritical Fluids. Appl. Catal., A. 2001, 222, 119

50. Tomasko DL, Li H, Liu D, Han X, Wingert MJ, Lee LJ and Koelling KW. A Review of CO_2 Applications in the Processing of Polymers. Ind. Eng. Chem. Res. 2003, 42, 6431

51. Kikic I and Vecchione F. Supercritical Impregnation of Polymers. Curr. Opin. Solid State Mater. Sci. 2003, 7, 399

52. Sperling LH. Introduction to Physical Polymer Science. 4th Ed. New Jersey: Wiley-Blackwell; 2006

53. Kazarian S. G. Polymer processing with supercritical fluids. Polym. Sci., Ser. C 2000, 42, 78

54. Condo PD, Sanchez IC, Panayiotou C and Johnston KP. Glass Transition Behavior Including Retrograde Virtrification of Polymer with Compressed Fluid Fluids. Macromol. 1992, 29, 6119

55. Chiou JS, Barlow JW and Paul DR. J. Appl. Plasticization of Glassy Polymers by CO_2. Poym. Sci. 1985, 30, 2633

56. Wissinger RG. and Paulaitis ME. Glass Transition in Polymer/CO_2 Mixtures at Elevated Pressure. J. Polym. Sci. Part B: Polym. Phys. 1991, 29, 631

57. Condo PD and Johnston KP. Retrograde Vitrification of Polymers with Compressed Fluid Fluids: Experimental Confirmation. Macromol. 1992, 25, 6730

58. Condo PD, Paul DR and Johnston KP. Glass Transition of Polymer with Compressed Fluid Fluids: Type II and III Behavior. Macromol. 1994, 27, 365

59. Handa YP, Zhang Z and Wong B. Effect of Compressed CO_2 on Phase Transitions and Polymorphism in Syndiotactic Polystyrene. Macromol. 1997, 30, 8499

60. Varma-Nair M, Handa PY, Mehta AK and Agarwal, P. Effect of Compressed CO_2 on Crystallization and Melting Behavior of Isotactic Polypropylene. Thermochim. Acta. 2003, 396, 9, 57

61. Garcia-Leiner M and Lesser AJ. CO_2-Assisted Polymer Processing: A New Alternative for Intractable Polymers. J. Appl. Polym. Sci. 2004, 4, 1501

62. Takada M, Tanigaki M and Ohshima M. Effects of CO_2 on Crystallization Kinetics of Polypropylene. Polym. Eng. Sci. 2001, 11, 1938

63. Zerda AS, Caskey TC and Lesser AH. Highly Concentrated, Intercalated Silicate Nanocomposites: Synthesis and Characterisation. Macromol. 2003, 36, 1603

64. Green JW, Rubal MJ, Osman BM, Welsch RL, Cassidy PE, Fitch JW and Blanda MT. Silicon-Organic Hybrid Polymers and Composites Prepared in Supercritical Carbon Dioxide. Polym. Adv. Technol. 2000, 11, 820

65. Li JB, Xu Q, Peng Q, Pang MZ, He SQ and Zhu CS. Supercritical CO_2-Assisted Synthesis of Polystyrene/clay Nanocomposites via in situ Intercalative Polymerisation. J. App. Polym. Sci. 2006, 1, 671

66. Garcia-Leiner M and Lesser AJ. Melt Intercalation in Polymer-Clay Nanocomposites Promoted by Supercritical Carbon Dioxide. Polym. Mater. Sci. Eng. 2003, 89, 649

67. Balow MJ. Global Trends for Polypropylene. Handbook of Polypropylene and Polypropylene Composites, Revised and Expanded. Karian HG Ed., New York: Marcel Dekker; 2003

68. Kissel WJ, Han JH and Meyer JA. Polypropylene: Structure, Properties, Manufacturing Processes, and Applications. In: Karian HG, editor. Handbook of Polypropylene and Polypropylene Composites. New York: Marcel Dekker; 1999

69. Deng H, Zhang R, Reynolds CT, Bilotti E and Peijs T. Carbon Nanotube Composite Tapes or Fibres with High Strength and Electrical Conductivity. Macromol. Mater. Eng. 2009, 294, 749

70. Liu XH and Wu QJ. PP/Clay Nanocomposites Prepared by Grafting-Melt Intercalation. Polym. 2001, 25, 10013

71. Kishimoto Y and Ishi R. Differential Scanning Calorimetry of Isotactic Polypropene at High CO_2 Pressures. *Polym.* 2000, 41,3483

72. Fleming G.K and Koros WJ. Dilation of Polymers by Sorption of Carbon Dioxide at Elevated Pressures. 1. Silicone Rubber and Unconditioned Polycarbonate. Macromol. 1986, 19, 2285

73. Sawan SP, Shien YT and Su JH. Evaluation of the-lnteractions Between Supercritical Carbon Dioxide and Polymeric Materials. Los Alamos, New Mexico: Los Alamos National Laboratory, 1994

74. Hull D and Clyne T. An Introduction to Composite Materials. Cambridge: University Press; 1981

Chapter 3

Polymer/Clay Nanocomposites using $ScCO_2$ Assisted Mixing

3.1 Introduction

In this research, $scCO_2$ was used to prepare PP/sepiolite nanocomposites with and without the presence of PP-g-MA as a compatibilizer. Bilotti *et al.*[1] previously reported the preparation of PP/sepiolite nanocomposites using the traditional melt compounding method. The benefits of performing this process with $scCO_2$ are investigated in this study. The morphologies of various nanocomposites were identified, and the thermal properties were investigated. In addition, as PP is a semicrystalline polymer, its crystalline structure and morphology were also studied,

as these may be greatly affected by the interaction of the polymer with the clay as well as the processing conditions[2].

3.2 Experimental

3.2.1 Materials and Equipments

The PP used was Moplen® HP500H from Basell. Moplen® HP500H, which has a softening temperature of 151 °C (A50 (50 °C/h 10 N)), density of 0.9 g/cm^3 at 20 °C and a melt flow rate (MFR) of 1.8 g/10min (230 °C/2.16kg). The clay used was Sepiolite Pangel® supplied by Tolsa (Spain). Sepiolite Pangel® has a bulk density of ~ 60 g/L. All materials were used as obtained. The average length of an individual sepiolite nano-fibre is 1-2 μm and its diameter is in the range of 20-30 nm. The compatibilizer used was PP-g-MA having a commercial grade of VINBOND® P series (VB100; 1 % grafted MA), and was purchased from Vin Enterprise Ltd. A liquid withdrawal CO_2 cylinder at 725 psi pressure was supplied by BOC gases. A custom-built stirred high-pressure autoclave with paddle type stirrer was used to prepare the nanocomposites. A Rondol laboratory bench-top hot-press was used to produce the dumbbell-shaped specimens.

3.2.2 Processing of PP/clay Nanocomposites

A custom-built high-pressure autoclave made from stainless steel was used with an ISCO pump. Fig. 3.1 shows the system diagram. Abbreviations in the Fig. 3.1 are explained as below: PR: Pressure Regulator, EP: Electronic Pressure Gauge (Transducer), T: TAP, TC: Temperature Controller, PG: Pressure Gauge, F: Filter, and BPR: Back Pressure Regulator.

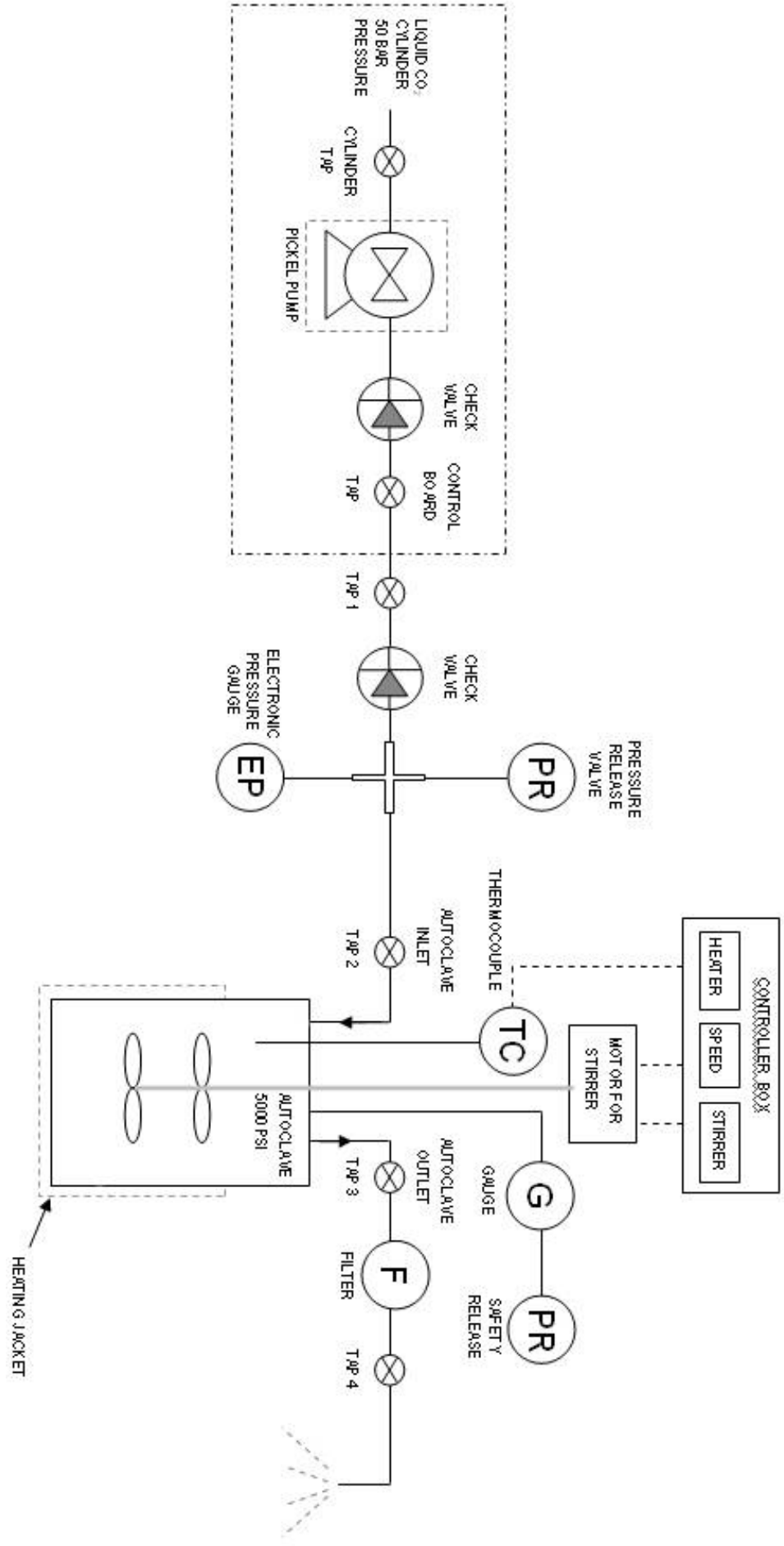

Fig. 3.1 *System diagram*

PP and sepiolite with and without PP-g-MA were loaded in the autoclave. The amount of PP-g-MA in the nanocomposites was equivalent to the amount of sepiolite (1:1 weight ratio). CO_2 was pumped into the autoclave via an Isco model 260D syringe pump after being chilled to -6 °C. The autoclave was heated up and held at 2175 psi and 200 °C under stirring using a pitched bladed turbine impeller for 30 min. The stirring speed was set at maximum power. After mixing, the autoclave was cooled in water to room temperature, and CO_2 was vented slowly. Nanocomposites having clay contents of 1 wt.%, 2.5 wt.%, 5 wt.% and 10 wt.% were obtained by selecting different weight ratios between the PP and the sepiolite. The bulk materials obtained from the autoclave were frozen in liquid nitrogen and then broken into pieces, which were subsequently used for hot pressing into dumbbell-shaped specimens according to ASTM D-638 at 200 ^{o}C under 5800 psi for 5 min. The samples were cooled down to room temperature using the water cooling system of the hot-press.

3.2.3 Characterization

Scanning Electron Microscopy (SEM) was used to investigate the morphological characteristics using a JEOL 6300^{TM} (accelerating voltage 10 kV) in the normal secondary electron imaging mode. Prior to the examination, the samples were freeze-fractured in liquid nitrogen and sputter coated with a thin layer of gold by using a sputter coater (Emitech K550). Transmission Electron Microscopy (TEM) was carried out using a JEOL JEM 2010 TEM. The ultra-thin samples were prepared by an ultra microtome.

DSC was performed using a Mettler Toledo DSC 822^{e}. Samples of about 5mg were heated from 30 to 250 ^{o}C at a heating rate of 10 ^{o}C/min in dry nitrogen and held for

10 min to erase any thermal history, and then cooled to -50 ºC using the same scan rate of 10 ºC/min.

X-ray diffraction (XRD) data were recorded for thin film samples using a Siemens D5000 Diffractometer, where the X-ray beam was Cu-K radiation ($k\alpha_1$ = 1.5406 Å) and the radiation operated at 40 kV. Data were collected over the 2θ range 5-30 º with a step size of 0.01 º and a step time of 1 sec.

Tensile tests were performed using an Instron 5584 tensile testing machine, equipped with a 1 kN load cell, standard grips and Merlin data acquisition software. The tests were conducted according to the ASTM D-638 standard. Crosshead displacements of 5 $mm.min^{-1}$ and 10 $mm.min^{-1}$ were used for measuring Young's modulus and tensile stress, respectively. The Modulus of each specimen was calculated as the gradient of the stress vs. strain curve between 0.05 % and 0.2 % strain. The values presented for all the properties are the average of 5 repetitions of each test.

3.3 Results and Discussion

Fig. 3.2 shows the morphology of the nanocomposites produced by $scCO_2$. A porous foamed structure is formed. The increase of the clay content results in the smaller size of pores. This porous structure will be removed during the hot pressing process performed afterwards, thus dense samples are produced.

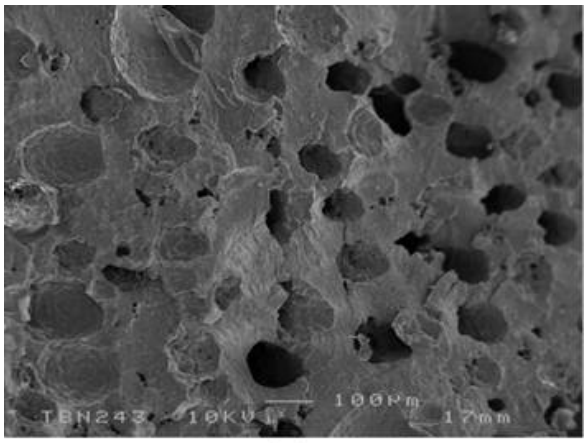

(a)

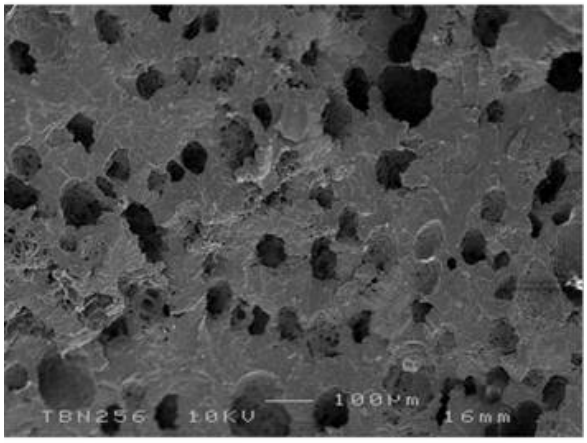

(b)

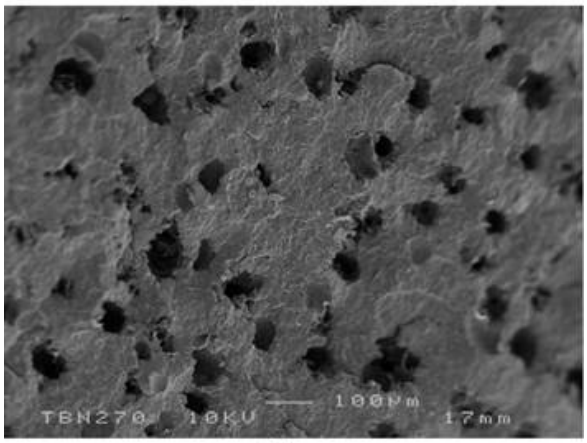

(c)

Fig. 3.2 *SEM images of $scCO_2$ processed nanocomposites before hot press (a) $scCO_2$ PP+1 wt.% sepiolite (b) $scCO_2$ PP+2.5 wt.% sepiolite and(c) $scCO_2$ PP+5 wt.% sepiolite showing that the porous structures were formed*

The SEM images of the samples after hot pressing are presented in Fig. 3.3. The bright spots represent sepiolite in the images. Under higher magnification, it is clear to see that the sepiolite fibres sticking out the fracture surface of polymer (Fig. 3.3b).

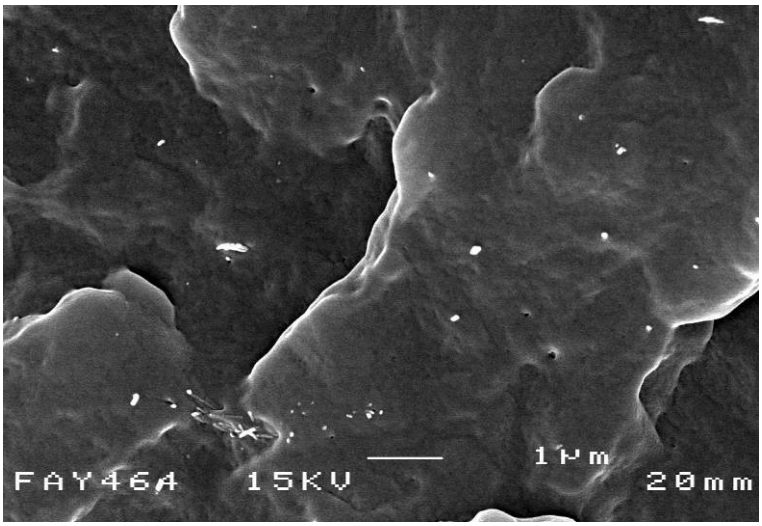

(a)

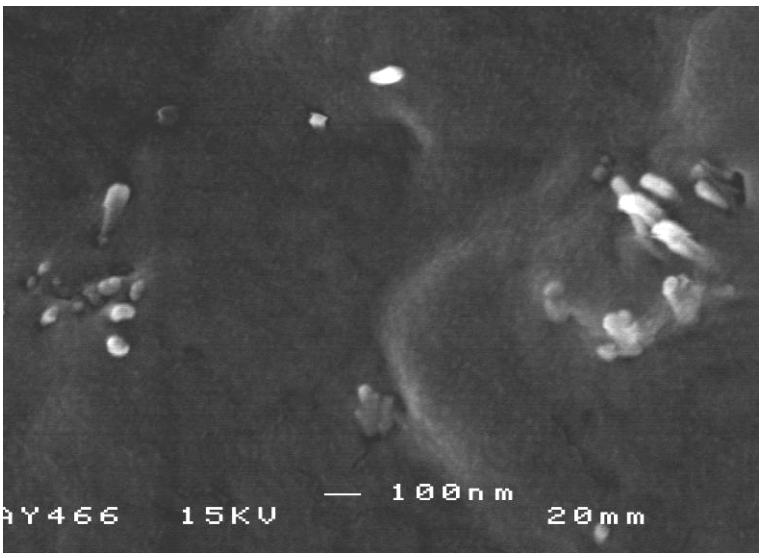

(b)

Fig. 3.3 *SEM images of freeze-fractured samples for $scCO_2$ PP+2.5 wt.% PP-g-MA+2.5 wt.% sepiolite (a) low magnification (b) high magnification*

The comparison between images of the $scCO_2$ processed nanocomposites and traditional melt compounded ones, which are from the work by Bilotti *et al.*[1], is shown in Fig. 3.4. The large aggregates of sepiolite fibres, as observed in melt compounded PP nanocomposite (see encircled regions in Fig. 3.4(a) and (b)), are not observed in the $scCO_2$ PP nanocomposites (Fig. 3.4(c) and (d)). This confirms the better dispersion of clay with $scCO_2$ assisted mixing suggested by other authors[3]. Especially, for the $scCO_2$ nanocomposites prepared without PP-g-MA (Fig. 3.4(c)), the dispersion of sepiolite in the PP matrix has improved significantly and is as good as the one using PP-g-MA as a compatibilizer in the $scCO_2$ assisted mixing (Fig. 3.4(d)). This indicates that PP-g-MA is not necessary to achieve a good dispersion in $scCO_2$ assisted processing. This is of particular relevance because the role of compatibilizers, such as PP-g-MA, is generally regarded as essential for the creation of well dispersed nanoclay composites using traditional melt compounding methods[1].

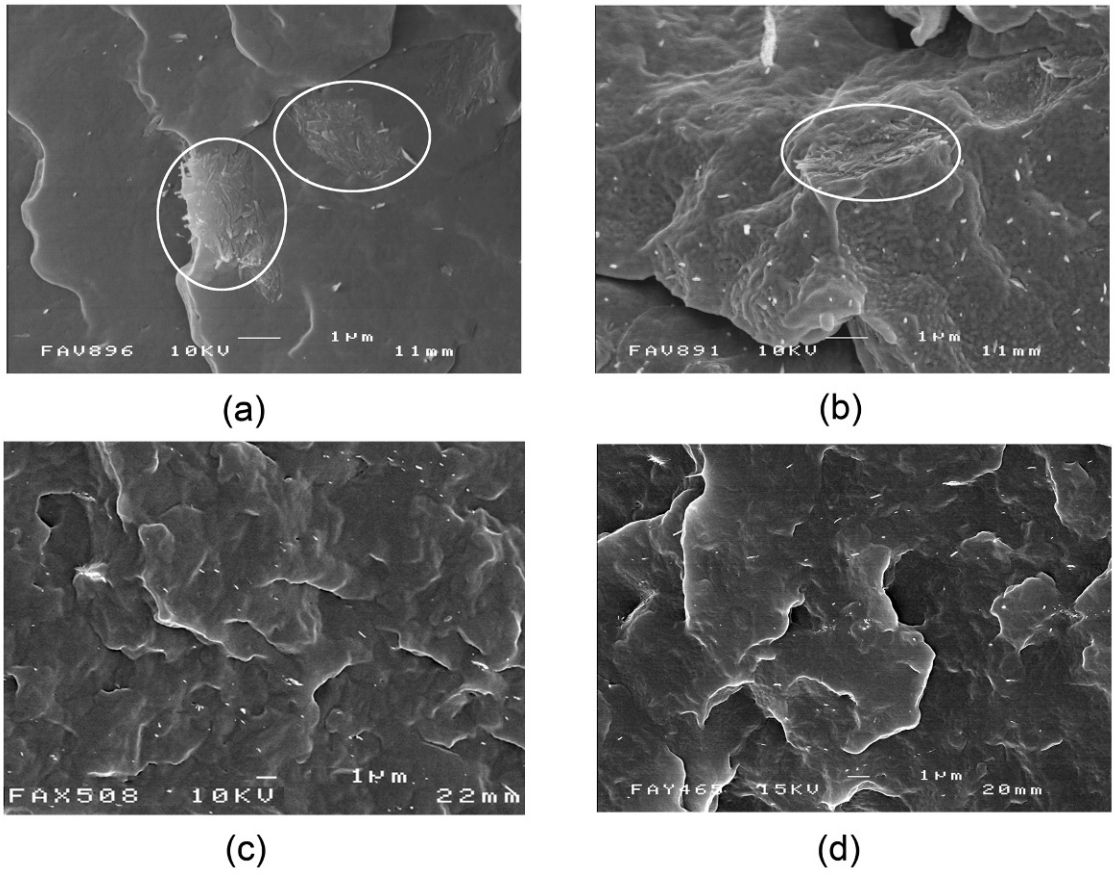

Fig. 3.4 *SEM images of freeze-fractured samples for (a) melt compounded PP+2.5 wt.% sepiolite[1] (b) melt compounded PP+2.5 wt.% PP-g-MA+2.5 wt.% sepiolite[1] (c) $scCO_2$ PP+2.5 wt.% sepiolite and (d) $scCO_2$ PP+2.5 wt.% PP-g-MA+2.5 wt.% sepiolite*

The TEM image (Fig. 3.5) of a $scCO_2$ PP nanocomposite is compared with the original sepiolite suspended in a water solution and also a melt compounded PP nanocomposite. A higher magnification was used for identifying the sepiolite in the nanocomposites because the sepiolite was widely dispersed inside the polymer and broken into much shorter length so that the lower magnification failed to present them clearly. Especially for melt compounded PP/sepiolite nanocomposite, on average of 10 pictures taken under TEM, the clearest picture we could get is Fig.

3.5(b)[1]. They reported significant reduction in sepiolite length due to the compounding process, while the fibre bundles and aggregates could not be effectively broken down (Fig. 3.5(b)). In this work, sepiolite needles appear to be separated from each other in $scCO_2$ PP nanocomposites (Fig. 3.5(c)). Although some reduction in fibre length seems to have occurred, a length of about 400-500 nm was still preserved after the $scCO_2$ assisted mixing process, which is much longer than that of the sepiolite fibres in the melt-compounded samples (see Fig. 3.5(b)). This indicates the greater efficiency of $scCO_2$ to prevent breakage and aggregation of sepiolite, which should lead to a higher reinforcing efficiency of the sepiolite.

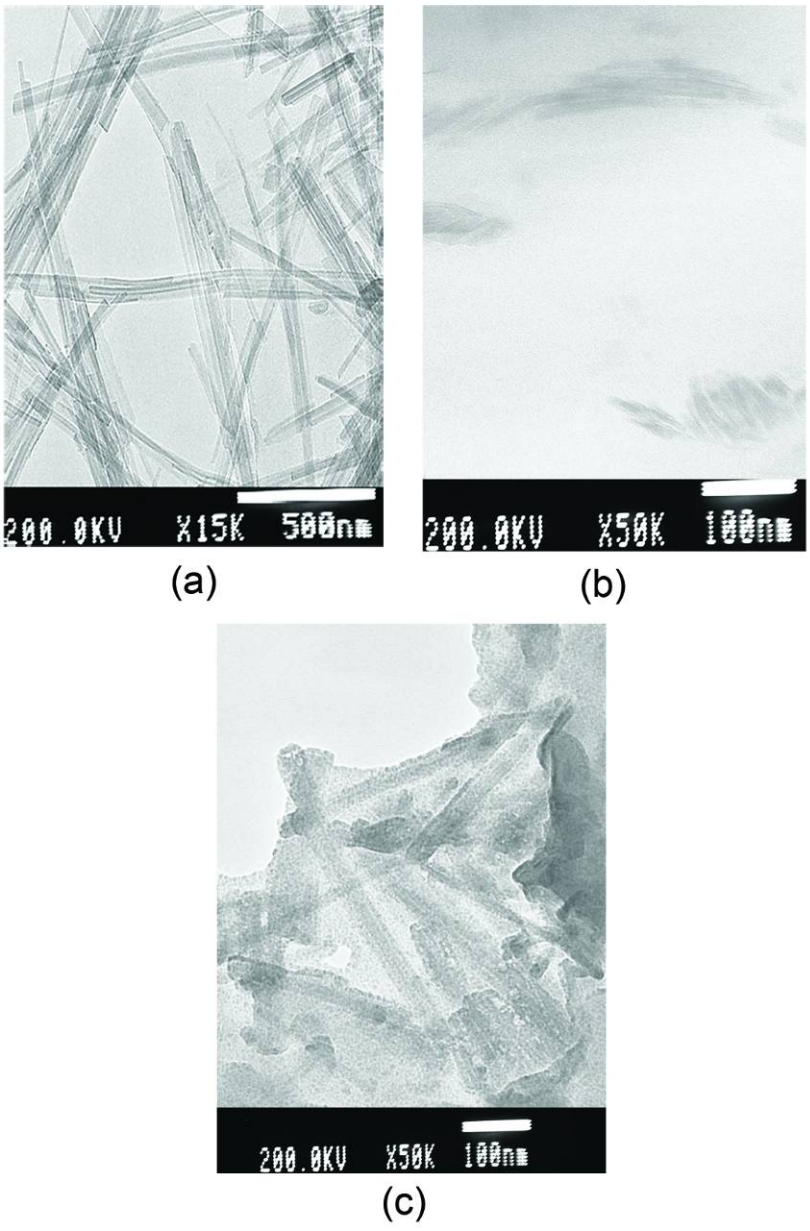

Fig. 3.5 *TEM images of (a) original sepiolite in aqueous solution[1] (b) melt compounded PP/sepiolite nanocomposite[1] and (c) $scCO_2$ PP/sepiolite nanocomposite showing less fibre length reduction for $scCO_2$ processed sample*

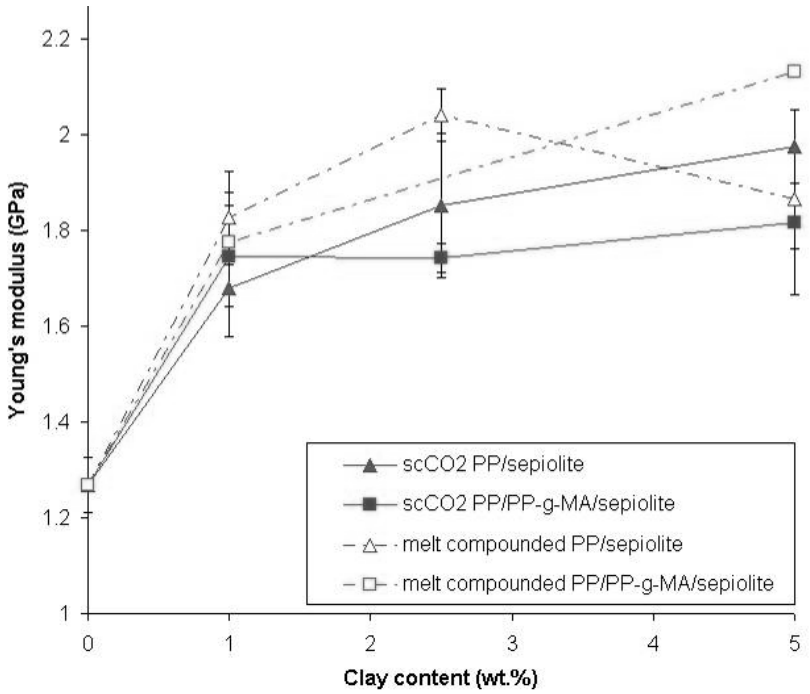

Fig. 3.6 *Young's modulus of PP nanocomposites prepared using different methods and clay contents*

The values of Young's modulus of $scCO_2$ PP nanocomposites with different clay content are presented in Fig. 3.6. For comparison, the results for melt compounded PP nanocomposites are also included[1]. The Young's modulus of melt compounded PP nanocomposites (no compatibilizer) shows a reduction with the increase of the clay content. This corresponds to the aggregation of clay at higher loadings with the absence of the compatibilizer (Fig. 3.4a and Fig. 3.5b), hence the modulus is reduced. This is in contrast to the analogous material with a compatibilizer, which shows a 68 % increase in modulus from 1 to 5 wt.% clay content. If one compares the two modulus plots for $scCO_2$ PP nanocomposites with and without a compatibilizer (Fig. 3.6), it can be seen that the modulus value for the plot with a compatibilizer remains roughly constant across the differing clay contents. In contrast, the plot without compatibilizer shows a steady increase in modulus (by up to 56 % for 5 wt.% sepiolite), suggesting that the compatibilizer has a negative effect on the modulus

(and indeed the yield stress; see discussion later). The increase of clay content compromises the ductile nature of the PP matrix. Yielding followed by drawing still occurred in the 1 wt.% sepiolite samples; while 2.5 wt.% and 5 wt.% sepiolite samples show brittle fractures at low strains (Fig. 3.7). The effects of $scCO_2$ processing on the mechanical properties of pure PP have been investigated in the past, and the research showed that little difference was made in both yield strength and modulus of PP[4]. The potential factors which would affect the mechanical properties of PP, such as changing in the degree of crystallinity, would be removed during the hot pressing procedure in the preparation of testing samples. The only remaining effect of $scCO_2$ processing is the extraction of small agents, such as monomers, or oligomers from PP, which would lead to a decrease of the weight[5].

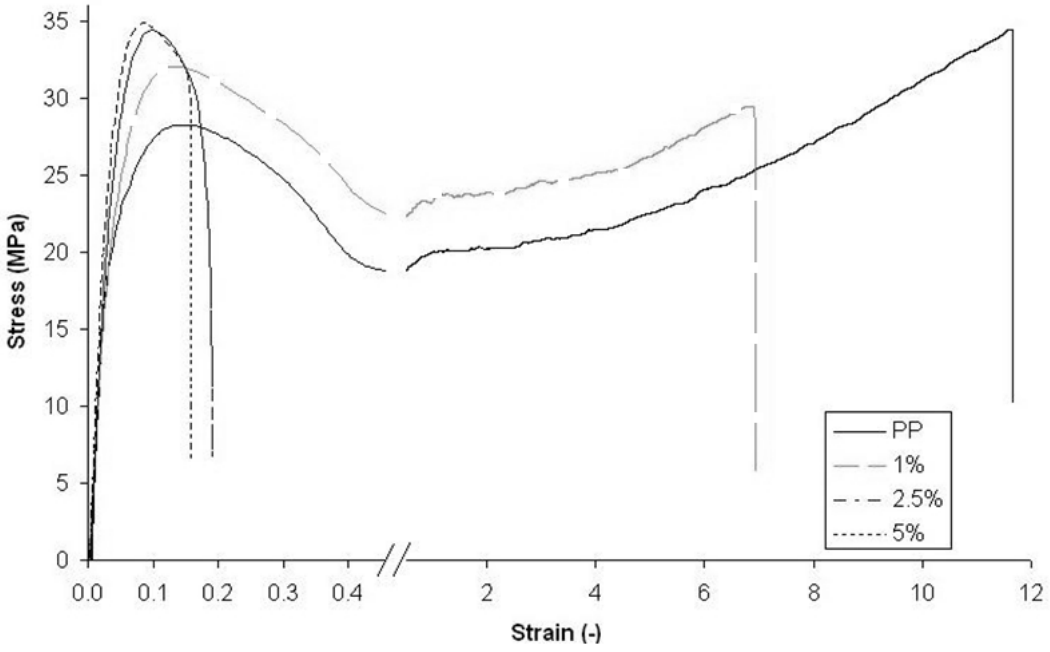

Fig. 3.7 *Stress-strain curves of $scCO_2$ PP/sepiolite nanocomposites with different clay contents*

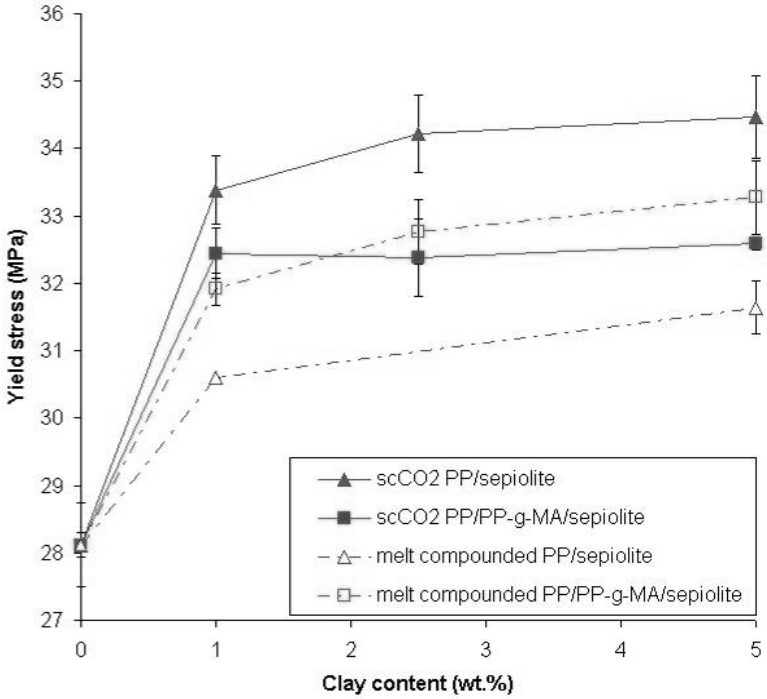

Fig. 3.8 *Yield stress of PP nanocomposites prepared using different methods and clay contents*

Fig. 3.8 shows an increase in yield stress for $scCO_2$ PP nanocomposites of up to 23 % for 5 wt.% sepiolite samples compared with pure PP and a significant improvement over those prepared using melt compounding was also observed, which confirms the good dispersion of the sepiolite in the PP matrix (Fig. 3.4c and d) and also the benefit of preserving the fibre length when using $scCO_2$ assisted mixing (Fig. 3.5c). Moreover, $scCO_2$ PP nanocomposites without the PP-g-MA compatibilizer, possess an even higher yield stress than those with the compatibilizer. The reasons for this are not immediately clear. However, because the compatibilizer may reduce the yield stress of $scCO_2$ PP nanocomposites, it may have resulted in $scCO_2$ forming interactions with the compatibilizer molecules, since $scCO_2$ has been identified as a good solvent and carrier agent for maleic[6]. These interactions may disrupt the normal compatibilizer behaviour. In contrast, for the melt compounded samples, the

compatibilizer is more likely to be able to act at the polymer/clay interface. Furthermore, the interactions between $scCO_2$ and the compatibilizer may also result in the compatibilizer being located unevenly in the PP phase by being trapped more around the micro-cells when CO_2 is vented, which may induce the uneven dispersion of the clay. Hence, the addition of the compatibilizer in the $scCO_2$ PP nanocomposites may not be acting effectively at the polymer/clay interface.

Fig. 3.9 presents the DSC cooling curves of pure PP and $scCO_2$ PP nanocomposites. The crystallization temperature (T_c) of the pure PP sample is 111 °C. However, for PP nanocomposites, it is observed that the crystallization temperature shifts to higher temperatures, which indicates that the sepiolite fibres act as nucleating agents for PP crystallization. This increase in crystallization temperature is dependent on the clay content, which suggests that higher loadings of sepiolite can provide higher nucleating efficiency. These results is corresponding well to the findings in the literature that both degree of crystallinity and crystallization rate are increased due to the nucleation effect of sepiolite[7].

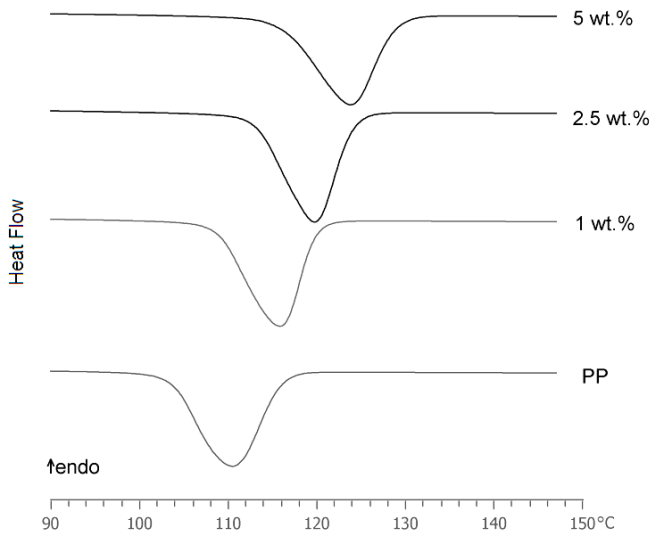

Fig. 3.9 *The DSC crystallisation peaks for typical $scCO_2$ PP/sepiolite nanocomposites*

The degree of crystallinity (X_c) is calculated from the melting heat (ΔH_m) obtained from DSC measurement according to the following equation[8]:

$$X_c = \frac{\Delta H_m}{\Delta H_0} \times f_c \qquad 3\text{-}1$$

where ΔH_0 = 209 J/g is the melting enthalpy of 100 % crystalline PP and f_c is a factor that simply takes into account the excluded mass of inorganic that does not melt. For instance, f_c is 0.99 for a 1 wt.% nanocomposite DSC data of the T_c and the X_c are presented in Table 3.1. The addition of clay has little influence on the X_c. All the samples with different clay content show very similar degree of crystallinity, which suggests that the increase in modulus and yield stress of PP nanocomposites were contributed mainly from the reinforcement of sepiolite fibres.

Table 3.1 *DSC measurement results*

Sample	Sepiolite [wt.%]	PP-g-MA [wt.%]	T_c [°C]	X_c [%]	ΔH_m J/g
PP	0	0	110.8	31.5	65.8
PP/sepiolite	1	0	115.6	31.0	65.4
	2.5	0	119.6	31.2	66.9
	5	0	123.8	29.1	64.0
PP/PP-g-MA/sepiolite	1	1	117.0	30.5	64.4
	2.5	2.5	120.5	29.4	63.0
	5	5	122.5	28.8	63.4

iPP can crystallize in three crystalline modification: monoclinic (α), hexagonal (β), orthorhombic (γ)[9]. These phases can be examined by XRD. The XRD patterns for all

the PP nanocomposites show peaks corresponding to PP α-phase at 2θ = 14, 17, 18.5, 21.5, 21.9 and 25.4 ° for six major reflections: (110), (040), (130), (111), (041) and (060) plane, respectively (Fig. 3.10). No other reflections for other forms of PP crystallites were detected. This indicates that the addition of sepiolite does not affect the crystal modification of the final PP molecules. However, it should be noted that the relative intensity of the peaks for (040) increased considerably with the presence of sepiolite, taking the (110) peak as reference. Data of relative intensities are listed in Table 3.2. This phenomenon has also been noticed by other researchers[1,10]. A possible reason for this increase is that the addition of sepiolite promotes a preferential orientation of PP crystals growing with (040) planes parallel to the sepiolite surface and the b-axes perpendicular to it[10,11].

Table 3.2 *Ratio of intensity between diffraction peaks of (040)α and (110)α in XRD patterns*

Sepiolite [wt.%]	0	1	2.5	5
PP/sepiolite	0.80	2.41	2.40	2.24
PP/PP-g-MA/sepiolite	0.80	1.40	3.00	2.71

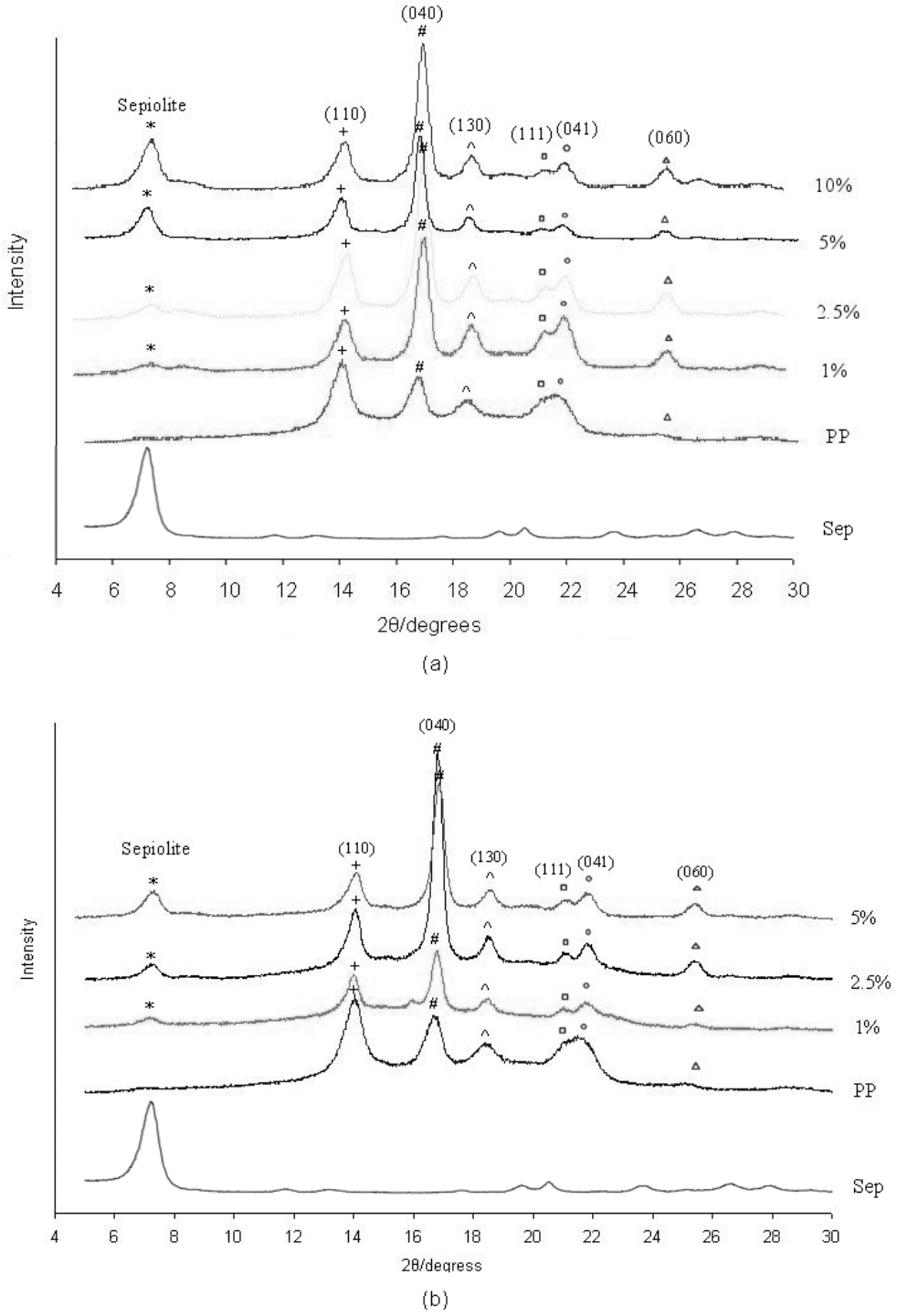

Fig. 3.10 *XRD patterns of (a) PP/sepiolite and (b) PP/PP-g-MA/sepiolite nanocomposites*

3.4 Conclusions

PP/sepiolite nanocomposites with and without PP-g-MA as a compatibilizer were prepared using $scCO_2$ assisted mixing and compared with those processed by a traditional melt compounding method. A relatively homogeneous dispersion of sepiolite was obtained throughout the PP matrix for the nanocomposites processed in $scCO_2$ even without the aid of PP-g-MA as the compatibilizer. Well separated sepiolite fibres were observed from TEM images and the fibre length in the $scCO_2$ assisted mixing is retained better than in melt compounding. Consequently, mechanical properties of PP nanocomposites prepared in $scCO_2$ were significantly improved, especially without the need of PP-g-MA. All these facts indicate that $scCO_2$ can give significant benefits for preparing PP/sepiolite nanocomposites. Especially, the fact that PP-g-MA, which is normally used as a compatibilizer in melt compounding, is not needed for the processing of high quality PP nanocomposites using $scCO_2$ is highly relevant from a technological and economical point of view. Similarly to other nanocomposite studies also in this study it was found that nanoclays can act as nucleating agents and increase the crystallization temperature of the PP matrix in nanocomposites. Moreover, the nanocomposites only contained PP α-phase crystallites with the clay inducing a preferred orientation for the PP.

3.5 References

1. Bilotti E, Fischer HR and Peijs T. Polymer Nanocomposites Based on Needle-Like Sepiolite Clays-Effect of Compatibilizers on Morphology, Crystallinity and Mechanical Properties. J. App. Polym. Sci. 2008, 2, 1116
2. Pukanszky B, Mudra I and Staniek P. Relation of Crystalline Structure and Mechanical Properties of Nucleated Polypropylene. J. Vinyl. Addit. Technol. 1997, 1, 53

3. Garcia-Leiner M and Lesser AJ. Polymer Nanocomposites Prepared by Supercritical Carbon Dioxide-Assisted Polymer Processing. Polym. Prepr. 2004, 45, 520
4. Shieh YT, Su Jh, Manivannan G, Lee PHC, Sawan HP and Spall WD. Interaction of Supercritical Carbon Dioxide with Polymers. I: Crystalline Polymers. J. Appl. Polym. Sci. 1996, 59, 695
5. Fleming GK and Koros WJ. Dilation of Polymers by Sorption of Carbon Dioxide at Elevated. Pressures. 1. Silicone Rubber and Unconditioned Polycarbonate. Macromol. 1986, 19, 2285
6. Galia A, Gregorio R, Spadaro G, Scialdone O and Filardo G. Grafting of Maleic Anhydride onto Isotactic Polypropylene in the Presence of Supercritical Carbon Dioxide as a Solvent and Swelling Fluid. Macromol. 2004, 12, 4580
7. Acosta JL, Ojeda MC, Morales E, and Linares A. Morphological, Structural, and Interfacial Changes Produced in Composites on the Basis of Polypropylene and Surface-Treated Sepiolite with Organic-Acids .3. Isothermal and Nonisothermal Crystallization. J. Appl. Polym. Sci. 1986, 32, 4119
8. Jang GS, Cho WJ and Ha CS. Crystallization Behavior of Polypropylene with or without Sodium Benzoate as a Nucleating Agent. J. Polym. Sci., Part B: Polym. Phys. 2001, 39, 1001
9. Bruckner S, Meille SV, Petraccone V and Pirozzi B. Polymorphism in Isotactic Polypropylene. Prog. Polym. Sci. 1991, 16, 361
10. Ferrage E, Martin F, Boudet A, Petit S, Fourty G, Jouffret F, Micoud P, De Parseval P, Salvi S, Bourgerette C, Ferret J, Saint-Gerard Y, Buratto S and Fortune JP. Talc as Nucleating Agent of Polypropylene: Morphology Induced by Lamellar Particles Addition and Interface Mineral-matrix Modelization. J. Mater. Sci. 2002, 37, 1561
11. Wang LH, and Sheng J. Preparation and Properties of Polypropylene/org-attapulgite Nanocomposites. Polym. 2005, 46, 6243

Chapter 4

Polymer/CNT Nanocomposites using $ScCO_2$ Assisted Mixing

4.1 Introduction

In this chapter, the use of $scCO_2$ to assist the preparation of PP/CNT nanocomposites and the potential benefits thereof are investigated. Two types of CNTs were used: pure MWNTs and 31.6 % MWNTs pre-dispersed in a HDPE coating (cMWNTs). The resulting morphology and thermal properties of the nanocomposites were studied using SEM, TEM, DSC and TGA. The dispersion, physical and mechanical properties of nanocomposites obtained using $scCO_2$ processing were compared with those of traditional melt compounded samples. Micromechanical modelling was used to analyse the effective properties of the CNTs in the nanocomposites. The current study also addresses the effects of PP matrix modification by the CNTs and their

effects on the mechanical properties of the nanocomposites.

4.2 Experimental

4.2.1 Materials and Equipments

The PP used was Moplen® HP500H from Basell (Melt Flow Index = 1.8 g/10 min). The pristine MWNT used was Nanocyl®-7000 from Nanocyl S.A. (Belgium), which is a thin MWNT produced via the catalytic chemical vapour deposition process, achieving a purity of 90 % carbon. Nanocyl®-9000 is an HDPE-coated MWNT (cMWNTs) which contains 31.6 % of nanotubes pre-dispersed in a polymer carrier using a proprietary technology[1,2]. All materials were used as received. A liquid withdrawal CO_2 cylinder at 725 psi pressure was supplied by BOC Gases. A custom-built stirred high-pressure autoclave with a paddle type stirrer was used to prepare the nanocomposites. The system diagram is presented in Fig. 3.1. A Rondol laboratory bench-top hot-press was used to produce the dumbbell-shaped specimens.

4.2.2 Processing of PP/MWNT Nanocomposites

MWNTs (or cMWNTs) were directly added to the PP matrix in an autoclave to obtain a CNT concentration of 0.1 wt.%, 0.25 wt.%, 0.5 wt.% and 1.0 wt.%. CO_2 was pumped into the autoclave via an Isco model 260D syringe pump after being chilled to -6 ^{o}C. The autoclave was filled with liquid CO_2 and held at 2175 psi and 200 °C under stirring, using a pitched blade turbine impeller for 30 min. After mixing, the autoclave was cooled in water to room temperature, and then the CO_2 was vented. In comparison, a masterbatch of 3.0 wt.% CNT content was prepared using $scCO_2$ assisted mixing under 2175 psi and 200 °C for 10 min before being diluted into

lower concentrations of 0.1 wt.%, 0.25 wt.%, 0.5 wt.% and 1.0 wt.% CNT using the same conditions as described above. The bulk materials obtained from the autoclave were frozen in liquid nitrogen and then broken into pieces, which were subsequently used for hot-pressing into dumbbell-shaped specimens according to ASTM D-638 at 200 ^{o}C under 5800 psi for 5 min. The samples were cooled down to room temperature using the water cooling system of the hot-press. The nanocomposites along with their compositions, including those from Deng *et al.* work[3], are listed in Table 4.1 for comparison.

Table 4.1 *The composition of PP/CNTs nanocomposites*

Sample	CNT type	Processing method
$scCO_2$PP/MWNT	Nanocyl®-7000	$scCO_2$
$scCO_2$.m PP/MWNT	Nanocyl®-7000	$scCO_2$; masterbatch
$scCO_2$PP/cMWNT	Nanocyl®-9000	$scCO_2$
$scCO_2$.mPP/cMWNT	Nanocyl®-9000	$scCO_2$,; masterbatch
melt.mPP/MWNT[3]	Nanocyl®-7000	melt compounded; masterbatch
melt.mPP/cMWNT[3]	Nanocyl®-9000	melt compounded; masterbatch

4.2.3 Characterization

SEM was used to investigate the morphological characteristics using a JEOL 6300 (accelerating voltage 10 kV) in the normal secondary electron imaging mode. Prior to the examination, samples were freeze-fractured in liquid nitrogen and sputter coated with a thin layer of gold. Transmission electron microscopy (TEM) was carried out using a JEOL JEM 2010. MWNTs were dispersed in ethanol using

ultrasonication for 5 min and then drops of suspension were deposited onto a copper grid for TEM observation.

DSC was performed using a Mettler Toledo DSC822e. Samples of about 5 mg were heated from -50 ºC to 200 ºC at a scan rate of 10 ºC/min and held for 10 min to erase any thermal history, and then cooled to -50 ºC using the same scan rate of 10 ºC/min. Thermogravimetric analysis (TGA) was carried out under nitrogen atmosphere in the temperature range of 20-1000 ºC by using a TA TGA Q500. The heating rate used was 20 ºC/min.

XRD data were recorded with a Siemens Diffractometer D5000, where the X-ray beam was Ni-filtered CuKα (λ = 1.5405 Å) and the radiation was operated at a rate of 40 kV with a filament current of 40 mA. Corresponding data were collected from 5 to 30 ° with a step size of 0.01 º and a step time of 1 sec.

Tensile tests were performed using an Instron 5566 machine, equipped with a 1 kN load cell, standard grips and Merlin data acquisition software. The tests were conducted according to the ASTM D-638 standard. The Young's modulus of each specimen was calculated and the gradient of the stress vs. strain curve was measured between 0.05 % and 0.2 % strain. The values presented for all the properties are the average of 5 repetitions of each test.

4.3 Results and Discussion

Fig. 4.1 shows the SEM images of the nanocomposites produced by $scCO_2$. Nanotubes are observed as bright spots and with the increase of the nanotube content, more bright spots can be seen from the images.

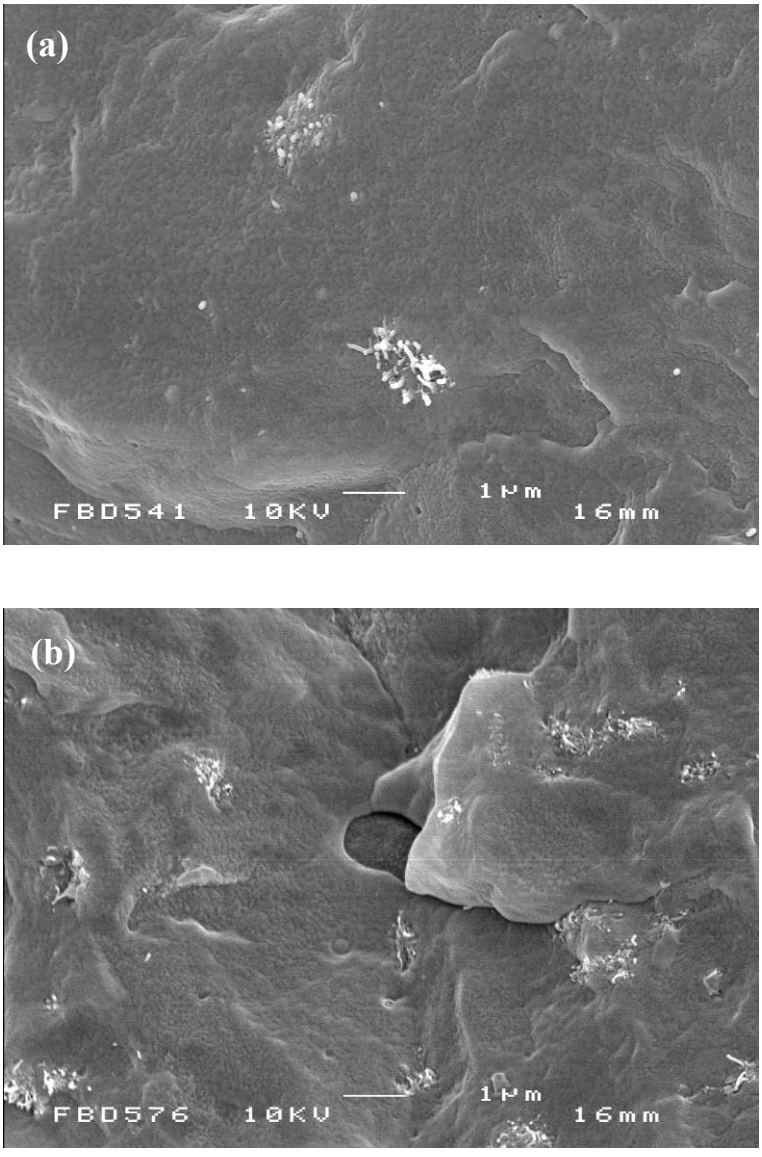

Fig. 4.1 *SEM images of freeze-fractured samples of PP nanocomposites with (a) 0.1 wt.% $scCO_2$.mPP/cMWNT (b) 0.5 wt.% $scCO_2$.mPP/cMWNT*

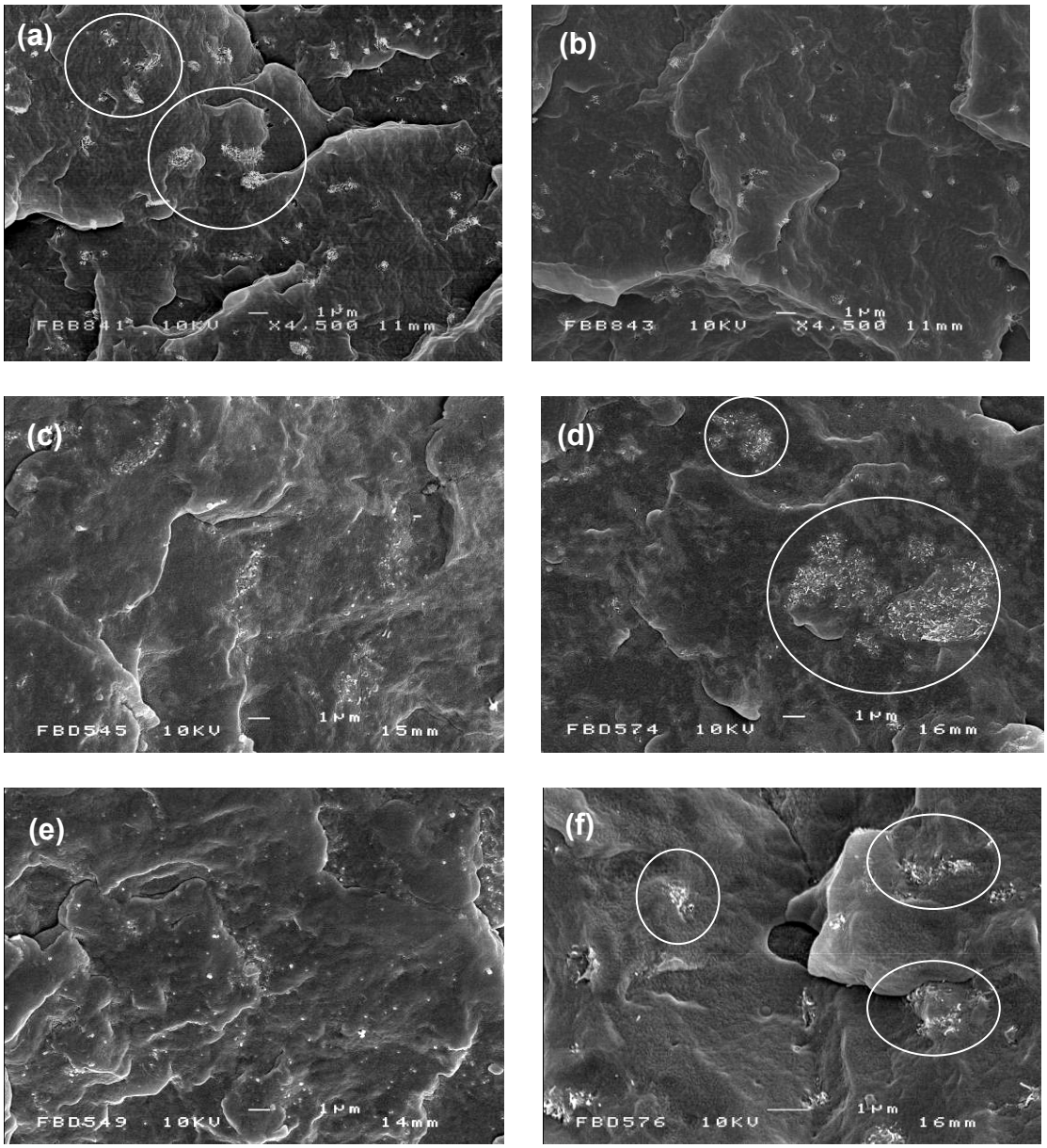

Fig. 4.2 *SEM images of freeze-fractured samples of PP nanocomposites with 0.5 wt.% MWNT loading (a) melt.mPP/MWNT[3] (b) melt.mPP/cMWNT[3] (c) $scCO_2$PP/MWNT (d) $scCO_2$ PP/cMWNT (e) $scCO_2$.mPP/MWNT and (f) $scCO_2$.mPP/cMWNT*

Fig. 4.2 compares the images of the $scCO_2$ processed nanocomposites and traditional melt compounded ones. In the case of conventional melt compounding, better

dispersions of CNTs were observed for the HDPE coated MWNTs samples, owing to the de-aggregated state of the cMWNTs[1]. (Fig. 4.2a and 2b) However, in the case of $scCO_2$ assisted mixing, large aggregates of cMWNTs were observed (Fig. 4.2d) and even when a masterbatch method was applied the cMWNTs were still not well dispersed (Fig. 4.2f). Interestingly, pristine MWNTs without HDPE coating provided a better and more homogeneous dispersion in the PP matrix (Fig. 4.2c). Similar improvements in dispersion, for $scCO_2$ assisted mixing without the use of compatibilizers were also reported for nanoclays in PP matrices. A better dispersion of MWNTs was observed using the masterbatch method (Fig. 4.2e).

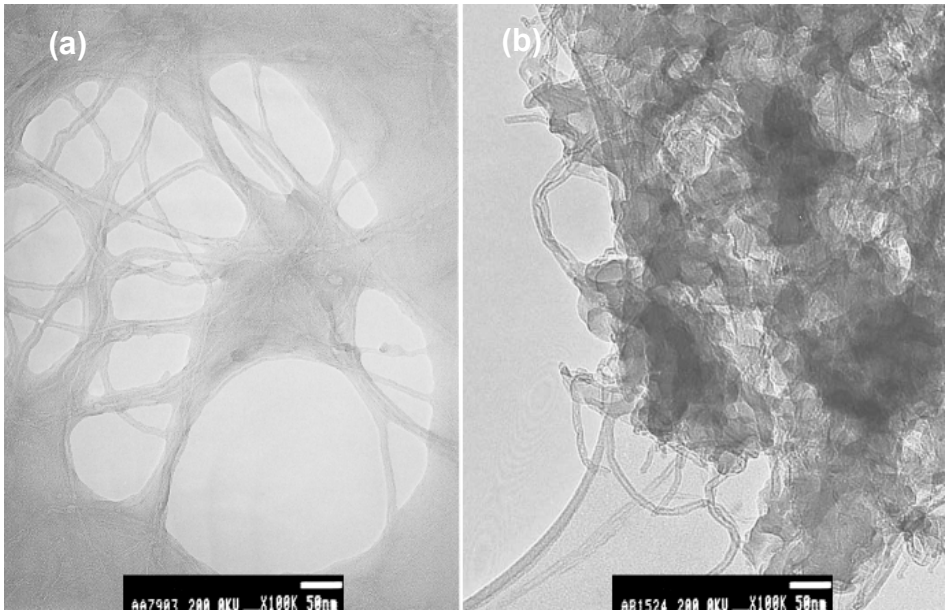

Fig. 4.3 *TEM images of (a) pristine MWNTs and (b) HDPE coated MWNTs*

The TEM images of MWNTs and cMWNTs, which are presented in Fig. 4.3 may help to explain why the dispersion of cMWNTs in the PP matrix was unsatisfactory in $scCO_2$ assisted mixing. Pristine MWNTs could be dispersed into individual tubes on the grid with no large aggregates remaining (Fig. 4.3a). However, cMWNTs (Fig. 4.3b) showed quite a different structure. The polymer coated MWNTs form large

agglomerates and although the HDPE coating helps to separate the individual nanotubes, the break up of these agglomerates still requires high shear forces. Therefore, cMWNTs can be dispersed well in conventional melt compounding processes in twin-screw extruders because of the high shear forces employed. However, a pitched blade turbine impeller, used in $scCO_2$ assisted mixing, generates much lower shear forces, thus leading to poor dispersion of these agglomerates.

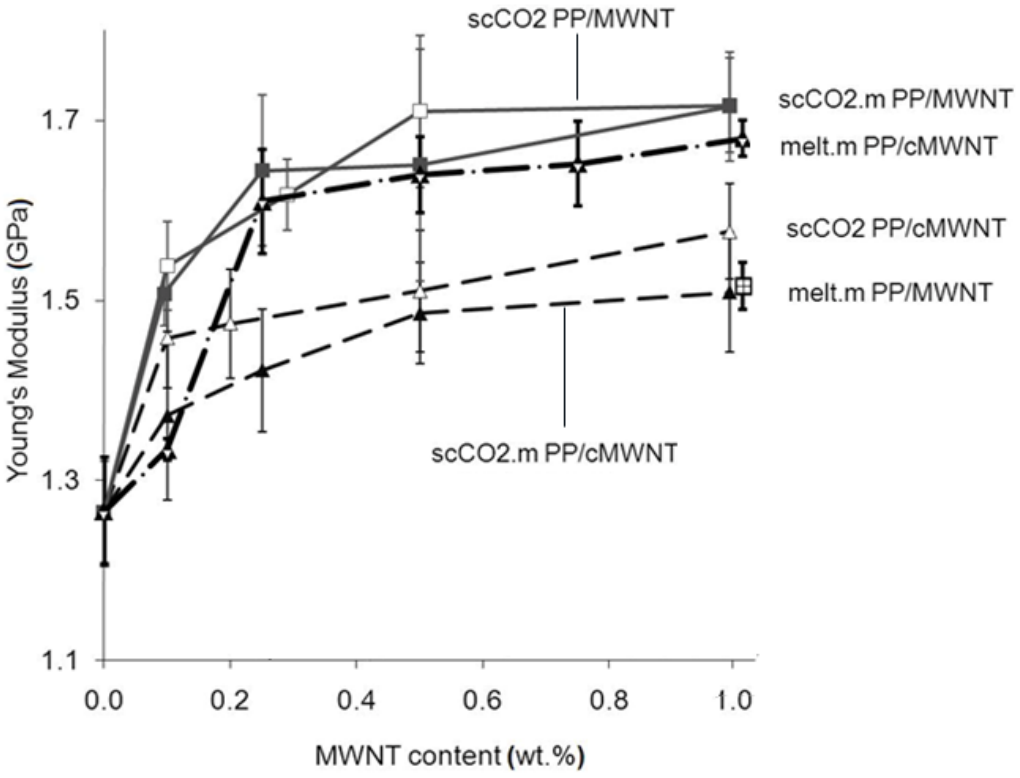

Fig. 4.4 *The Young's modulus of PP nanocomposites as a function of MWNT loading, showing that a similar modulus is achieved for $scCO_2$ processed nanocomposites with pristine MWNTs and melt-compounded nanocomposites with coated cMWNTs. Solid lines represent results of nanocomposites with pristine MWNTs, whereas dashed lines represent nanocomposites with coated cMWNTs*

The values of Young's modulus of the nanocomposites with different MWNT

loadings are presented in Fig. 4.4. As a result of the de-aggregation of the MWNT bundles by the HDPE coating, the melt-compounded and masterbatch based PP/cMWNT composites show a continuous modulus increase up to 1.7 GPa from zero to 1.0 wt.% CNT loading[3]. Based on uncoated MWNTs, the same melt-compounded and masterbatch systems only displayed a Young's modulus value of 1.5 GPa for 1.0 wt.% CNT loading, due to the poor dispersion of pristine MWNTs in the PP matrix[3] (Fig. 4.2a) . Interestingly, $scCO_2$ processed nanocomposites with pristine MWNTs showed an increase in Young's modulus, which is as good as, or even better than, that of melt.m PP/cMWNT. However, cMWNTs showed the lowest reinforcing efficiency in the case of $scCO_2$ processed nanocomposites. It is in the agreement with results from the SEM images that MWNT can achieve better dispersion than cMWNT in the $scCO_2$ processing (Fig. 4.2c and e comparing with Fig. 4.2d and f). Furthermore, the use of masterbatch in the $scCO_2$ assisted mixing method did not show improvements in terms of Young's modulus, as shown for both $scCO_2$.mPP/MWNT and $scCO_2$.mPP/cMWNT composites. The reason may be the long processing times needed at these high temperature conditions causing a degradation of the PP matrix.

Similarly, increases in yield stress were observed for all $scCO_2$PP/MWNT samples, with a significant 6 % increase from zero to 0.1 wt.% CNT loading followed by roughly constant values across the rest of the CNT loading range up to 1 wt.% (Fig. 4.5). The degree of reinforcement of pristine MWNTs is as good as for melt-compounded coated PP/cMWNT composites. PP/cMWNTs composites, showing poor nanofiller dispersion in the case of $scCO_2$ assisted mixing, give lower yield stresses. Although the HDPE coating indeed helps the dispersion of cMWNTs in melt compounding processes, the HDPE coating could also act as a weak interface between the matrix and the CNTs, leading to a poor stress transfer, thereby

weakening the nanocomposites. This potential effect is however not found here. $ScCO_2$ assisted mixing achieves a better dispersion of CNTs without the need for HDPE coating, therefore eliminating the potential drawbacks of HDPE coating, leading to greater thermal and mechanical reinforcing effects from the MWNTs. Also, the relatively low shear forces involved in $scCO_2$ assisted mixing cause less nanotube breakage and damage (Fig. 4.3c).

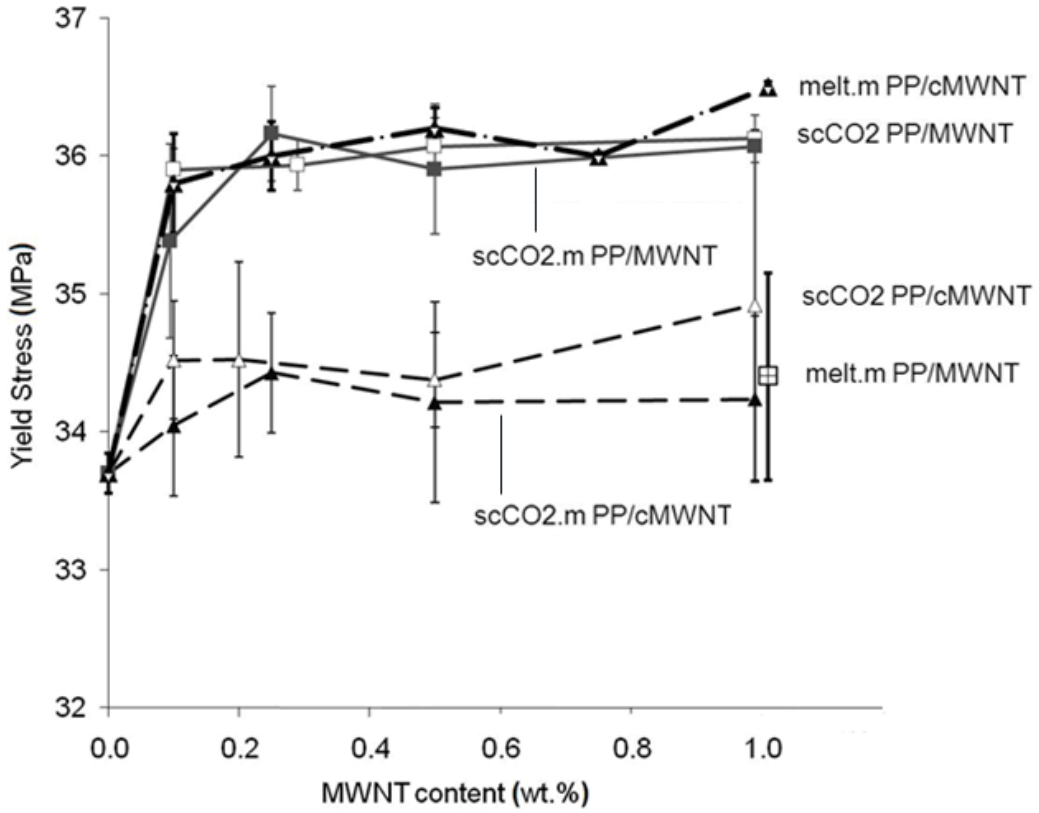

Fig. 4.5 *The Yield stress of PP nanocomposites as a function of MWNT loading, showing that a similar yield stress is achieved for $scCO_2$ processed nanocomposites with pristine MWNTs and for melt-compounded and masterbatch based nanocomposites with HDPE coated MWNTs. The solid lines represent the results of nanocomposites with pristine MWNTs, whereas the dashed lines represent those of the nanocomposites with coated cMWNT*

From Fig. 4.6, strain at break was observed to decrease significantly with the CNT loading for all sets of samples which indicates that the increase of CNT loading compromises the ductile nature of the PP matrix. Not surprisingly, the strain values of $scCO_2$PP/cMWNTs are the lowest among all due to its large aggregations of MWNTs in the nanocomposites which act as defects accelerating the final failure of the sample under stress. Furthermore, the increase in the crystallinity of PP by the addition of MWNTs, which will be discussed in the later text, has been suggested as one of factors causing the decrease of the strain at break[4].

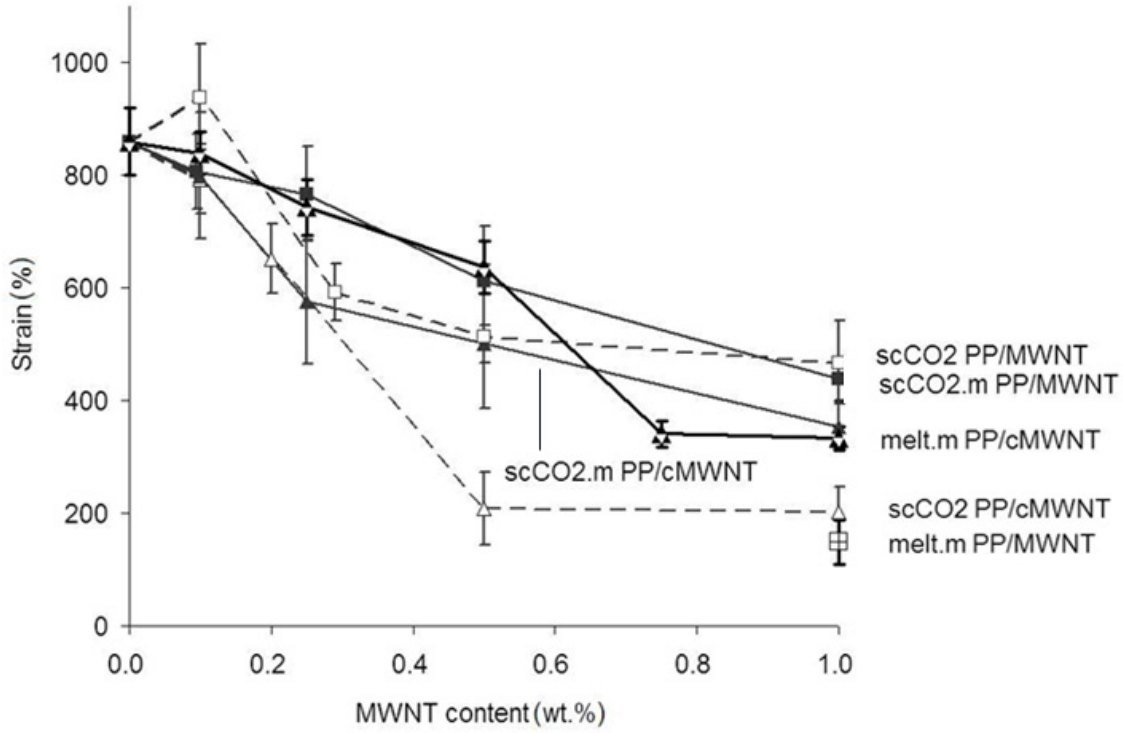

Fig. 4.6 *Strain curves of the nanocomposites prepared using different methods and MWNT loading*

To calculate the reinforcing efficiency of the CNTs in composites, as introduced in the Chapter 2, the rule of mixture is applied to quantify the effective Young's modulus of the CNTs. For composites in which discontinuous fibres are not perfectly

aligned, the Young's modulus of the composite (E_c) can be written as[5]:

$$E_c = \eta_o \eta_L V_f E_f + (1 - V_f) E_m \qquad 4\text{-}1$$

where η_L is the length efficiency factor, η_o is the orientation factor, E_m and E_f are the Young's modulus of the matrix and the fibre respectively, and V_f is the volume fraction of the fibre. η_L can vary between 0 and 1. η_o is equal to 1 for fully aligned fibres, 3/8 for random (in-plane) 2D orientation and 1/5 for random 3D orientation. A similar equation can be formulated for the strength, where σ_m, σ_m and σ_f are the tensile strengths of the composites, matrix and fibre, respectively.

$$\sigma_c = \eta_L \eta_o V_f \sigma_f + (1\text{-}V_f)\, \sigma_m \qquad 4\text{-}2$$

Therefore, equations 4-1 and 4-2 can be used to evaluate the effective mechanical properties of CNTs in the composites. In the calculation, the random 3D orientation value of 1/5 was chosen for η_o, η_L equals 1 for high fibre aspect ratios (1/d) > 100. The volume fractions were deduced from the weight fractions and densities of the materials.

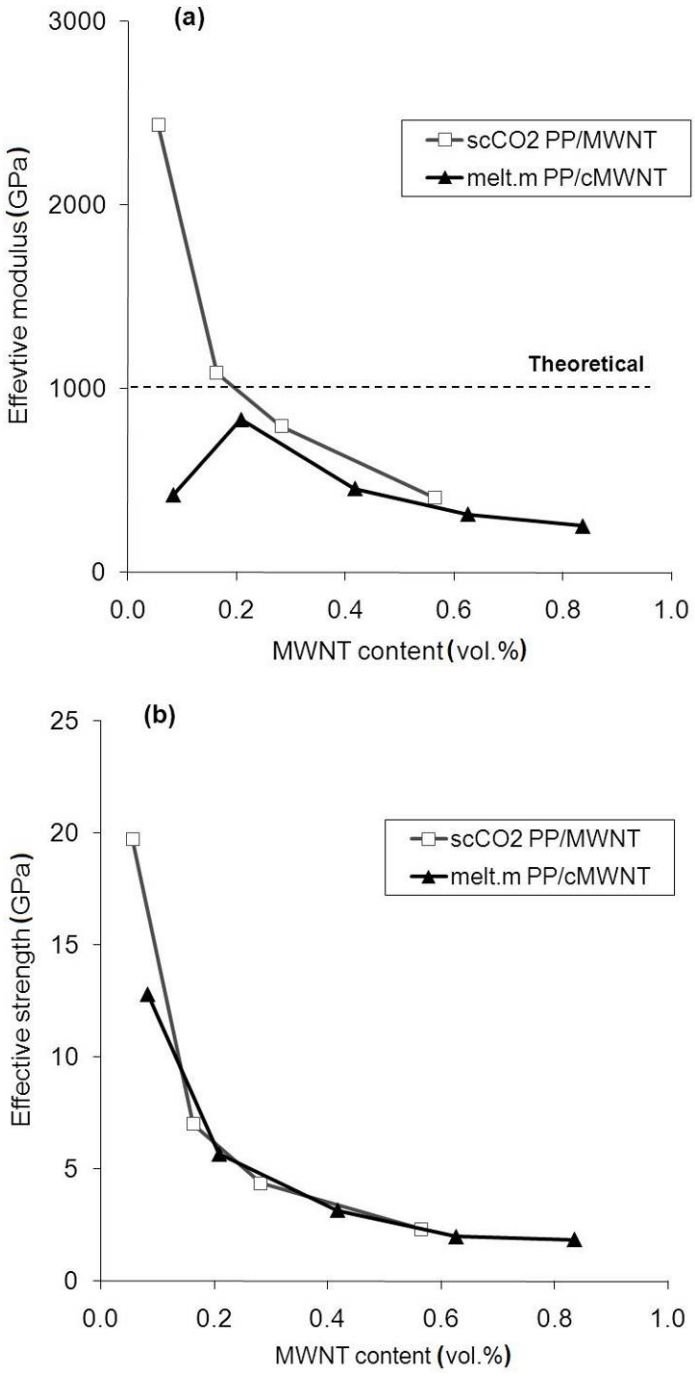

Fig. 4.7 *(a) Effective Young's modulus and (b) effective strength of MWNTs as calculated from the rule of mixtures, showing that $scCO_2$ processed nanocomposites incorporating pristine MWNTs result in nanotube efficiency similar to that of melt-compounded and masterbatch based nanocomposites based on HDPE coated MWNTs. The line represents the upper-bound for nanotube moduli*

Fig. 4.7 illustrates the back-calculated effective Young's modulus and tensile stress of CNTs. Generally, the effective properties decrease with increasing nanotube content. The effective properties of pristine MWNTs in nanocomposites processed using $scCO_2$ are as good as, or even better than, those for coated cMWNTs in nanocompsoites processed using melt-compouding and masterbatch. From direct individual CNT testing, Young's moduli of the order of 1 TPa and tensile strength values ranging from 10 to 150 GPa have been reported in the literature [6-9]. However, often back-calculated values of effective nanotube properties are significantly lower than experimentally measured values of isolated CNTs, presumably due to difficulties in achieving good dispersions of the nanotubes, a strong nanotube-matrix interface and nanotube alignment. Our calculated values of strength are reasonable among the experimental data for CNTs[8,9]. However, the effective modulus values, deduced from nanocomposites with a very low nanotube content (0.06 vol.%), are significantly higher than the theoretical modulus values for nanotubes indicated by the drawn line in Fig. 4.6a. The reason for this could be related to a modification of the matrix through the addition of CNTs, which can cause errors in the selected value of E_m. Because of the high matrix content, the calculated results are strongly affected by the variation of E_m. Small changes of E_m values of 1.25 MPa to 1.40 MPa will result in an effective modulus reduction from 2435 GPa to 1200 GPa in the calculations. In Coleman *et al*. work, the Young's modulus of the composites has been reported to increase with polymer matrix crystallinity[10]. Similar results were also shown in other studies that changes in the crystallinity and the crystalline morphology of the polymer matrix can have pronounced effects on the mechanical properties of nanocomposites[11-13].

Table 4.2 *DSC measurement results*

Sample	CNT [wt.%]	T_m [˚C]	T_c [˚C]	X_c [%]
Pure PP	0	166.0	110.3	37.9
$scCO_2$PP/MWNT	0.1	164.7	118.9	43.7
	0.25	164.2	119.0	43.1
	1.0	165.0	119.9	41.0
$scCO_2$.mPP/MWNT	0.1	164.4	119.0	42.3
	0.25	165.0	119.5	42.4
	1.0	164.4	119.9	43.4
$scCO_2$PP/cMWNT	0.1	164.9	116.2	43.3
	0.25	164.4	115.7	44.6
	1.0	127.0 / 166.0	116.5	42.9
$scCO_2$.mPP/cMWNT	0.1	164.2	115.5	43.7
	0.25	164.7	116.2	43.3
	1.0	127.3 / 165.7	116.4	43.7
melt.mPP/MWNT[3]	1.0	165.0	121.9	40.2
melt.mPP/cMWNT[3]	1.0	165.4	117.8	39.8

The melting temperature was calculated from the first heating, the crystallinity was calculated from the second heating, and the crystallization temperature was measured from the first cooling.

DSC data of the melting temperature (T_m), the crystallization temperature (T_c) and the crystallinity (X_c) of the PP nanocomposites are presented in Table 4.2. The addition of nanotubes only slightly decreases the T_m of PP at 166 ˚C by 1 ˚C. A T_m of around 165 ˚C indicates the melting of α-crystals of PP. Additionally, samples with HDPE coated MWNT content above 0.5 wt.% show an additional broad peak at around 127 ˚C corresponding to the melting of the HDPE coating (Fig. 4.8).

Interestingly, the $scCO_2$ processed sample before hot-pressing shows a broad peak in the 150-160 ˚C temperature range as well as the peak of 166 ˚C. This lower T_m around 155 ˚C, suggests the melting of polypropylene β-phase crystals[12,14]. Our XRD results also confirm the presence of a γ-phase of PP which is discussed in the text below. All samples after hot-pressing only show the T_m, at 166 ˚C, indicating no change to the PP α-crystals upon the addition of CNTs, which is in agreement with previous reports in the literature[15,16]. Therefore, it is assumed that the β and γ-phase crystal formation of PP during $scCO_2$ processing was erased from the final specimens after hot-pressing.

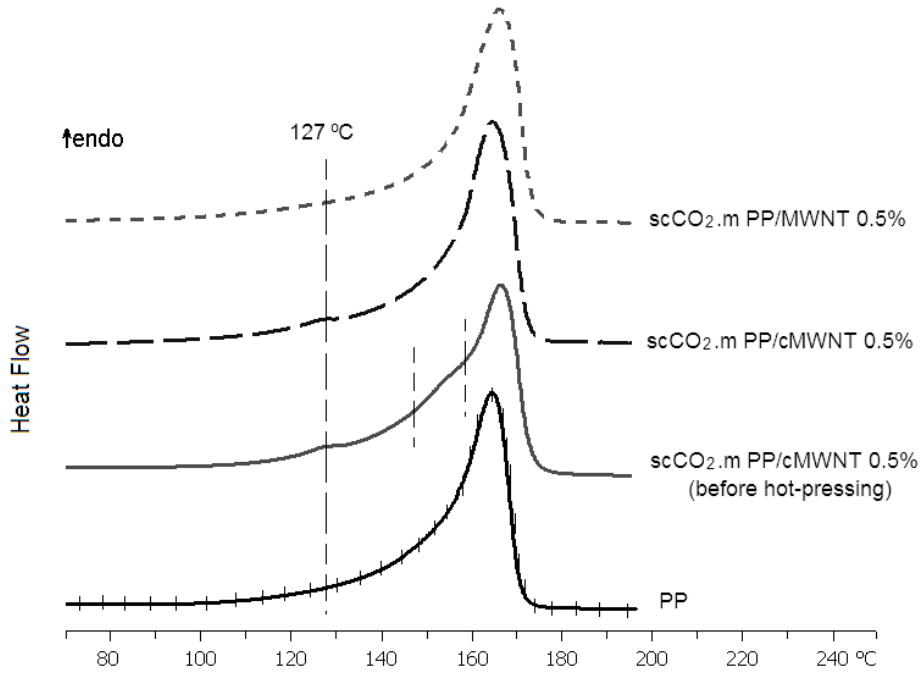

Fig. 4.8 *The DSC heating scan for typical PP/MWNT nanocomposites, showing an additional broad peak at around 127 ˚C for samples with cMWNTs*

T_c and X_c are increased by the addition of MWNTs or cMWNTs into the PP, suggesting that nanotubes act as nucleating agents which reduce the spherulites' size, induce the crystals' growth at higher temperatures and enhance crystallization.

Furthermore, pristine MWNTs give a higher T_c of PP nanocomposites than cMWNTs, which indicates a stronger nucleation effect from MWNTs than from coated MWNTs. Clearly, the surface of any nucleating agent plays an important role in the crystallization process[17,18]. MWNTs have high surface energies which can absorb the polymer preferentially along their crystal structure and act as nuclei for polymer crystals. HDPE coatings decrease this surface free energy, resulting in a reduced nucleating efficiency. Results also show a small variation in the T_c with different CNT loadings. Although nucleating agents significantly increase the number of nucleation sites, above certain loadings the introduction of more CNTs may hinder chain mobility and retard crystal growth. This may explain the more pronounced nucleating effect observed for very low CNT loadings. Hence, the mechanical reinforcing effects observed are a combination of the modification of the PP matrix through increased crystallinity as well as true reinforcing effects from CNT fillers[13].

Fig. 4.9 shows the XRD patterns for pure PP and $scCO_2$ processed nanocomposites before and after hot-pressing. MWNTs do not have peaks at $2\theta < 25$ °. The pattern of pure PP shows peaks corresponding to a PP α-phase at 2θ = 14, 17, 18.5, 21.5, 21.9 and 25.4 ° for six major reflections: (110), (040), (130), (111), (041) and (060) plane, respectively[19]. For $scCO_2$ processed pure PP and PP nanocomposites, an additional peak at 2θ of 20.1 ° is detected, which corresponds to the characteristic (117) plane of the γ-phase of PP[20]. The γ-phase is only obtained in some special cases such as under high pressure and by the crystallization of very low molar mass fractions[20]. In our case, the high pressure used in the $scCO_2$ processing promoted the formation of γ-phase crystals. Apart from the peaks of α and γ-phases, a broad small peak observed at 2θ of 16° for the $scCO_2$.mPP/cMWNT 0.5 wt.% sample before hot-pressing corresponds to the (300) plane of the β-phase of PP[21]. Other β-phase peaks such as 2θ of 16.7 ° (008) and 21 ° (301) are too close to the strong α-phase

peaks to be identified. The PP nanocomposite sample after hot-pressing only shows an α-phase of PP which is in close agreement with our DSC results, suggesting that the thermal history from $scCO_2$ processing was erased after hot-pressing. The preferential orientation of PP crystals growth along the (040) planes is also found here with the addition of MWNTs in PP, similar to the phenomenon observed from PP/sepiolite nanocomposites (studied in Chapter 3).

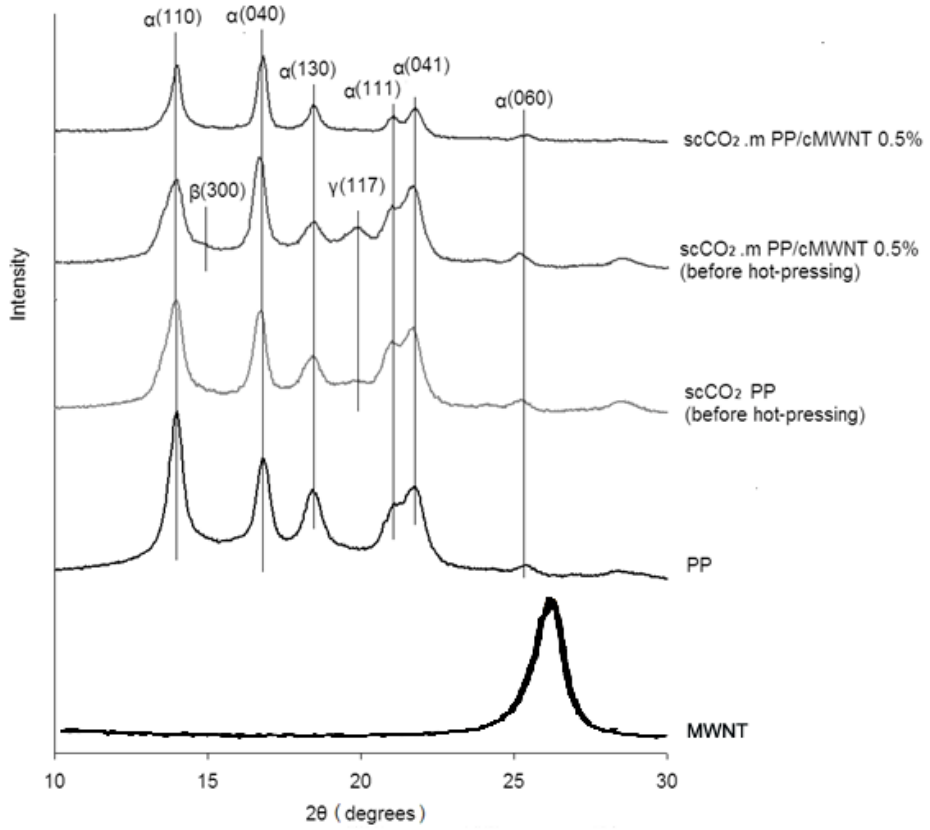

Fig. 4.9 *X-ray diffraction spectra for typical PP/MWNT nanocomposites, confirming the presence of α-phase crystals of PP in the nanocomposites*

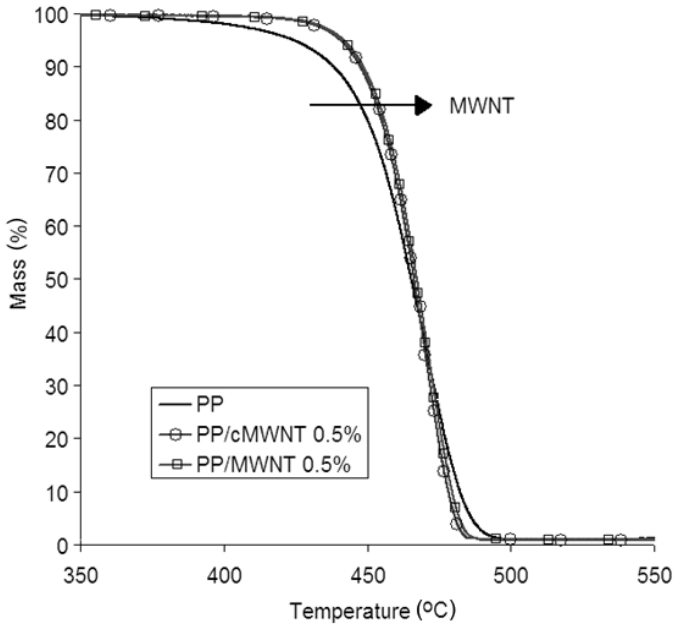

Fig. 4.10 *The TGA of PP/MWNT nanocomposites processed using $scCO_2$ assisted mixing, showing a retarded thermal degradation of nanocomposites by the presence of MWNTs*

Finally, the thermal stability of the nanocomposites was investigated by TGA (Fig. 4.10). The thermal degradation of PP is substantially retarded by the presence of CNTs. The onset decomposition temperatures, T_{onset}, are higher for PP/MWNT nanocomposites because the CNTs hinder the flux of degradation products and improve the heat dissipation within the composites[22]. However, above 470 °C the composites seem to degrade at a slightly higher rate than the neat polymer. A similar T_{onset} was observed for both the PP/cMWNT and PP/MWNT nanocomposites, indicating that the HDPE coating of cMWNTs had no significant effect on the thermal degradation behaviour.

4.4 Conclusions

This chapter described the preparation of PP/MWNT nanocomposites using the

$scCO_2$ assisted mixing method and the results were compared with those processed by a traditional melt compounding method. Results showed that by using $scCO_2$ assisted mixing, both the yield stress and the Young's modulus of the nanocomposites increase with MWNT loading. However, unlike in melt compounding processes, with which the use of HDPE coated MWNTs is essential for improved dispersion and properties, in the case of $scCO_2$ assisted mixing, similar good dispersions and mechanical properties are achieved with pristine MWNTs, which in addition to obvious cost benefits may also benefit from a lower viscosity of the polymer melt under $scCO_2$ conditions and a better preservation of nanotube lengths. It is interesting that techniques designed to achieve high quality PP nanocomposites, such as the use of masterbatches or polymer coated MWNTs, are not strictly necessary when using $scCO_2$ assisted mixing. In accordance with many other nanocomposite studies, the addition of CNTs enhanced the PP nucleation process. The resulting increase in crystallinity is an important additional factor responsible for the enhanced mechanical properties of the final nanocomposites.

4.5 References

1. Dubois P and Alexandre M. Performant Clay/Carbon Nanotube Polymer Nanocomposites. Adv. Eng. Mater. 2006, 8, 147
2. Alexandre M, Bonduel D, Claes M, Dubois P, Peeterbroeck S, Pegel S and Potschke P. Method for Dispersing Carbon Nanocubes in a Polymer Matrix. US 2008/0207824A1
3. Deng H, Bilotti E, Zhang R, Peijs T. Effective Reinforcement of Carbon Nanotubes in polypropylene Matrices. J. Appl. Polym. Sci. 2010, 118, 30
4. Fayolle B, Richaud E, Verdu J and Farcas F. Embrittlement of Polypropylene Fibre During Thermal Oxidation. J. Mater. Sci.2008, 43, 1026
5. Hull D and Clyne T. An Introduction to Composite Materials. Cambridge: University

Press; 1981

6. Treacy MM, Ebbesen TW and Gibson LM. Exceptionally High Young's Modulus Observed for Individual Carbon Nanotubes. Nature. 1996, 381, 678
7. Yu MF, Lourie O, Dyer MJ, Moloni K, Kelly TF and Ruoff RS. Strength and Breaking Mechanism of Multiwalled Carbon Nanotubes under Tensile Load. Science. 2000, 287, 637
8. Barber AH, Andrews R, Schadler LS and Wagner HD. On the Tensile Strength Distribution of Multiwalled Carbon Nanotubes. Appl. Phys. Lett. 2005, 203, 106
9. Barber AH, Cohen SR, Eitan A, Schadler LS and Wagner HD. Fracture Transitions at a Carbon-Nanotube/Polymer Interface. Adv. Mater. 2006, 18, 83
10. Ryan KP, Cadek M, Nicolosi V, Blond D, Ruether M, Armstrong G, Swan H, Fonseca A, Nagy JB, Maser WK, Blau WJ and Coleman JN. Carbon Nanotubes for Reinforcement of Plastics? A Case Study with Poly(vinyl alcohol). Compos. Sci. Technol. 2007, 67, 1640
11. Coleman JN, Cadek M, Blake R, Nicolosi V, Ryan KP, Belton C, Fonseca A, Nagy JB, Gun'ko YK and Blau WJ. High Performance Nanotube-Reinforced Plastics: Understanding the Mechanism of Strength Increase. Adv. Funct. Mater. 2004, 14, 791
12. Bhattacharyya AR, Sreekumar TV, Liu T, Kumar S, Ericson L.M, Hauge H and Smalley RE. Crystallization and Orientation Studies in Polypropylene/Single Wall Carbon Nanotube Composite. Polym. 2003, 44, 2373
13. Wang Z, Ciselli P and Peijs T. The Extraordinary Reinforcing Efficiency of Single-Walled Carbon Nanotubes in Oriented Poly(vinyl alcohol) Tapes. Nanotechnol. 2007, 18, 455709
14. Mandelkern L and Alamo RG. Thermodynamic Quantities Governing Melting. In: Mark JE, editor. Physical Properties of Polymers Handbook. New York: American Institute of Physics; 1996
15. Bao SP and Tjong SS. Mechanical Behaviours of Polypropylene/Carbon Nanotube

Nanocomposites: The Effects of Loading Rate and Temperature. Mater. Sci. Eng., A. 2007, 485, 508

16. Andrews R, Jacques D, Minot M and Rantell T. Fabrication of Carbon Multiwall Nanotube/Polymer Composites by Shear Mixing. Mater. Eng. 2002, 287, 395
17. Tang JG, Wang Y, Liu HY and Belfiore LA. Effects of Organic Nucleating Agents and Zinc Oxide Nanoparticles on Isotactic Polypropylene Crystallization. Polym. 2004, 45, 2081
18. Wittmann JC and Lotz B. Epitaxial Crystallization of Polymers on Organic and Polymeric Substrates. Prog. Polym. Sci. 1990, 15, 909
19. Natta G and Corradini P. Structure and Properties of Isotactic Polypropylene. Nuovo. Cimento. Suppl. 1960, 15, 40
20. Brückner S, Philips PJ, Mezghani K and Meille SV. On the Crystallization of γ-isotactic Polypropylene: A High Pressure Study. Macromol. Rapid Commun. 1997, 18, 1
21. Meille SV, Ferro DR, Brückner S, Lovinger AJ and Padden FJ. Structure of Beta-Isotactic Polypropylene: A Long-Standing Structural Puzzle. Macromol. 1994, 27, 2615
22. Huxtable ST, Cahill DG, Shenogin S, Xue LP, Ozisik R, Barone P, Usrey M, Strano MS, Siddons G, Shim M and Keblinski P. Interfacial Heat Flow in Carbon Nanotube Suspensions. Nat. Mater. 2003, 2, 731

Part B:

Processing of Polymer Drug Delivery Systems for Controlled Release

Chapter 5

Drug Delivery Systems

A wide variety of biomaterials are used as components of the various formulations and devices that are routinely used for delivering drugs to the body today. These devices are referred to as being a drug delivery system (DDS), a system which releases drugs in a controlled manner[1]. So, why use a DDS? Let's start with the changes in blood plasma levels following a single dose administration of a therapeutic agent. Fig. 5.1 shows that the blood plasma level rapidly rises and then exponentially decays as the drug is metabolised and/or eliminated from the body. The figure also shows drug concentrations above which the drug produces undesirable (e.g. toxic) side effects and below which it is not therapeutically effective. Although we can increase the size of the dose to achieve longer time for which the concentration of the drug is above the minimum effective level, blood

plasma concentrations will extend into the toxic response region (dotted line). Alternatively, safe doses can be repeatedly administered at periodic intervals to maintain a desired drug concentration level; however, this is inconvenient, and patient compliance is often poor.

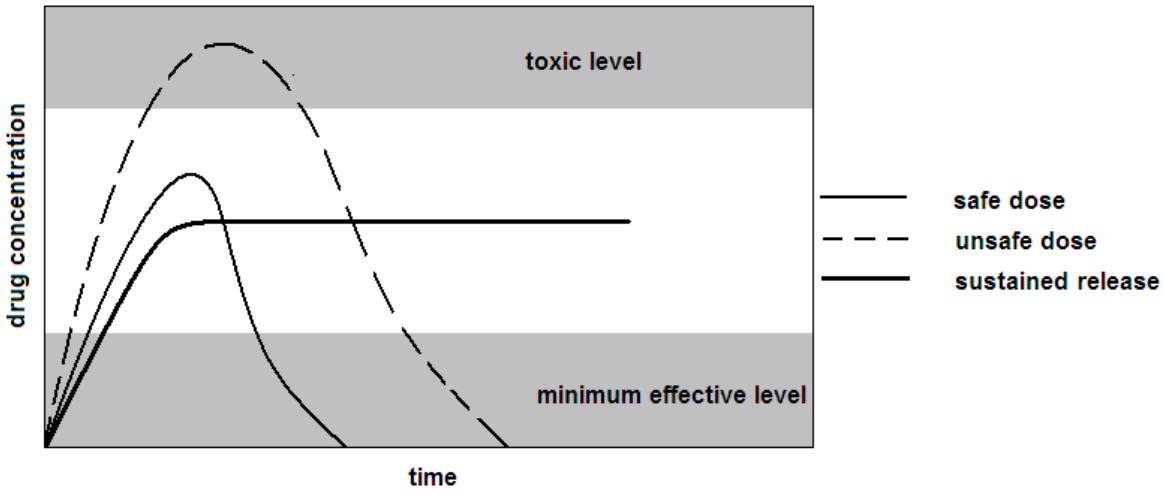

Fig. 5.1 *Drug concentration as a function of time following absorption of a therapeutic agent*[1]

For these reasons, there has been great interest in developing sustained-release formulations and devices that can maintain a desired blood plasma level for a certain period of time without reaching a toxic level or dropping below the minimum effective level. The sustained-release systems became the primary objective of DDS to control the release of drugs. Nowadays, sustained-release systems are designed to achieve the controlled release of drugs by reproducible and predictable kinetics. Also, a concerted effort was made to develop controlled release systems for drug targeting, a method by which a drug is delivered to a specific tissue or organ using carriers or chemical conjugates[2]. Drug delivery is one of the most clinically-commercialised areas of biomaterials. The world market of advanced drug delivery systems was valued at $139 billion in 2009 and is estimated to be worth $196.4 billion by 2014[3].

Here are some commercial device examples. The Ocusert system, developed by Alza Corp., which is inserted in the lower cul-de-sac and releases pilocarpine in the treatment of glaucoma[4]. Capronor® is designed for contraceptive steroids based on the biodegradable polymer polycaprolactone to release levonorgestrel at a constant rate for one year and to completely bio-erode in three years[5]. Nutropin® is a product which encapsulates recombinant human growth hormone using poly(lactic-co-glycolic acid) (PLGA). It provides elevated blood plasma levels for more than one month[6]. Gliadel®Wafers is a unique form of treatment for brain tumours. It is based on polyanhydride wafers which slowly release carmustine (an anti-brain tumour drug) and can be implanted into the tumour site[7].

5.1 Types of Drug Delivery System

There are several methods used to classify DDS. According to their delivery routes, DDS can be divided into four types: pulmonary delivery, oral delivery, transdermal delivery and other delivery routes[8]. The correct delivery route could significantly increase drug action efficiency and decrease its side-effects and systemic toxicity. All of these delivery routes could provide a novel drug delivery path for specific diseases at specific sites.

According to the release mechanism, DDS can be classified into diffusion controlled DDS, water penetration controlled DDS, chemically controlled DDS, responsive DDS and particulate DDS[9]. Sometimes, one drug release device will release a drug under combinations of several of the release mechanisms mentioned above. For example, the drug release from biodegradable polymer devices can be controlled by the diffusion of the drug as well as the chemical degradation of the polymer carriers.

As mentioned in the previous context, DDS can also be classified into sustained release and drug targeting systems based on their action mechanism and functions. In this thesis, if not mentioned, controlled release means sustained release.

According to materials utilized for drug delivery, there are two main groups: liposome-based drug delivery systems and polymer-based drug delivery systems. Small lipid vesicles known as liposomes have been extensively studied and encapsulating drugs within these vesicles has the potential advantage of providing a transdermal path and a higher drug delivery capacity[10]. The technology of polymer drug delivery has been studied in detail over the past 30 years and numerous excellent reviews are available[8,11,12]. A more detailed review of polymer drug delivery systems is stated in the following section.

5.2 Design of Drug Delivery Devices

In recent years, there have been numerous developments in designing different devices to fulfil various requirements in the field of drug delivery[9]. The most used designs are:

- Drug surrounded by a thin polymer membrane (reservoir devices)
- Drug uniformly dispersed or dissolved in a polymer matrix (monolithic devices)
- Soluble polymers with covalently attached pendant drug molecules
- Osmotic pumps by which the drug release rate is controlled dynamically
- Biodegradable reservoir and monolithic systems
- Biodegradable polymer backbones with pendant drugs
- Responsive smart systems, such as temperature- and pH-responsive, mechanical- and physically-responsive, self-regulated systems

- Polymeric colloidal particles or microencapsulates (microparticles, microspheres or nanoparticles)
- Polymer drug conjugates
- Polymeric micelles
- Liposomes

5.3 Polymer Drug Delivery Systems

There is a range of polymers which have been employed to control the release of drugs. Polymer delivery systems can be classified into non-biodegradable and biodegradable delivery systems. However, in principle there is no sharp boundary between biodegradable and stable polymers. The difference between non-biodegradable and biodegradable polymers is a matter of degree, conditions and time scale. For example, proteins are biodegradable polymers which are degraded by the hydrolysis of the amide bond by the mediation of enzymes. Polyamides, which are widely used as non-biodegradable polymers, are also subject to enzymic degradation, but at a significantly lower rate. Therefore, classifying polymers into non-bio- and biodegradable is based on whether the polymer is used deliberately for its biodegradability or for its non-biodegradability[1,8].

5.3.1 Non-Degradable Polymer Delivery Systems

The first polymer drug release system was based on non-biodegradable polymers. In 1964, Folkman and Long reported the use of silicone tubes filled with drug suspension for sustained release[13]. Their findings initiated the field of controlled release technology and led to the development of Norplant®, a contraceptive which can remain therapeutically effective release for as long as five years[13].

5.3.1.1 Overview of Non-Degradable Polymers

To be successfully used in controlled drug delivery formulations, a material must be chemically inert and free of leachable impurities. It must also have an appropriate physical structure, with minimal undesired ageing, and be readily processable. Some of the materials that are currently being used or studied for controlled drug delivery include: polyurethanes[14], silicones[13], poly(2-hydroxy ethyl methacrylate)[15,16], poly(vinyl alcohol)[17], poly(vinyl pyrrolidone)[18], poly(methyl methacrylate)[19], poly(acrylic acid)[20], polyacrylamide[20], poly(ethylene-co-vinyl acetate)[20], poly(ethylene glycol)[21], poly(methacrylic acid)[20,22], etc.

5.3.1.2 Poly(ethyl methacrylate/tetrahydrofurfuryl methacrylate)

In dentistry, to avoid repeated mouth washes, polymer drug delivery systems are being researched extensively for the release of antibacterial, anti-fungal and antiviral drugs in order to treat oral infections[23]. It is claimed that these systems have fewer side effects by comparison with conventional forms, because of the continual presence of the drug at the site of action, which means that a smaller amount of the drug is needed to achieve the therapeutic effect[24]. They were also believed to be of high benefit for both physically and mentally compromised patients[25].

Among the employed polymers, the poly(ethyl methacrylate/tetrahydrofurfuryl methacrylate) (PEM/THFM) polymer system is widely used and well documented[26-30]. This chemical structure is shown below in Fig. 5.2.

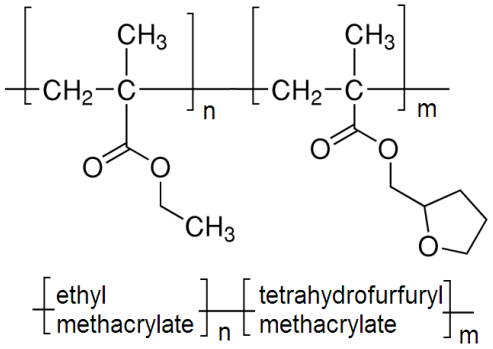

Fig. 5.2 *The chemical structure of PEM/THFM*

The suitability of PEM/THFM in drug delivery applications is due to its various unique properties, which include:

- Unusual water uptake properties. Although the solubility of THFM monomer in water is only 3 %, poly(THFM) absorbs more than 70 % water[27]. The mechanism is a two-stage process involving an initial Fickian process, followed by a stage characterised by a slower growth of droplets (clustering mechanism)[27]. The second stage is controlled by stress relaxation. If the clustering or stress relaxation can be prevented, the polymer behaves in an ideal, Fickian manner which will be perfect candidate for drug release. It has been shown that copolymerisation of THFM with other monomers, e.g., PEM, successfully suppresses this secondary process[29,31].
- Cold cure polymer systems. The polymerisation of the copolymer happens at room-temperature. This mode of polymerisation has a low polymerisation exotherm, which does not adversely affect the efficacy of the anti-fungal drugs[28]. It is proven that PEM/THFM has superior biocompatibility than poly(methyl methacrylate) and is more efficient at delivering drugs[28].

PEM/THFM has been proved to be an effective system as a delivery vehicle for chlorhexidine diacetate[23,25,26,28], fluoride release[30], gentamicin[28] and bone morphogenetic protein[28,31]. The system is also biocompatible with bone and used to promote bone and cartilage regeneration.

5.3.2 Biodegradable Polymer Delivery Systems

Non-biodegradable materials are stable and can be used easily to make specific structures. On the other hand, biodegradable polymers are polymers that are used in biomedical technology and medicine specifically for their biodegradability. Biodegradable delivery systems do not need to be surgically removed; they can be metabolized and excreted by natural pathways. Therefore, some of the problems related to the long-term safety of permanently implanted devices can be circumvented. The polymer is used to protect a drug during its transfer through the body until it is released, or is used to control the release rate of a drug. Selecting a suitable polymer is critical to the design of a desired controlled release system. These degradable materials must fulfil more stringent requirements in terms of their biocompatibility than non-biodegradable materials. Since all the degradation products are released into the body of the patient, the potential toxicity requires careful consideration.

5.3.2.1 An overview of Degradable Polymers

Biodegradable polymers include natural, modified natural and synthetic polymers. Collagen, cellulose, and chitosan are examples of natural polymers. Natural polymers have been tested as drug delivery matrices for the delivery of protein based drugs. Modified natural polymers are natural polymers that are altered in order to suit a

particular application. The reason for the modification is that these polymers often take more time to degrade within the body. Over the past few decades, synthetic polymers have been actively studied for use in DDS. These include polyhydroxybutyrate, polyhydroxyvalerate, and copolymers thereof, polycaprolactone, polyanhydrides, polycyanoacrylates, poly(amino acids), polyphosphazenes, poly(phosphoesters), polyorthoesters, and polylactides (PLA), polyglycolides (PGA), and the copolymers PLGA[16,32-34].

Although a variety of polymers are available, degradable polymers are still too limited to cover a wide enough range of diverse material properties. Thus, the design and synthesis of new, degradable materials is currently an important research challenge.

5.3.2.2 The Process of Biodegradation

One of the most important prerequisites for the successful use of a degradable polymer for any medical application is a thorough understanding of the way the device will degrade and ultimately absorb from the implant site. The bio-erosion process of a solid, polymeric implant is associated with macroscopic changes in the appearance of the device, changes in its physical processes such as swelling, softening, deformation, stress cracking, or structural disintegration, weight loss, and the eventual depletion of the drug or a loss of its function[8,11].

The two main biodegradation mechanisms in biomedical polymers are hydrolysis and oxidation. These reactions may or may not be catalysed by enzymes, depending on detailed characteristics of the polymer itself (e.g., chemical structure, molecular weight (M_w), morphology), and on device shape and its location in the body.

Hydrolysis is the scission of covalent bonds by water. Susceptibility of polymers to hydrolysis depends on their chemical structure, morphology and dimensions, and also on their immediate environment. Hydrolysis may be catalysed by acids, bases, salts and enzymes.

5.3.2.3 Two Modes of Biodegradation

Two distinct modes of biodegradation have been described in the literature. They are surface erosion and bulk erosion[35] (Fig. 5.3).

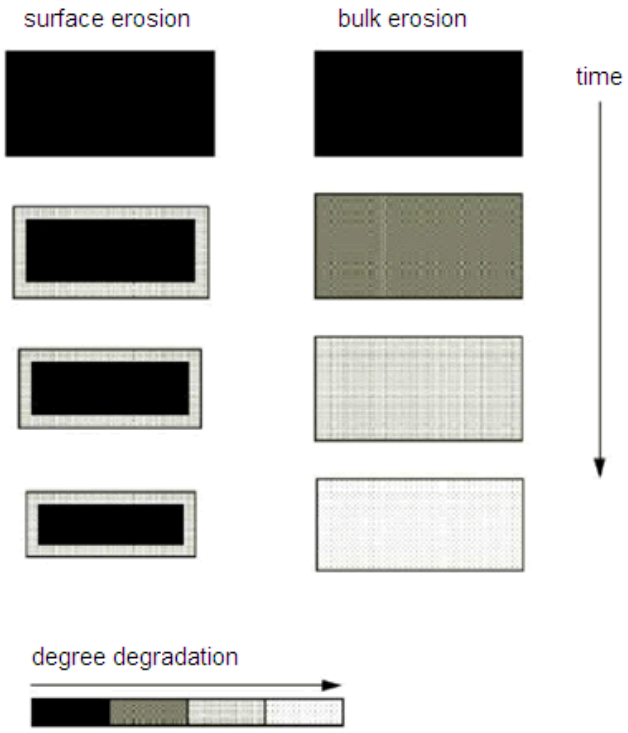

Fig. 5.3 *A schematic illustration of surface erosion and bulk degradation*

In "surface erosion", degradation occurs when the penetration of water into the polymer bulk is much slower than the hydrolysis. The degradation process is limited

to the surface of the device. Therefore, the device will become thinner with time, while maintaining its structural integrity throughout much of the erosion process[35]. Alternatively, in "bulk erosion", the rate of water penetration into the solid device is much faster than the degradation reaction; hence degradation takes place at nearly equal rates throughout the polymer surface and bulk. Because of the rapid penetration of water into the matrix of hydrophilic polymers, most of the currently available polymers will give rise to bulk eroding devices.

Bulk erosion may be autocatalysed by the acidity of the degradation products, or changes in the biodegradation environment. This effect may lead, somewhat counter intuitively, to faster degradation in larger devices (lower surface to volume ratios), and inside the device bulk, due to the slower release of soluble acidic degradation product in larger devices.

However, in practice, biodegradation must be regarded in terms of the various intermediates of these two extremes, i.e. in "erosion zones" of finite thickness at the surface where degradation takes place. Most typical examples of bulk and surface degrading polymers are aliphatic polyesters and polyanhydrides, respectively.

5.3.2.4 Factors Influencing Biodegradation

The rate of biodegradation of a given polymer is not an unchangeable property. The main factors that determine the overall rate of the biodegradation process are:

- Polymer properties: crystallinity, T_g, M_w, M_w distribution, the hydrophilic/hydrophobic character of the repeat units, wettability (swelling, water uptake)

- The manufacturing process of the polymer devices: morphology, geometry (specifically the surface area to volume ratio)
- External factors: temperature, pH, additives, enzymes

5.3.2.5 Poly(lactic-co-glycolic acid)

Among these biodegradable polymers, PLA and PGA and their copolymer PLGA have been investigated for more applications than any other degradable polymer[16,32-34]. The high interest in these materials is based, not on their superior materials properties, but mostly on the fact that these polymers have already been used successfully in a number of approved medical implants and are considered safe, non-toxic, and biocompatible by regulatory agencies. It has received abundant research for its effective usage in drug delivery.

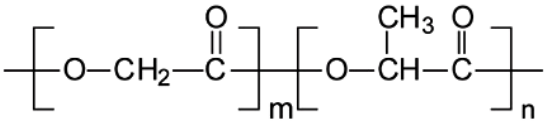

Fig. 5.4 *The chemical structure of PLGA*

Fig. 5.4 shows the chemical structure of PLGA. PLGA has been successful as a biodegradable polymer because it undergoes hydrolysis to yield lactic acid and glycolic acid monomers and these two monomers are normal by-products of cellular metabolism in the body. Since the body deals effectively with the two monomers, there is very minimal systemic toxicity associated with using PLGA for drug delivery or biomaterial applications.

The degradation of PLGA has been described very well as bulk erosion[36]. The erosion process can be split into 3 stages. In stage 1, water diffuses into the polymer

and ester bond cleavage starts producing a primary alcohol and a carboxylic acid. In stage 2, differentiation between the surface and interior begins, with a drastic decrease in molecular weight in the inner part of the matrix. The accumulation of carboxylic acid hydrolysis products will reduce the pH which will enhance hydrolysis inside the PLGA resulting in an autocatalysis of the hydrolysis reaction. However, the diffusion of the degradation segments out of the polymer is limited by their sizes, therefore, the mass of the PLGA will remain unchanged. In stage 3, a network of pores is formed allowing for the release of fragments, i.e. erosion occurs.

PLGA degradation is strongly determined by the properties of the polymer. Different forms of PLGA can be obtained depending on the ratio of the lactide to the glycolide monomer used for the polymerisation. The higher the content of glycolide units, the lower the time required for degradation. A low molecular weight PLGA polymer degrades faster than PLGA composed of high molecular weight polymer chains. Since water does not penetrate as easily into the crystalline regions, the PLGA degradation rate is decreased with the increase of the crystallinity of the polymer[33]. Factors such as sample size, shape, and surface morphology can also influence PLGA degradation.

5.4 Drug Release Prediction

Mathematical modelling is used to aid in predicting the drug release rates and diffusion behaviour of these systems by the solution of an appropriate model. It also aids in understanding the physics of a particular drug transport phenomenon, thus facilitating the development of new pharmaceutical products.

5.4.1 Mechanisms of Drug Release

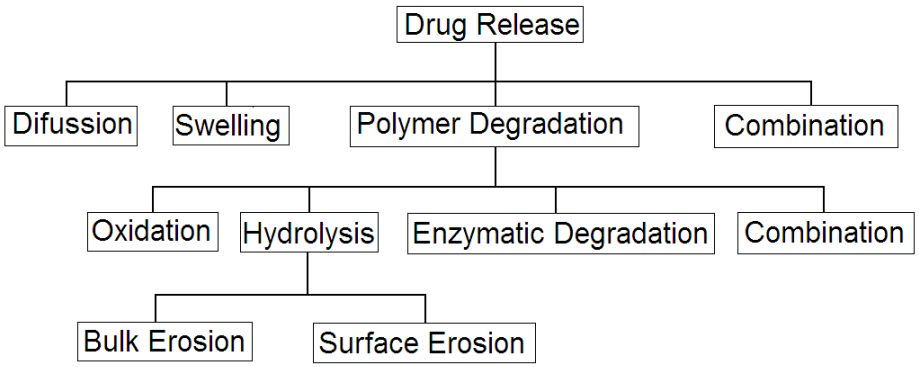

Fig. 5.5 *Drug release mechanisms for polymer drug delivery*

Depending on the release mechanism, the controlled release systems can be classified into diffusion-controlled, polymer degradation-controlled, swelling-controlled, and a combination of the above mechanisms, as shown in Fig. 5.5. Diffusion is the principal release mechanism, and it takes place at varying degrees in both degradation and swelling-controlled systems[37]. The diffusion-controlled systems follow the fundamental Fick's law. For degradation-controlled systems, the rate of drug release is controlled by oxidation, hydrolysis, enzyme assistance, or a combination thereof.

The burst effect, an initial large portion of drug which is released before the release rate reaches a stable profile, has usually not been considered as one of the phases of release[38].

5.4.2 Kinetic Equations for Evaluation

Drug release from polymer matrices has been described by kinetic models in which the dissolved amount of drug (Q) is a function of time (t). Modelling studies allow

the elucidation of underlying mass transport mechanisms and offer the possibility of predicting the effect of matrix design parameters (shape, size and composition of matrix tablets) on the resulting drug release rate[39-51]. The kinetic equations which have been widely applied are zero order, first order, the Higuchi equation and the Korsmeyer-Peppas equation, which is also called the power law.

5.4.2.1 Zero Order Kinetics

A zero-order equation describes a constant rate of drug release over time:

$$Q_t = Q_0 + K_0 t \qquad 5\text{-}1$$

Where Q_t is the amount of the drug dissolved in time t, Q_0 is the initial amount of the drug in the solution (most times, $Q_0 = 0$) and K_0 is the zero order release constant. The drug delivery system, following this profile, releases the same amount of drug in each unit of time and is the ideal method of drug release in order to achieve a pharmacological prolonged action[40]. The zero order model has a large application in coated dosage forms or membrane controlled dosage forms.

5.4.2.2 First Order Kinetics

A first-order equation can be rewritten as a log cumulative percentage of drug remaining vs. time:

$$Log\ Q_t = Log\ Q_0 - K_1 t/2.303 \qquad 5\text{-}2$$

where Q_t is the amount of the drug released in time t, Q_0 is the initial amount of the

drug in the solution and K_1 is the first order constant.[41] In this way a graphic of the decimal logarithm of the released amount of drug versus time will be linear. The pharmaceutical dosage forms following this dissolution profile, such as those containing water-soluble drugs in porous matrices[42], release the drug in a way that is proportional to the amount of drug remaining in its interior, and so that the amount of drug released in each unit of time diminishes.

5.4.2.3 Higuchi's Equation

In 1961, Higuchi derived an equation to describe drug release from a planar system consisting of a homogeneous matrix in the form of an ointment base containing a finely dispersed drug[43]:

$$q(t) = A\sqrt{D(2c_0 - c_s)c_s t} \quad , \qquad c_0 > c_s \tag{5-3}$$

Where $q(t)$ is the amount of drug released after time t, A is the surface area of the ointment exposed to the absorbing surface, D is the diffusion coefficient of the drug in the matrix medium, and C_0 and C_s are the initial drug concentration and the solubility of the drug in the matrix, respectively.

The Higuchi equation describes a linear relationship between the cumulative amount of drug released and the square root of time, which is an indicator of diffusion controlled release (no erosion occurring)[43]. Although a planar matrix system was postulated in the original analysis, modified forms of equation 5-3 were subsequently applied to other types of matrices. Desai *et al.*[44] employed inert matrix tablets with only one flat surface exposed to the dissolution media. Drug release was found to be linear with square root time. Lapidus and Lordi[45] showed that when drug release was

restricted to a planar surface of a hydroxypropyl methylcellulose (HPMC) matrix tablet, linearity between drug release and square root time was observed even though the matrix was not inert.

The classical Higuchi equations were derived under pseudo-steady state assumptions and, in general, cannot be applied to practical systems. The assumptions were summarized by Siepman and Peppas[46]: (i) the initial drug concentration in the system is much higher than the solubility of the drug in the matrix, (ii) mathematical analysis is based on one-dimensional diffusion (negligible edge effects), (iii) swelling or dissolution of the matrix is negligible, (iv) constant drug diffusivity and (v) perfect sink conditions are maintained. Although these assumptions are not valid for most hydrophilic matrices, the Higuchi equation is often employed to analyse the drug release to gain a rough idea of the underlying drug release mechanism due to its simplicity.

Equation 5-3 is frequently written in simplified form[47]:

$$M_t/M_\infty = Kt^{1/2} \qquad 5\text{-}4$$

where M_t and M_∞ are the absolute cumulative amounts of drug released at time t and infinite time, respectively and K is the Higuchi dissolution constant. The drug release rate derived from the Higuchi equation predicts a zero intercept. However, negative or positive intercepts on the Y-axis might be obtained from a curve-fitting of dissolution data to the equation. The former indicates a failure of the drug delivery system to immediately attain a state of equilibrium diffusion described by the Higuchi equation (lag time) while the latter represents a burst release of the drug prior to the development of the diffusion-controlling barrier.

The analytical expression allows experimental determination of K from early release curves when Higuchi conditions are still prevailing.

5.4.2.4 Korsmeyer-Peppas' Equation (Power Law)

The Higuchi equation does not apply to swellable polymer system because swelling leads to moving (diffusion) boundary conditions which violates one of the assumptions of the Higuchi equation. Korsmeyer *et al*.[48] proposed the use of a simple, semi-empirical model, also known as power law, to describe drug release from a single face of a swelling hydrophilic matrix under perfect sink conditions:

$$M_t/M_\infty = Kt^n \qquad 5\text{-}5$$

where M_t/M_∞ is the fractional release of the drug, t is the release time, K is a kinetic constant characteristic of the drug/polymer system, and n is the release exponent indicative of the drug release mechanism. In 1987, Ritger and Peppas[49, 50] showed that the equation can be used to describe the general drug release behaviour of non-swelling and swelling polymer matrices in the form of films, cylinders and spheres.

Table 5.1 lists the values of n for different geometries of polymer matrices and the corresponding release mechanisms. For a polymer film or slab, when n = 0.5, pure Fickian diffusion operates and results in diffusion-controlled drug release. When n = 1.0, case II transport is the predominant mechanism. It is in the same form as the zero-order equation Case II transport generally refers to the swelling-controlled systems due to the relaxation of the polymer chain. In addition to Case II transport (relaxation-controlled mechanisms), other mechanisms also give rise to linear drug

release kinetics. In swellable-erodible polymer matrices, a constant drug delivery rate can be achieved when a constant gel layer thickness is attained by synchronization of the swelling and eroding fronts[40]. A constant drug release rate was also observed with matrices consisting of low viscosity polymers where polymer dissolution controlled the rate of drug release[51]. An intermediate value of n ($0.5 < n < 1.0$) indicates a combination of Fickian diffusion and Case II transport, which is usually called anomalous transport or non-Fickian diffusion.

For cylindrical and spherical matrices, the exponent n has a slight different value to identify the drug release mechanism. (Table 5.1)

Table 5.1 *The values of the exponent n in equation 5-5 and the corresponding release mechanisms from polymer delivery systems of various geometries*

Exponent n			Release
Film	Cylinder	Sphere	mechanism
0.5	0.45	0.43	Fickian diffusion
$0.5 < n < 1.0$	$0.45 < n < 0.89$	$0.43 < n < 0.85$	Anomalous transport
1.0	0.89	0.85	Case II transport

The power law equation is only valid for the first 60 % of the drug release. However, recent work has shown that the equation can be applied to the entire release profile[51]. This model is generally used to analyse the release of a pharmaceutical polymer system, when the release mechanism is not well known or when more than one type of release phenomena could be involved.

In order to choose the best model to study drug release phenomena, the coefficient of determination (R^2), absolute sum of squares (sum of the squares of the vertical distances of the points from the curve), and the standard deviation of the residuals (standard deviation of the vertical distances of the points from the line) are

commonly used to compare the goodness-of-fit of the dissolution data to a model equation.

5.4.3 Factors Influencing Drug Release

Drug release from a polymeric matrix is affected by various factors including polymer properties, drug properties and the morphology of the matrix. Obviously, polymer properties are the fundamental factors when designing a drug delivery device in the first place. Drug properties include stability, solubility, charge, and protein binding propensity, etc. Morphology of the polymer matrix also plays an important role in governing the release characteristics of the encapsulated drug. The polymer matrix could be formulated as microspheres, gel, film, cylinders, rods etc. The shape of the polymer is important to the drug release kinetics, which has been described in detail in section 5.4.2.2. The surface morphology, porosity and the size distribution also affect the performance of the drug delivery device.

5.5 Drugs Involved in the Study

5.5.1 Chlorhexidine

Chlorhexidine (CX) is a conventional antimicrobial drug which has been widely used to treat and prevent skin and mucosal infections with a low topical toxicity[52]. In addition, it has been demonstrated that chlorhexidine has a strong substantivity within the oral cavity, making it efficient in inhibiting dental plaque and gingivitis[53]. The structure of CX is symmetrical with two identical epitopes. (Fig. 5.6)

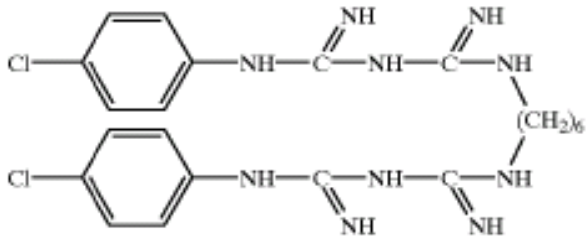

Fig. 5.6 *The molecular structure of chlorhexidine*

CX is used as a rinse solution between 0.2 % and 0.5 % (w/v). However, the use of the mouth-rinse containing CX salt usually provides short-term efficiency, requiring repeated applications to maintain antibacterial activity. This shortcoming led to the use of controlled release devices for the long-term release[54]. Later development yielded devices made of an acrylic-based strip[55], a cross-linked collagen chip[56], and biodegradable polyesters[57]. Also, a number of researches were based on the PEM/THFM system[26,28].

5.5.2 Bovine Serum Albumin

Despite the fast development of protein delivery systems, there are several problems facing protein delivery. The most significant issue is the denaturation and degradation. Proteins are polymers made up mainly of amino acids, which polymerize to give long chains that then fold into a functional 3-dimensional structure. This 3-dimensional structure, however, is held in place by weak forces that can be broken easily. Once this configuration is destroyed, the proteins lose their activity, and, in essence, are denatured. Proteins can lose their activity easily when subjected to adverse conditions such as high temperature, mechanical agitation and extreme pH etc. Protein stabilization is one of the most important issues that researchers must take into consideration during the design of controlled release systems.

Albumins form a group of acidic proteins which occur plentifully in body fluids and tissues of mammals and in some plant seeds. Albumins are readily soluble in water and their solution stability is very good. Albumin binds water, Ca^{2+}, Na^{+}, and K^{+}. Due to a hydrophobic cleft, albumin binds fatty acids, bilirubin, hormones and drugs[58]. The main biological function of albumin is to regulate the colloidal osmotic pressure of blood. The albumin form bovine serum (BSA) is widely used in the field due to its lack of effect in many biochemical reactions and its low cost since large quantities of it can be readily purified from bovine blood. BSA is a single polypeptide chain consisting of about 583 amino acid residues and no carbohydrates. The molecular weight of BSA has frequently been cited as 66430[59]. BSA is often used as standard in protein calibration studies. BSA is also the commonly used protein during the development of controlled release systems. To evaluate the characteristics of the polymer delivery vehicles, fluorescein isothiocyanate labelled BSA (FITC-BSA) has often been used as a model drug to allow the visualization of the protein localization within the microparticles and the detection of microparticles in cell cultures or tissues[60].

5.6 Techniques Involved in the Preparation of Drug Delivery System

5.6.1 The Layer by Layer Technique

Encapsulation is a process whereby particles are surrounded by a shell to give small capsules desired properties. This encapsulation can be achieved by a number of techniques such as phase separation, spray-drying, spray-coating, solvent evaporation etc. Amongst these methods, one technique, called layer-by-layer (LbL) polyelectrolyte assembling[61], was established in 1992 and has been of great interest for the last 20 years. Initially, LbL polyelectrolyte adsorption utilised electrostatic

interaction between oppositely charged macromolecules at each adsorption to make multilayer films onto flat macroscopic substrates[62]. Then in the late 1990s, this technology was extended to non-planar surfaces by Sukhorukov *et al*. in the form of colloidal particles[63]. An "onion-like" structure was achieved by assembling multilayer of various polyelectrolyte combinations for colloidal particles. Once the desired number of layers has been assembled, the template particle is decomposed to form hollow polyelectrolyte microcapsules. The steps for microcapsule assembly are presented in Fig. 5.7. This enables an alternating polyelectrolyte assembly on different kinds of templates.

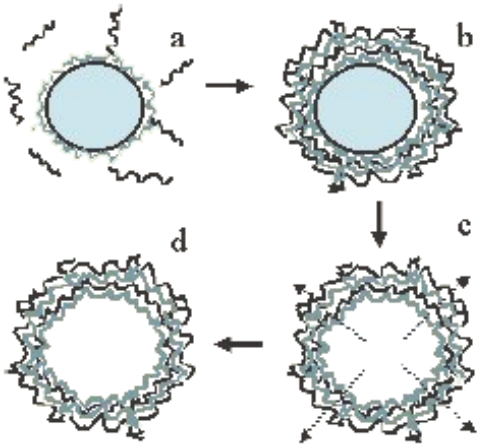

Fig. 5.7 *A schematic of general LbL assembly of polymeric microcapsules. a: coating a charged colloid with a polyelectrolyte and repeating with a second polyelectrolyte of opposite charge. b: the desired number of layers are obtained. c: decomposing the template. d: leaving a hollow polyelectrolyte capsule*

There are several general approaches using the LbL technique to encapsulate the biomacromolecules into polyelectrolyte capsules. Molecules like protein aggregates, dye or drug nanocrystals, and compact forms of DNA can be used as the template for LbL assembly, then leading to encapsulation[64]. The macromolecules can also be incorporated from the surrounding medium into preformed hollow capsules by

switching the permeability of the hollow capsule shell[65]. Another popular approach is that of using porous calcium carbonate ($CaCO_3$) microparticles as the template to capture proteins inside polyelectrolyte microcapsules[66]. The porous $CaCO_3$ microparticles have a high adsorption capacity which benefits the encapsulation of proteins and other macromolecules. Protein-loaded $CaCO_3$ microparticles can be prepared either by physical adsorption in which proteins are adsorbed from the solutions onto $CaCO_3$ microparticles, or by coprecipitation in which proteins are captured in the growth process of $CaCO_3$ microparticles. Then, the required number of polyelectrolyte layers poly(allylamine hydrochloride)/poly(sodium 4-styrenesulfonate) (PAH/PSS) is assembled. Compared with physical adsorption, the coprecipitation procedure is very mild; coprecipitation was found to be about five times more effective than the former with the same amount of captured proteins; the concentration of protein inside the microcapsules can be controlled easily. Moreover, because it is universal, a wide range of macromolecular compounds and bioactive species can be encapsulated by the coprecipitation method.

The LbL technique provides a unique architecture which is perfectly suited to the delivery of sensitive contents and active agents. Compared with other approaches, this method is quite simple and a high yield and tunable size of microcapsules can be achieved.

5.6.2 Electrospinning

Synthetic fibres, which can provide both physical and pharmaceutical support, have a wide range of applications in the biomedical field. Drug-loaded fibres have been proposed for a number of applications such as nanofibre-based supports for enzymes and catalysts, fibrous membranes for wound healing and scaffolds for tissue

engineering[67-70]. The most commonly used technique for the creation of drug-loaded fibres is electrospinning. Electrospinning is a straightforward, relatively easy and cheap method. This technique involves drawing a continuous filament from a polymer solution or melt through a spinneret by high electrostatic forces and then depositing it on a grounded conductive collector (Fig. 5.8). The process offers the advantages of operating at ambient temperature and there being no coagulation chemistry involved. This ensures that the functionality of the drug is well preserved throughout the manufacturing process. The diameters of electrospun fibres can range from nanometers to micrometers. Extensive research based on PLA, poly(ethylene-co-vinyl acetate), PLGA, poly(ethylene glycol)-g-chitosan has taken place over the past few years and the drugs employed include tetracycline hydrochloride, ibuprofen, plasmid DNA, etc[67,68,70,71].

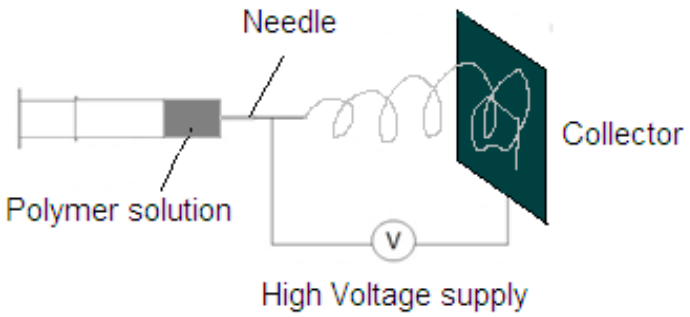

Fig. 5.8 *A schematic illustration of electrospinning*

However, this method has still some unsolved problems:

- Water-soluble drugs have proved difficult to incorporate in the process, because electrospinning requires a full dissolution of all the components in the polymer solution;

- The direct blend-electrospinning procedure leads to a high initial drug release from the fibres, and this burst release phenomenon reduces the effectiveness of the drug release system[72];
- The Denaturation and degradation of the bioactive agents happen during the preparation of the spinning solution and the electrospinning process due to the long exposure to harsh organic solvents[73,74].

To rise to this challenge, several improvements have been made. Water-in-oil (W/O) and oil-in-water (O/W) emulsions have been employed in the electrospinning processes to improve the incorporation of functional particles[75]. Coaxial electrospinning has also been designed and core-shell structures have been developed to protect bioactive agents. However, judicious adjustments of operational conditions were involved to ensure desired results[76]. Research into more effective modifications to electrospinning process is urgently required to address these issues.

5.7 Objectives for Part 2

Since sustained release is essential and an ultimate goal in drug delivery, the aim of the study for this part of the thesis was to develop polymer sustained release devices with improved efficiency of drug release. One non-biodegradable polymer and one biodegradable polymer were chosen.

The PEM/THFM system is one of the most employed non-biodegradable polymer systems in DDS. It has been widely researched based on its use as a drug carrier for anti-fungal and anti-infection drugs to achieve prolonged antimicrobial activity locally. Changing the morphology of the polymer matrix, porosity for example, will have a great impact on the drug release profile as it is expected that porous structures

should enhance the release. Therefore, research was carried out based on a PEM/THFM system with the assistance of a $scCO_2$ foaming technique. The research focuses are summarized as follows:

1. To modify the traditional PEM/THFM copolymer system with the assistance of a $scCO_2$ foaming technique
2. To investigate the morphology, drug properties, and drug release efficiency under different fabrication conditions
3. To investigate the drug release under different fabrication conditions

As for biodegradable polymers, PLGA was chosen for its wide usage in the area of medical applications. PLGA has been employed as porous biodegradable matrices to guide tissue regeneration in the body. In addition, it can be modified by loading with growth factors, which can be released to enhance cell growth. The scaffold may also include additional residues for mimicry of extracellular matrix components or other biologically active molecules for therapeutic amelioration. Drug-loaded fibres have also been proposed for applications such as nanofibre-based supports for enzymes and catalysts and fibrous membranes for wound healing. However, the preparation procedure, electrospinning, is only valid for non-water soluble drugs and the harsh solvents involved significantly reduce the efficiency of the drugs. Therefore, the current study focuses on introducing a second barrier around the drug using the LbL technique in combination with electrospinning. It is believed that as such a new route for the impregnation of water-soluble drugs into PLGA fibres can be achieved. In detail, the research strategy was as follows:

1. To fabricate PLGA fibres with water-soluble drugs using a combination of LbL techniques and electrospinning

2. To investigate the loading efficiency of the drugs, morphology, polymer properties and drug release efficiency under different fabrication conditions
3. To study the mechanism of drug release from the fibres
4. To explore the stability of the encapsulated drugs

5.8 References

1. Roseman TJ and Yalkowsky SH. Importance of Solute Partitioning on the Kinetics of Drug Release from Matrix Systems. In: D. R. Paul DR and Harris FW, editors. Controlled Release Polymeric Formulations. Washington DC: American Chemical Society; 1976
2. Mathiowitz E, Kreitz MR, Brannon-Peppas L. Microencapsulation. In: Mathiowitz E, editor. Encyclopedia of Controlled Drug Delivery. New York, NY: John Wiley & Sons, Inc; 1999
3. Shahani S. Advanced Drug Delivery Systems: New Developments, New Technologies. Pharmaceuticals. 2009
4. Domb, AJ. Ocular Inserts. United States Patent 5660851, 1997
5. Pitt CG and Schindler A. A Biodegradable Delivery System for Levonorgestrel. In: Zatuchni GL, Goldsmith A, Shelton JD, Sciarra JJ, editors. Long Acting Contraceptive Delivery Systems. Philadelphia: Harper and Row Publishers; 1984
6. Johnson OFL, Cleland JF, Lee HJ, Charnis M, Duenas E, Jaworowicz W, Shepard D, Shazamani A, Jones AJS and Putney CD. A Month-Long Effect from a Single Injection of Microencapsulated Human Growth Hormone. Nat. Med. 1996, 2, 795
7. Westphal M, Ram Z, Riddle V, Hilt D and Bortey E. Gliadel Wafer in Initial Surgery for Malignant Glioma: Long-Term Follow-up of a Multicenter Controlled Trial. Acta Neurochir (Wien). 2006, 148, 269
8. Langer R. New Methods of Drug Delivery. Science. 1990, 249, 1527

9. Ratner BD, Hoffmon AS, Schoen FJ and Lemons JE. Biomaterials Science: An Introduction to Materials in Medicine. 2nd ed. Elsevier Academic Press; 2004
10. Bangham AD. Liposomes: a Historical Perspective, In: Liposomes, New York: Marcel Dekker; 1983
11. Lu Y and Chen SC. Micro and Nano-Fabrication of Biodegradable Polymers for Drug Delivery. Adv. Drug Delivery Rev. 2004, 11, 1621
12. Pillai O and Panchagnula R. Polymers in Drug Delivery. Curr. Opin. Chem. Biol. 2001, 4, 447
13. Folkman J and Long DM. The Use of Silicone Rubber as a Carrier for Prolonged Drug Therapy. J. Surg. Res. 1964, 4, 139
14. Hasirci N. Polyurethanes. In: High Performance Biomaterials. Lancaster: Technomic Publishing Co Inc.;1991
15. Dziubla TD, Torjman MC, Joseph JI, Murphy-Tatum M and Lowman AM. Evaluation of Porous Networks of Poly(2-hydroxyethyl methacrylate) as Interfacial Drug Delivery Devices. Biomater. 2001, 21, 2893
16. Willerth SM and Sakiyama-Elbert SE. Approaches to Neural Tissue Engineering using Scaffolds for Drug Delivery. Adv. Drug Delivery Rev. 2007, 4, 325
17. Morita R, Honda R and Takahashi Y. Development of Oral Controlled Previous Preparations, a PVA Swelling Controlled Previous System (SCRS). I. Designing of SCRS and Its Previous Controlling Factor, J. Control. Rel. 2000, 63, 297
18. Tantishaiyakul V, Kaewnopparat N and Ingkatawornwon S. Properties of Solid Dispersions of Piroxicam in Poly(previous termvinyl pyrrolidone). Int. J. Pharm. 1999, 181, 143
19. Mishima K, Matsuyama K, Tanabe D, Yamauchi S, Young TJ and Johnston KP. Microencapsulation of Proteins by Rapid Expansion of Supercritical Solution with a Non-Solvent, AIChE J. 2000, 46, 857

20. Bajpai AK, Shukla SK, Bhanu S and Kankane S. Responsive Polymers in Controlled Drug Delivery. Prog. Polym. Sci. 2008, 11, 1088
21. Katre NV. The Conjugation of Proteins with Polyethylene Glycol and Other Polymers: Altering Properties of Proteins to Enhance Their Therapeutic Potential. Adv. Drug Delivery Rev. 1993, 1, 91
22. Qiu Y and Park K. Environment Sensitive Hydrogels for Drug Delivery. Adv. Drug Delivery Rev. 2001, 3, 321
23. Wilson SJ and Wilson HJ. The Release of Chlorhexidine from Modified Dental Acrylic Resin. J. Oral Rehabil. 1993, 20, 311
24. Garcia CR, Siqueiros A and Benet LZ. Oral Controlled Release Preparations. Pharm. Acta. Helv. 1978, 53, 99
25. Mirth DB, Bartkiewicz A, Shern RJ and Little WA. Development and in vitro Evaluation of An Intra-oral Controlled-Release Delivery System for Chlorhexidine. J. Dent. Res. 1989, 68, 1285
26. Riggs PD, Braden M and Patel M. Chlorhexidine Release from Room Temperature Polymerising Methacrylate Systems. Biomater. 2000, 4, 345
27. Patel MP and Braden M. Heterocyclic Methacrylates for Clinical Applications. III. Water Absorption Characteristics. Biomater. 1991, 12, 653
28. Patel MP, Cruchley AT, Coleman DC, Swai H, Braden M and Williams DM. A Polymeric System for the Intra-oral Delivery of an Anti-fungal Agent. Biomater. 2001, 17, 2319
29. Riggs PD, Clough AS, Jenneson PM, Drew DW, Braden M and Patel MP. ^{3}He Ion-beam Analysis of Water Uptake and Drug Delivery. J. Controlled Release. 1999, 27, 165
30. Patel MP, Pearson G J, Braden M and Mirza MA. Fluoride Ion Release from Two Methacrylate Polymer Systems. Biomater. 1998, 21, 1911

31. Patel MP, Pavlovic P, Hughes FJ, King GN, Cruchley A and Braden M. Release of Recombinant Human Bone Morphogenetic Protein-2 from Heterocyclic Methacrylate Polymer Systems. Biomater. 2001, 1, 2081
32. Pouton CW and Akhtar S. Biosynthetic Polyhydroxyalkanoates and Their Potential in Drug Delivery. Adv. Drug Delivery Rev. 1996, 2, 133
33. Luten J, Van-Nostrum CF, De Smedt SC and Hennink WE. Biodegradable Polymers as Non-viral Carriers for Plasmid DNA Delivery. J. Controlled Release. 2008, 2, 97
34. Pitt CG. Polycaprolactone and Its Copolymers. In: Chasin M and Langer R, editors. Biodegradable Polymers as Drug Delivery Systems. New York: Marcel Dekker; 1990
35. Mathiowitz E, Jaco J, Pekarek K and Chickering D. Morphological Characterization of Bioerodible Polymer, 3. Characterization of the Erosion and Intact Zones in Polyanhydrides using Scanning Electron Microscopy. Macromol. 1993, 26, 6756
36. Göpferich A. Polymer Bulk Erosion. Macromol. 1997, 9, 2598
37. Shah SS, Cha Y and Pitt CG. Poly(glycolic acid-co-dl-lactic acid): Diffusion or Degradation Controlled Drug Delivery? J. Control Rel. 1992, 18, 261
38. Huang X and Brazel CS. On the Importance and Mechanisms of Burst Release in Matrix-Controlled Drug Delivery Systems. J. Control. Rel. 2001, 73, 121
39. Siepmann J and Gopferich A. Mathematical Modeling of Bioerodible, Polymeric Drug Delivery Systems. Adv. Drug Deliv. Rev. 2001, 48, 229
40. Conte U, Colombo P, Gazzaniga A, and La Manna A. Swelling-Activated Drug Delivery Systems. Biomater. 1988, 9, 489
41. Bourne DW. Pharmacokinetics. In: Banker GS, Rhodes CT, editors. Modern Pharmaceutics. 4th ed. New York: Marcel Dekker Inc; 2002
42. Mulye, NV and Turco SJ. A Simple Model Based on First Kinetics to Explain Release of Highly Water Soluble Drugs from Porous Dicalcium Phosphate Dihydrate Matrices. Drug Dev. Ind. Pharm. 1995, 21, 943

43. Higuchi T. Mechanism of Sustained Action Medication. Theoretical Analysis of Rate of Release of Solid Drugs Dispersed in Solid Matrices. J. Pharm. Sci. 1963, 52, 1145
44. Desai SJ, Simonelli AP, Higuchi WI. Investigation of Factors Influencing Release of Solid Drug Dispersed in Inert Matrices. J. Pharm. Sci. 1965, 54, 1459
45. Lapidus H and Lordi NG. Drug Release from Compressed Hydrophilic Matrices. J. Pharm. Sci. 1968, 57, 1292
46. Siepmann J and Peppas N. A. Modeling of Drug Release from Delivery Systems Based on Hydroxypropylmethylcellulose (HPMC). Adv. Drug Deliv. Rev. 2001, 48, 139
47. Costa P and Lobo JMS. Modeling and Comparison of Dissolution Profiles. Eur. J. Pharm. Sci. 2001, 13, 123
48. Korsmeyer RW, Gurny R, Doelker E, Buri P and Peppas NA. Mechanisms of Solute Release from Porous Hydrophilic Polymers. Int. J. Pharm. 1983, 15, 25
49. Ritger PL, Peppas NA. A Simple Equation for Description of Solute Release. I. Fickian and Non-Fickian Release from Non-Swellable Devices in the Form of Slabs, Spheres, Cylinders or Discs. J. Control Release. 1987, 5, 23
50. Ritger PL and Peppas NA. A Simple Equation for Description of Solute Release. I. Fickian and Anomalous Release from Swellable Devices. J. Control Release. 1987, 5, 37
51. Rinaki E, Valsami G and Macheras P. The Power Law Can Describe the 'Entire' Drug Release Curve from HPMC-Based Matrix Tablets: a Hypothesis. Int. J. Pharm. 2003, 255, 199
52. Emilson CG. Potential Efficacy of Chlorhexidine against Mutans Streptococci and Human Dental Caries. J. Dent. Res. 1994, 73, 682
53. Axelsson P and Lindhe J. Efficacy of Mouthrinses in Inhibiting Dental Plaque and Gingivitis in Man. J. Clin. Periodontol. 1987, 14, 205

54. Coventry J and Newman HN. Experimental Use of a Slow Release Device Employing Chlorhexidine Gluconate in Areas of Acute Periodontal Inflammation. J. Clin. Periodontol. 1982, 9, 129
55. Addy M, Rawle L, Handley R, Newman HN and Coventry JF. The Development and in vitro Evaluation of Acrylic Strips and Dialysis Tubing for Local Drug Delivery. J. Periodontol. 1982, 53, 693
56. Jeffcoat MK, Bray KS, Ciancio SG, Dentino AR, Fine DH, Gordon JM. Adjunctive Use of a Subgingival Controlled Release Chlorhexidine Chip Reduces Probing Depth and Improves Attachment Level Compared with Scaling and Root Planing Alone. J. Periodontol. 1998, 69, 989
57. Yue IC, Poff J, Cortes ME, Sinisterra RD, Faris CB and Hildgen P. A Novel Polymeric Chlorhexidine Delivery Device for the Treatment of Periodontal Disease. Biomater. 2004, 25, 3743
58. Scott T and Eagleson M. Concise Encyclopedia: Biochemistry, 2nd ed. New York: Walter de Gruyter; 1988
59. Hirayama K, Akashi S, Furuya M and Fukuhara KI. Rapid Confirmation and Revision of the Primary Structure of Bovine Serum Albumin by ESIMS and FRIT-FAB LC/MS. Biochem. Biophys. Res. Commun. 1990, 2, 639
60. Wischke C and Borchert HH. Fluorescein Isothiocyanate Labelled Bovine Serum Albumin (FITC-BSA) as a Model Protein Drug: Opportunities and Drawbacks. Pharmazie. 2006, 9, 770
61. Petrov AI, Volodkin DV and Sukhorukov GB. Protein-Calcium Carbonate Coprecipitation: A Tool for Protein Encapsulation. Biotechnol. Prog. 2005, 21, 918
62. Decher G, Hong JD and Schmitt J. Buildup of ultrathin multilayer films by a self-assembly process 1. Consecutive adsorption of anionic and cationic bipolar amphiphiles on charged surfaces. Thin Solid Films. 1992 , 1, 831

63. Sukhorukov GB. Novel Methods to Study Interfacial Layers. In: Möbius D and Miller R, editors. Studies in Interface Science. Amsterdam: Elsevier; 2001
64. Volodkin DV, Balabushevitch NG, Sukhorukov GB and Larionova NI. Model System for Controlled Protein Release: pH-sensitive Polyelectrolyte Microparticles. STP Pharm. Sci. 2003 , 3, 163
65. Sukhorukov GB, Antipov AA, Voigt A, Donath E and Möhwald H. pH-Controlled Macromolecule Encapsulation in and Release from Polyelectrolyte Multilayer Nanocapsules. Macromol. Rapid Commun. 2001, 1, 44
66. Volodkin DV, Petrov AI, Prevot M, and Sukhorukov GB. Matrix Polyelectrolyte Microcapsules: New System for Macromolecule Encapsulation. Langmuir. 2004, 8, 3398
67. Kenawy ER, Bowlin GL, Mansfield K, Layman J, Simpson DG, Sanders EH and Wnek GE. Release of Tetracycline Hydrochloride from Electrospun Poly(ethylene-co-vinylacetate), Poly(lactic acid), and a Blend. J. Control. Release. 2002, 81, 57
68. Luu YK, Kim K, Hsiao BS, Chu B and Hadjiargyrou M. Development of a Nanostructured DNA Delivery Scaffold via Electrospinning of PLGA and PLA-PEG Block Copolymers. J. Control. Release. 2003, 89, 341
69. Chew SY, Wen J, Yim EKF and Leong KW. Sustained Release of Proteins from Electrospun Biodegradable Fibers. Biomacromol. 2005, 6, 2017
70. Huang ZM, Zhang YZ, Kotaki M and Ramakrishna S. A Review on Polymer Nanofibers by Electrospinning and Their Applications in Nanocomposites. Compos. Sci. Technol. 2003, 63, 2223
71. Jiang H, Fang D, Hsiao B, Chu B. and Chen W. Preparation and Characterization of Ibuprofen-Loaded Poly(lactide-co-glycolide)/Poly(ethylene glycol)-g-chitosan Electrospun Membranes. J. Biomater. Sci. Polym. Ed. 2004, 15, 279
72. Huang X and Brazel CS. On the Importance and Mechanisms of Burst Release in

Matrix-Controlled Drug Delivery Systems. J. Control. Release. 2001, 73, 121

73. Van de Weert M, Hennink WE and Jiskoot W. Protein Instability in Poly(lactic-co-glycolic acid) Microparticles. Pharm. Res. 2000, 17, 1159
74. Houchin ML and Topp EM. Chemical Degradation of Peptides and Proteins in PLGA: A Review of Reactions and Mechanisms. J. Pharm. Sci. 2008, 97, 2395
75. Xu XL, Yang LX, Xu XY, Wang X, Chen XS, Liang QZ, Zeng J and Jing XB. Ultrafine Medicated Fibers Electrospun from W/O Emulsions. J. Control. Release. 2005, 108, 33
76. Sun ZC, Zussman E, Yarin AL, Wendorff JH and Greiner A. Compound Core-shell Polymer Nanofibers by Co-electrospinning. AdV. Mater. 2003, 15, 1929

Chapter 6

Drug Release from Poly(ethyl methacrylate/tetrahydrofurfuryl methacrylate) Systems

6.1 Introduction

Changing the polymer morphology is one of the ways to influence drug release behaviour. A porous polymer matrix will enhance the drug release from the system. The applicability of supercritical fluid foaming technology has already proved to be beneficial in the area of biomedical and tissue engineering[1-3]. Barry *et al.*[1] have demonstrated the potential usage of porous poly (ethyl methacrylate / tetrahydrofurfuryl methacrylate) (PEM/THFM) system as non-degradable scaffold for the tissue engineering of cartilage. They applied $scCO_2$ foaming technique to fabricate the porous structure of the polymer and studied the effects of changes in the processing conditions on the porosity, pore size, etc. Described in this Chapter,

research focused on the applications of PEM/THFM system in the drug delivery. Traditionally cured PEM/THFM system was foamed by $scCO_2$ and used as a drug carrier. Chlorhexidine (CX) was chosen as the dispersed drug. The morphology, density and porosity of the system were studied. The effects of $scCO_2$ foaming conditions on the CX release behaviour were investigated. Higuchi's model and Korsmeyer-Peppas' model were used to study the drug release kinetics.

6.2 Experimental

6.2.1 Materials and Equipments

PEM, a powder containing 0.6 wt.% residual benzoyl peroxide was used as supplied (Bonar polymers Ltd, Newton Aycliffe Co., Durham, UK). The THFM was obtained from Rohm Chemie, GmbH (Darmstadt, Germany) and the N,N-dimethyl-p-toluidine was acquired from Aldrich (UK). The chlorhexidine diacetate salt hydrate was purchased from Sigma (UK) (Fig. 6.1). All materials were used as supplied without further purification.

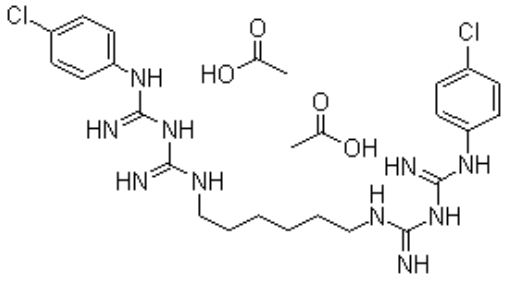

Fig. 6.1 *The molecular structure of chlorhexidine diacetate salt hydrate*

A liquid withdrawal CO_2 cylinder at 725 psi pressure was supplied by BOC gases. The CO_2 was chilled to -6 °C before being delivered via an Isco model 100D syringe pump with a chilled piston barrel. The custom made 450 ml high pressure autoclave

as described in Chapter 3 was used in all experiments. In addition, without exception, the water used was prepared in a three-stage Millipore Milli-Q Plus 185 purification system and had a resistivity higher than 18.2 MΩcm.

6.2.2 Synthesis

All samples were initially prepared using a similar procedure as follows: The CX was blended with the PEM powder at 3 levels, 6 wt.%, 12 wt.% and 18 wt.%. The N,N-dimethyl-p-toluidine (DMPT: a room temperature polymerization activator) was added to the THFM monomer at a level of 2.5 vol.% The CX-PEM powder was added to the THFM monomer at a ratio of 1 g powder to 0.6 ml monomer. After mixing, the material was placed in the circled cavity of a Teflon mould, 13.5 mm × 1.5 mm, between two microscope slides covered with acetate sheets. Then, the sandwiched mould was held together under a pressure of ca. 29 psi and allowed to cure at room temperature for 12 hr.

$ScCO_2$ assisted foamed samples were prepared as follows: samples were placed into the autoclave which was sealed and filled with liquid CO_2 at 725 psi. The temperature of the autoclave was then held at 40 °C and different pressures were applied for various periods. All conditions are listed in Table 6.1. At the end of the experiment, the CO_2 was released over a period of 5 min or 30 min.

Table 6.1 *Supercritical CO_2 conditions applied*

Name	CX loading [wt.%]	T [°C]	P [psi]	$T_{saturation}$	$T_{depressurization}$
6%2200psi3hr5min	6	40	2200	3hr	5
6%2200psi3hr30min	6	40	2200	3hr	30
6%1300psi3hr5min	6	40	1300	3hr	5
6%1300psi3hr30min	6	40	1300	3hr	30
12%2200psi3hr5min	12	40	2200	3hr	5
12%2200psi3hr30min	12	40	2200	3hr	30
12%1300psi3hr5min	12	40	1300	3hr	5
12%1300psi3hr30min	12	40	1300	3hr	30
18%2200psi3hr5min	18	40	2200	3hr	5
18%2200psi3hr30min	18	40	2200	3hr	30
18%2200psi1hr5min	18	40	2200	1hr	5
18%2200psi1hr30min	18	40	2200	1hr	30
18%1300psi3hr5min	18	40	1300	3hr	5
18%1300psi3hr30min	18	40	1300	3hr	30
18%1300psi1hr5min	18	40	1300	1hr	5
18%1300psi1hr30min	18	40	1300	1hr	30

6.2.3 Characterization

All the specimens were freeze dried over 22 hr before any characterization.

X-ray powder diffraction (XRD) data were recorded using a Siemens D5000 Diffractometer, for which the X-ray beam was Cu-K radiation ($k\alpha_1$ = 1.5406 Å) and

the radiation operated at 40 kV. Data were collected over the 2θ range 5-45 º with a step size of 0.01 º and a step time of 1 sec.

SEM was carried out on the products using a JEOL 6300 (accelerating voltage 10 kV). Prior to examination, samples were mounted onto 5 cm diameter circular aluminium stubs using carbon cement, coated with gold.

The DSC was calibrated using a pure sample of indium. For DSC runs, samples were carefully weighed in aluminium pans and covered with aluminium lids incorporating a pinhole. DSC curves were obtained from the first heating run at a rate of 10 °C/min under a dry nitrogen atmosphere from 30 to 200 °C.

Fourier transform infrared spectroscopy (FTIR) spectra were obtained using a Thermo Nicolet FTIR 8700 spectrometer equipped with a drift cell. Spectra were obtained at 8 cm^{-1} resolution, averaging 256 scans. The sampling chamber of the photoacoustic cell was pre-purged with helium.

The skeletal density was determined by automated helium displacement pycnometry using the Ultrapycnometer 1000 (Quantachrome) using a known mass of foamed samples under vacuum at room temperature.

Mercury intrusion porosimetry was performed using the PoreMaster 60 porosimeter. Pressure intrusion porosimetry (0-60000 psi) was employed to obtain pore diameter distributions in the range of 3.6 nm-360 μm.

The release of CX from supercritical fluid foamed CX-PEM/THFM samples was monitored using UV-Vis spectroscopy dissolution tests (LAMBDA 950

Spectrophotometer). 100 ml of sterile deionized water was used as the dissolution medium and was maintained at temperature of 37±0.5 °C, stirred with a magnetic stirrer at a rate of 100 rpm. Samples containing an equivalent quantity of 20 mg CX were immersed in the medium. 3 ml aliquots were collected and the same volume of fresh deionised water was immediately replaced. The aliquots were obtained at 2 hr, 6 hr, and 1, 2, 3, 4, 7, 9, 11, and 14 days, respectively. The CX concentration was determined using a UV-Vis spectrophotometer and the UV absorption was measured at 255 nm. The concentration of CX in the solution was calculated using the calibration curve established using a known concentration. The cumulative percentage of CX release over time was calculated using a spreadsheet package (Microsoft Excel).

6.2.4 Mathematical Modelling of Drug Release Kinetics

Data obtained from in-vitro release studies were analyzed according to different kinetic equations to identify the drug release mechanisms. The kinetic models studied were Higuchi's model and Korsmeyer-Peppas' equation, which are described in detail in Section 5.4.2.

6.3 Results and Discussion

6.3.1 Morphology

Using $scCO_2$ during processing has led to materials with significantly porous morphologies and micro-cellular polymer formation. The morphologies of all the $scCO_2$ treated samples are presented in Fig. 6.2. The unfoamed traditional sample is glassy opaque. After foaming with $scCO_2$, the samples lost the glassy opaque

appearance and became white. Also, the sizes of the samples after $scCO_2$ treatment were bigger compared with traditional dense samples. CO_2 depressurization time of 30 min clearly resulted in a bigger size than 5 min for all the samples treated with 1300 psi saturation pressure. 5 min depressurization time allows a more rapid loss of gas through the fast diffusion of CO_2 which results in a low expansion ratio. By contrast, the reduced rate of gas lost in 30 min gives a higher expansion ratio. However, for samples treated under 2200 psi CO_2 condition, there was no obvious size difference with different depressurization times, regardless of the CX content. The possible reason for this is that CO_2 at 2200 psi possess much more gas than CO_2 at 1300 psi, so the depressurization rate of both 30 min and 5 min are relatively fast and so did not produce a significant difference in the expansion ratio.

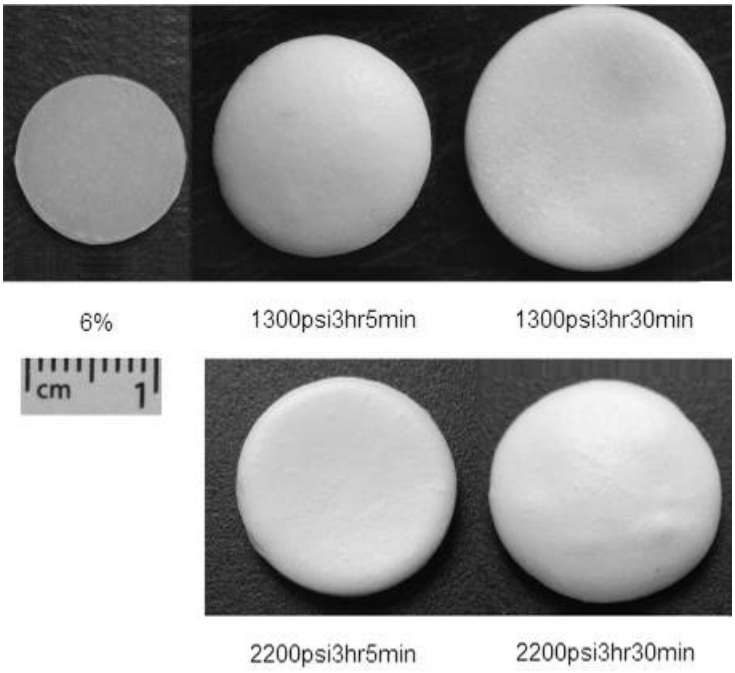

Fig. 6.2 *The morphologies of traditional cured and $scCO_2$ foamed 6 wt.% CX samples under different $scCO_2$ processing conditions*

SEM images were obtained for $scCO_2$ foamed samples with different CX content.

Fig. 6.3 shows a porous core structure encased by a nonporous skin after $scCO_2$ foaming processing. Previously, it was found that the thickness of this non-porous skin decreases with increasing CO_2 saturation pressure with PMMA[4]. This was suggested by our results with PEM/THFM as well (Fig. 6.3b).

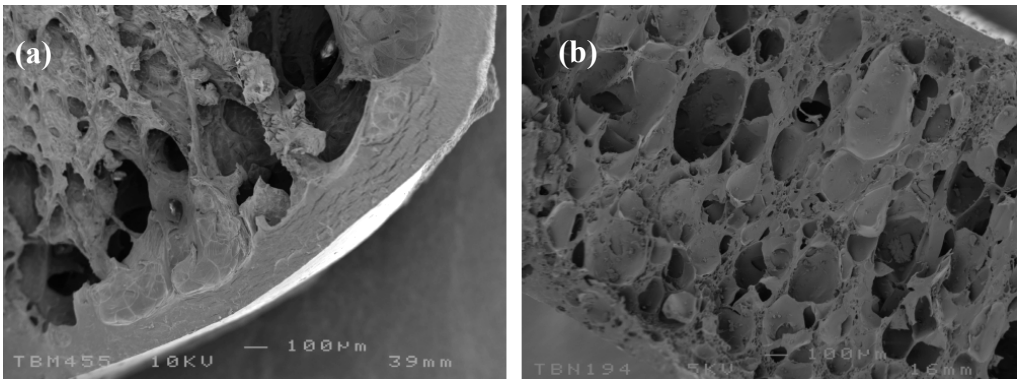

Fig. 6.3 *SEM images of $scCO_2$ foamed 6 wt.% CX samples showing dense skin with porous foam structure inside treated under (a) 1300 psi and (b) 2200 psi*

The porous structure of the polymer was produced based on the expansion of a gaseous phase dispersed throughout the polymer melt. In other words, they are produced through the utilization of the thermodynamic instability of a gas and polymer system[5]. Three major steps must be performed in order to make use of such instability: saturation of a polymer with CO_2; formation of expandable bubbles (nucleation); cell growth and density reduction. The critical parameters for controlling foam development in a CO_2 foaming process are the concentration of CO_2 in the polymer and the rate of CO_2 escaping from the polymer[6].

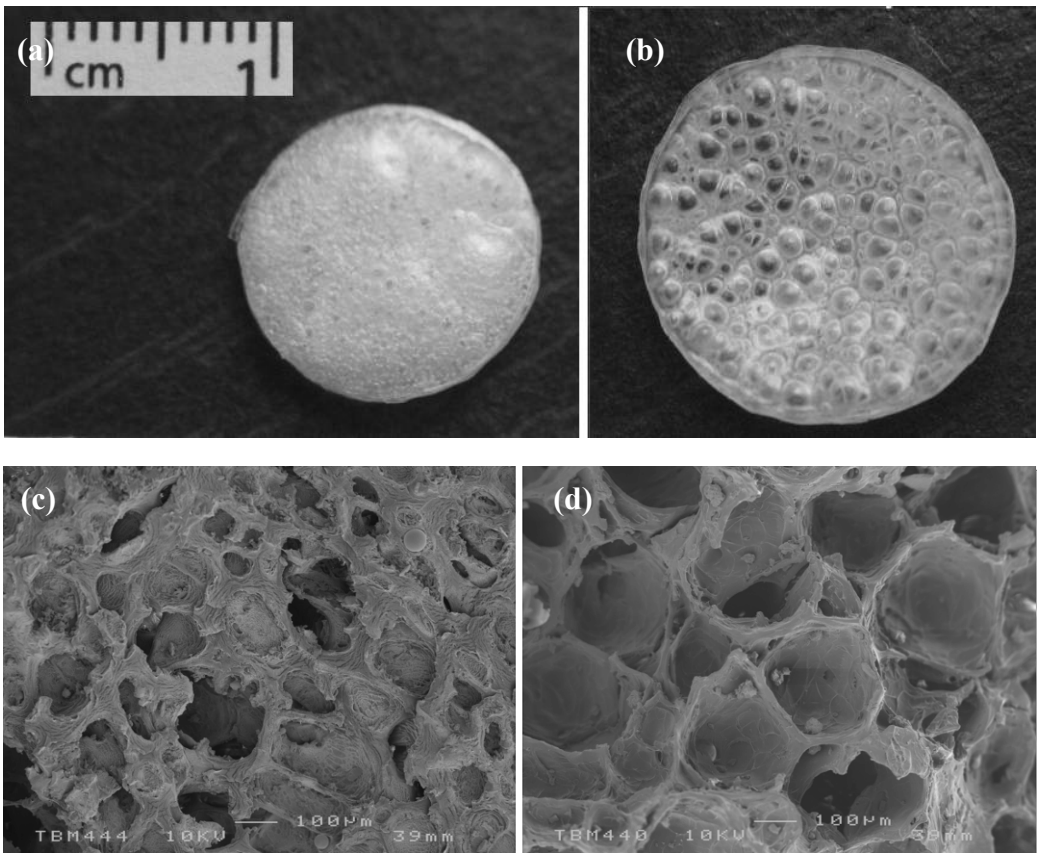

Fig. 6.4 *Images showing $scCO_2$ treated samples with different depressurization time Other processing conditions: 1300 psi saturation pressure, 3 hr saturation time. Pure PEM/THFM sample (a) 5 min, (b) 30min. 6 wt.% CX-PEM/THFM samples: (c) 5min, (d) 30 min*

The study on the effect of depressurization time was carried out while keeping other operating conditions constant, e.g., 1300 psi saturation pressure with 3hr saturation time. When depressurization occurred rapidly at 5 min, the samples displayed a small pore structure (Fig. 6.4a and c) compared with the larger pores obtained by the slow 30 min venting process (Fig. 6.4b and d). A difference in depressurization time gives a different depressurization rate, which plays an important role in the foaming process. A faster depressurization rate resulted in higher supersaturation, leading, in turn, to a higher nucleation rate. Decreasing the depressurization rate permits the

nucleation sites to grow into larger pores, whilst also allowing the pores to coalesce into more open structures[7]. This effect has been proved by many reserachers[2,7-9]. In Barry et al.' research on PEM/THFM, within 30s vent, pore size is found within 50 - 150 μm and 200 - 900 μm for a 60 min vent[2]. Similar observations have also been found for other foamed polymer systems previously, such as PS, PLGA and PMMA [7-9].

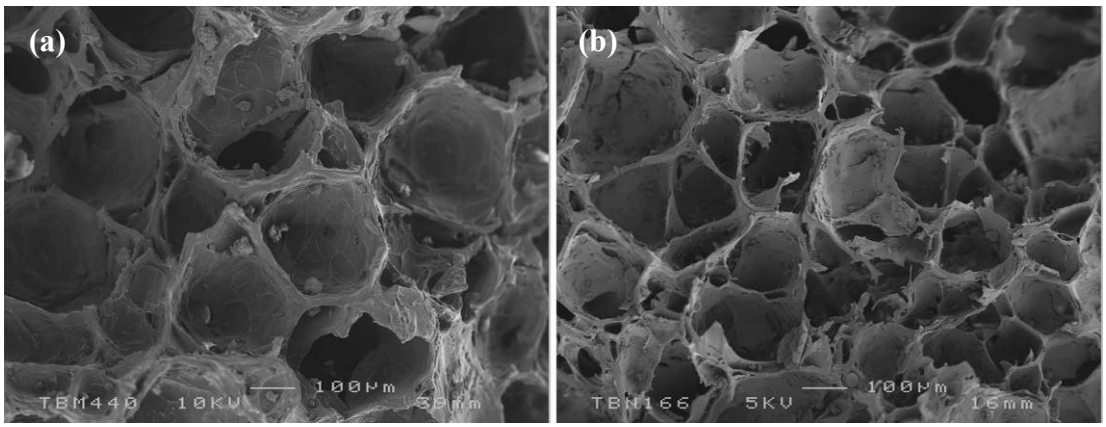

Fig. 6.5 *SEM images showing 6 wt.% CX-PEM/THFM samples treated with $scCO_2$ under different saturation pressure: (a) 1300 psi and (b) 2200 psi. Processing conditions: 3 hr saturation, 30 min depressurization*

The effect of saturation pressure, in which 1300 and 2200 psi were chosen; on the foam structure was studied keeping the other parameters constant, e.g., 3 hr saturation time and 30 min depressurization time. The images in Fig. 6.5 show that the pore size is shifted towards smaller sizes and size distribution becomes narrower with increased CO_2 saturation pressure. The saturation pressure directly determines the concentration of CO_2 in the polymer. With increasing saturation pressure, the concentration of CO_2 in the matrix increased, as well as the dissolution of CO_2[8,10]. Therefore, a greater amount of CO_2 is incorporated into PEM/THFM at a higher CO_2 saturation pressure, providing more CO_2 molecules for foaming upon the release of

pressure. This will produce a higher nucleation density due to lower interfacial tension and viscosity in the polymer matrix. A change in temperature has an effect as well[8]. An expansion in the gas will cause a drop in temperature. Lower saturation pressure produces a smaller temperature drop, hence the actual temperature following depressurization is higher, by comparison. Therefore, in this case, pores have more time to grow before they are frozen. Moreover, although the depressurization time is the same, the depressurization rate for 1300 psi is much slower than for 2200 psi due to the pressure difference, which also favours larger pores, as discussed in the previous paragraph.

A comparison of the porous structure of the samples with different CX content is presented in Fig. 6.6. The images of 18 wt.% CX samples show more CX particles, which is as expected. With the increase of the CX content, the size of the pores becomes smaller and CX particles inside the matrix decrease the available free volume in the matrix. During polymer expansion, the CX particles tend to lock the polymer chains and decrease the CO_2 absorption in the polymer. During the depressurization, CX particles inhibit the escape of CO_2 from the polymer and give less opportunity for CO_2 expansion; thereby promoting slow pore growth leading to smaller pore structures.

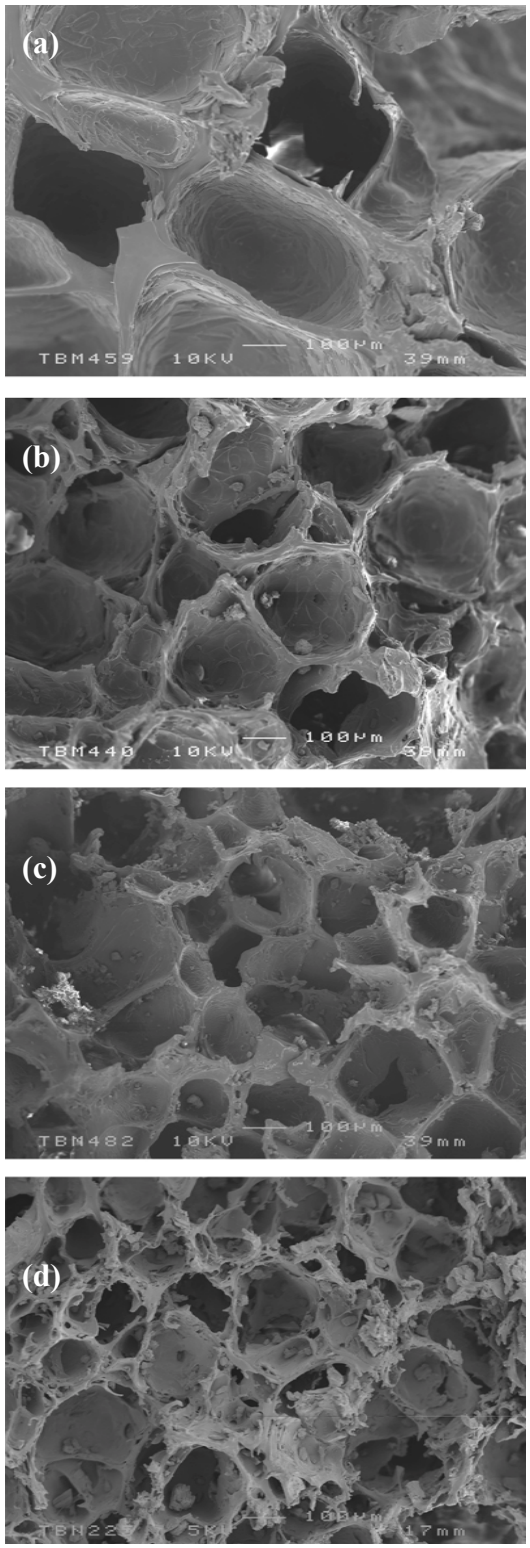

Fig. 6.6 *SEM images of $scCO_2$ foamed samples containing (a) pure PEM/THFM (b) 6 wt.%, (c) 12 wt.% and (d) 18 wt.% CX under 1300 psi for 3 hr with 30 min depressurization time*

The effect of changing the saturation time was studied by saturating of the sample under $scCO_2$ conditions for 1 hr or 3 hr with other parameters remaining constant. The difference is not obvious between the results for 6 wt.% CX samples and those from the SEM observation. However, with the increase of the CX constant, for samples with 18 wt.% CX, a shorter saturation time (1 hr) produced a broader distribution of large pores (Fig. 6.7), while a longer saturation time (3 hr) produced smaller pores with a narrow distribution. CO_2 might not be distributed uniformly throughout the polymer within a short saturation time especially with more CX particles inside the matrix retarding the absorption of the CO_2. While longer saturation time allows for a full diffusion of CO_2 into the polymer, leading to more uniform porous structures.

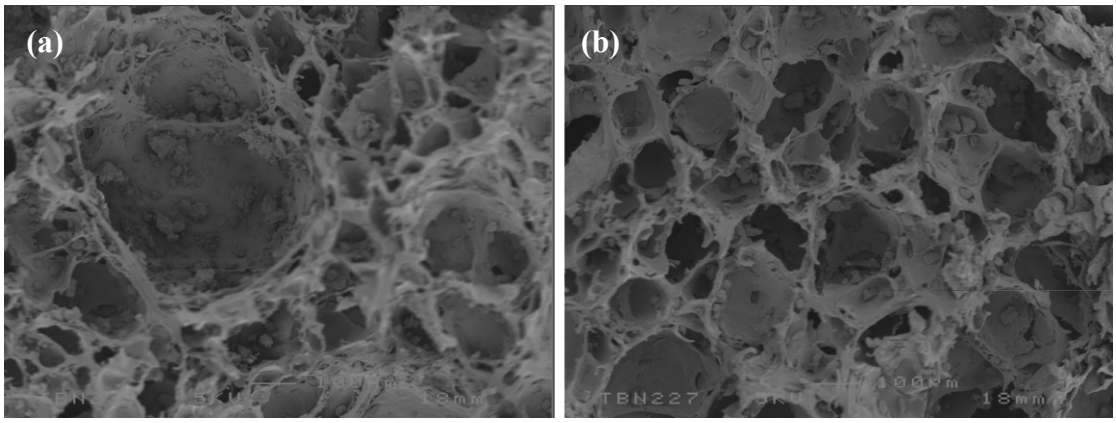

Fig. 6.7 *SEM images of 18 wt.% CX samples treated with $scCO_2$ under different saturation times: (a) 1 hr and (b) 3 hr. Processing conditions: 1300 psi saturation pressure, 30 min depressurization*

.

Helium pycnometry was used to analyse the density of the samples. For $scCO_2$ treated samples, the non-porous skin was removed prior to the measurement. The densities of traditional and $scCO_2$ foamed samples, the comparison of the densities in terms of CO_2 depressurization time and the CO_2 saturation pressure are presented in Fig. 6.8. $ScCO_2$ foaming significantly decreases the density of the sample as

expected. Increasing depressurization time from 5 min to 30 min results in a lower density for all samples (Fig. 6.8b), which agrees with the microscope results showing higher expansion ratios for samples with longer depressurization time. Moreover, higher CO_2 saturation pressure (2200 psi) results in a slightly lower density than for those using 1300 psi (Fig. 6.8c).

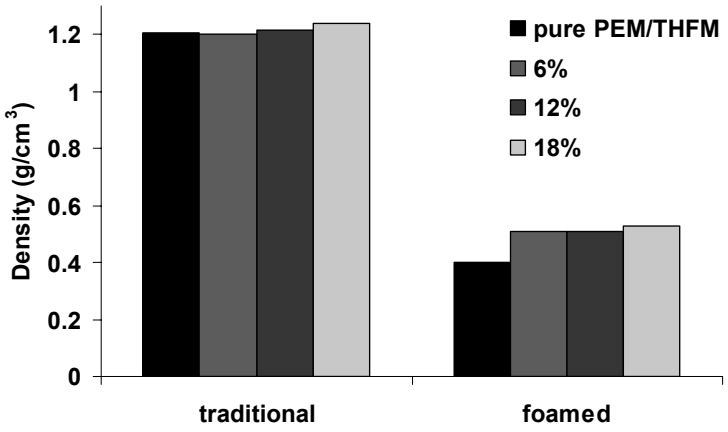

(a)

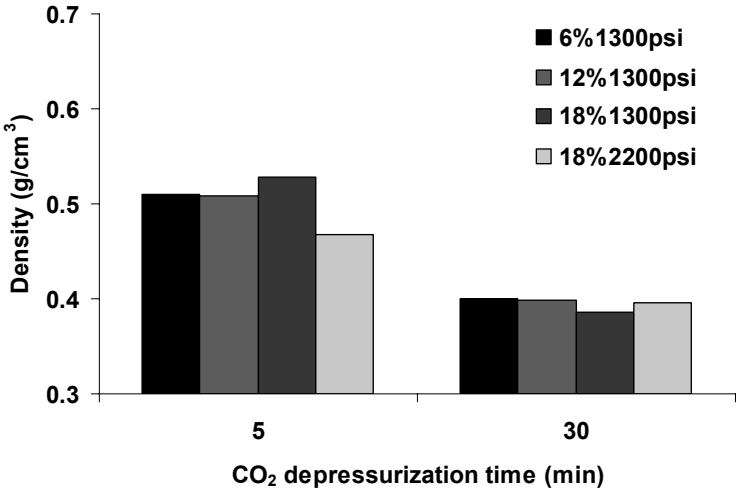

(b)

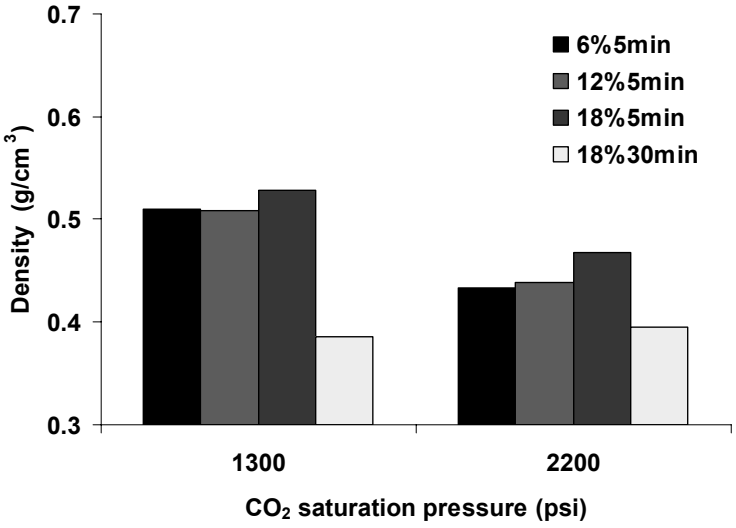

(c)

Fig. 6.8 *A comparison of the densities of the samples in terms of (a) traditional vs. foamed samples under 1300 psi saturation pressure, 3hr saturation time, 5 min depressurization time (b) CO_2 depressurization time and (c) CO_2 saturation pressure. Both (b) and (c) are under 3hr saturation time.*

Table 6.2 *The porosity of traditional cured and scCO_2 foamed samples (operation condition: 1300 psi saturation pressure, 3 hr saturation time, 30 min depressurization time)*

Sample	Mean pore diameter [μm]	Porosity [%]
Traditional pure PEM/THFM	0.19±0.03	0.73±0.1
Foamed pure PEM/THFM	25.9±2.2	80.1±1.2
6 wt.%	22.1±3.6	70.1±2.3
12 wt.%	19.3±1.9	56.2±1.3
18 wt.%	18.0±3.3	49.4±5.3

The pore structure was also analysed by MIP. The data of the mean pore diameter and porosities are summarized in Table 6.2. It was found that the porosity and mean

pore size significantly decreased when the content of CX increased. (from 70 % porosity for 6 wt.% CX samples to 49 % porosity for 18 wt.% CX samples). Although the porosity results are in agreement with the SEM observations, these images show much larger pore diameters (in the order of 200 μm). Barry *et al.*[2] also witnessed this phenomenon and they attributed this finding to the differences in the theories of these two techniques. Porosimetry measures the diameter of the pore opening can be smaller than the pore cavity diameter[2]. Therefore, when a large number of very small pore openings (< 20 μm) is presented, the result detected by porosimetry would be dramatically smaller than the one observed from SEM. The combination of different methods in the analysis facilitates the extraction of information in a more exhaustive way.

6.3.2 Thermal Analysis

The thermal behaviour of materials is examined by DSC analysis, which is presented in Fig. 6.9. A peak at around 152 ºC which indicates the melting of crystallized CX can be observed in all the CX-PEM/THFM samples. A glass transition temperature (T_g) of around 55 ºC for PEM/THFM polymer systems was also observed. The $scCO_2$ foamed samples show higher T_g than unfoamed samples regardless of CX content. Fig. 6.6 only presents the foamed sample of 18 wt.% CX content. (T_g around 55 ºC) Data of samples of other CX content can be found in Table 6.3.

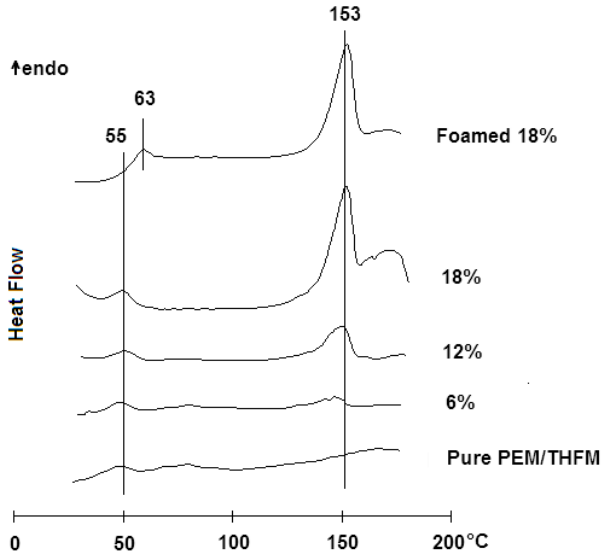

Fig. 6.9 *The DSC curves for traditional cured pure PEM/THFM, 6 wt.%, 12 wt.%, 18 wt.% CX content samples and scCO₂ foamed 18 wt.% CX samples. (operation condition: 1300 psi saturation pressure, 3 hr saturation time, 30 min depressurization time)*

Table 6.3 *DSC data of T_g onset and T_m of samples*

Sample	T_g [ºC]	T_m [ºC]
Pure PEM/THFM	54	--
Pure CX	--	156.3
6 wt.%	51	150.4
6%1300psi3hr5min	61	152.4
6%2200psi3hr5min	63	151.5
12 wt.%	50	152.8
12%1300psi3hr30min	61	154.5
12%2200psi3hr30min	64	153.8
18 wt.%	51	153.9
18%1300psi3hr5min	63	155.3
18%2200psi3hr5min	63	156.0

6.3.3 FTIR Results

FTIR spectra of the $scCO_2$ foamed CX-PEM/THFM samples were collected and compared with the traditional cured samples (Fig. 6.10). The peak at 1635 cm^{-1} indicates a C=N stretching from the CX. The carbonyl bands (C=O) of PEM and THFM in the traditionally cured system were observed at 1731 and 1719 cm^{-1}, respectively (Fig. 6.10a). Only one single peak of C=O was observed in the traditionally cured CX-PEM/THFM samples. This peak slightly shifted to lower wave numbers (1727 cm^{-1}) with the increase of CX content (18 wt.%). Similarly, $scCO_2$ foamed CX-PEM/THFM systems have the same trend with drug loading (Fig. 6.10b). Gong *et al*.[11] found a larger shift of C=O peak (from 1724 to 1704 cm^{-1}) in the $scCO_2$ samples with the increase of CX content suggesting H-bonding interaction with the N-H groups of CX molecules. However, in this study, the shift is too tiny and happens in both traditional and foamed samples. The evidence is not good enough to conclude that the same interaction between polymer matrix and drug molecules appears after being treated with $scCO_2$ in this case. For the $scCO_2$ treated samples under different $scCO_2$ conditions, no obvious differences are observed in the FTIR curves.

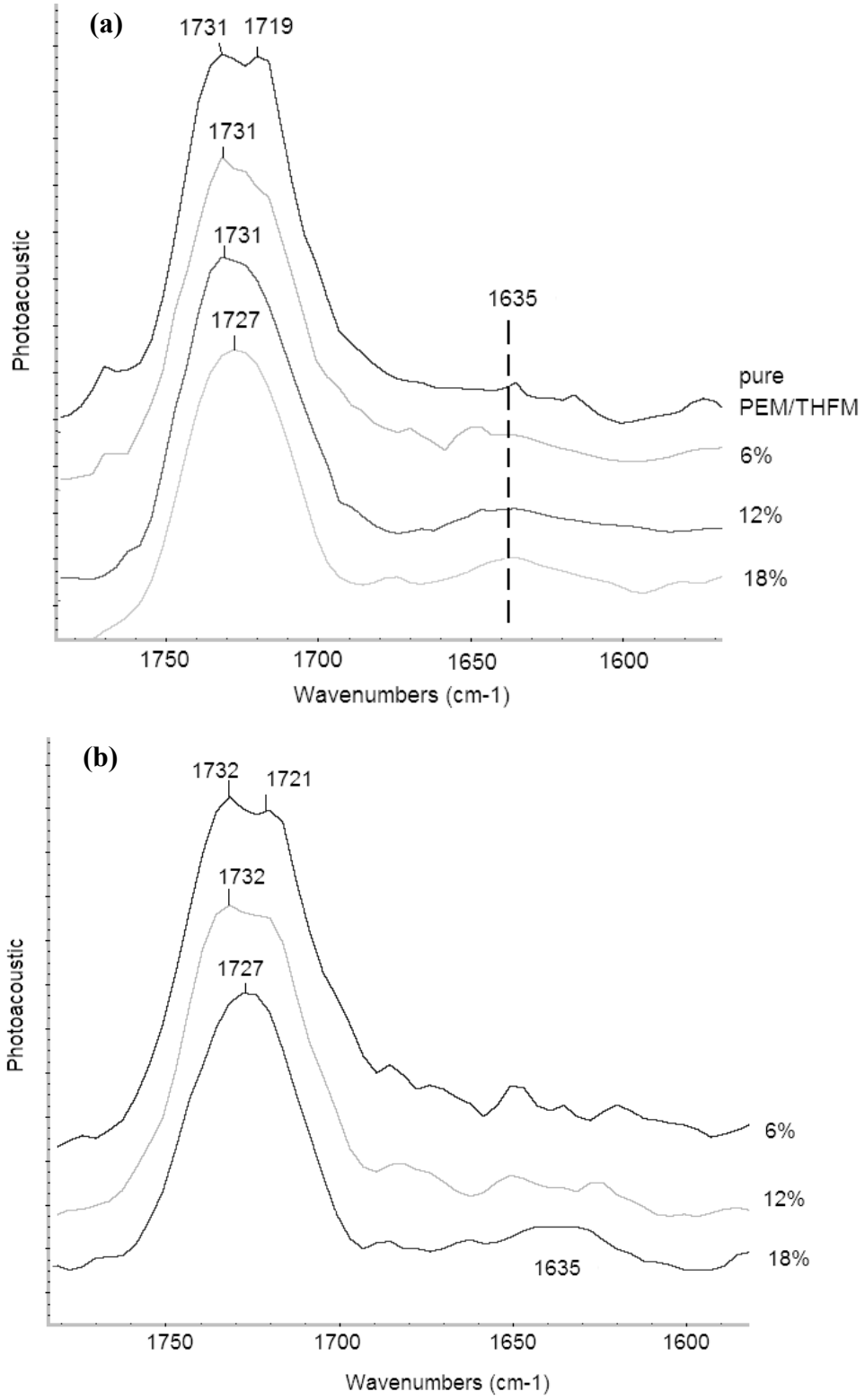

Fig. 6.10 *The FTIR curves of (a) traditionally cured and (b) $scCO_2$ foamed CX-PEM/THFM systems with different CX content*

6.3.4 XRD Results

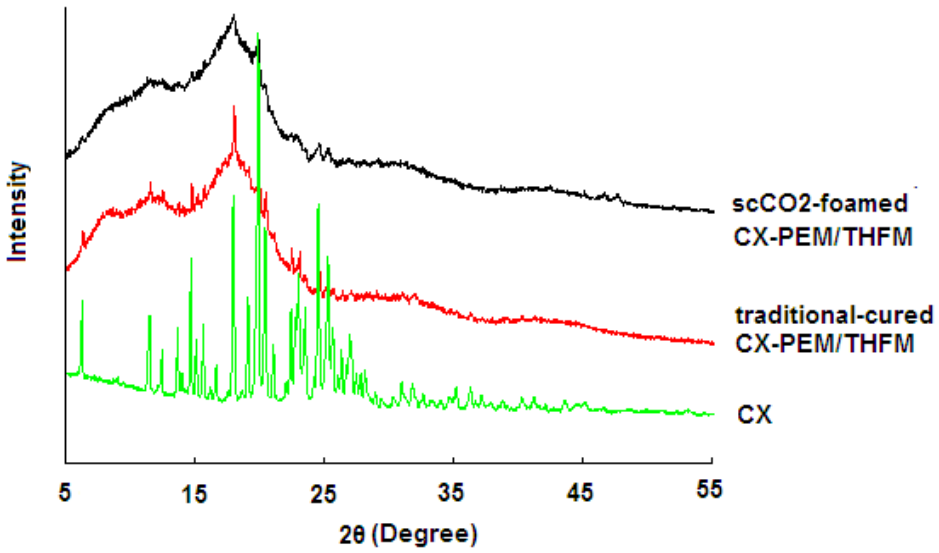

Fig. 6.11 *XRD analysis for pure CX, traditional cured samples (12 wt.% CX) and $scCO_2$ foamed samples (12 wt.% CX)*

The crystallinity of CX was analysed by XRD. The XRD patterns of pure CX powder and cured CX-PEM/THFM systems, both before and after $scCO_2$ processing, are presented in Fig. 6.11. The XRD pattern of pure CX powder shows strong characteristic peaks. After being cured in the PEM/THFM system, the peaks showing characteristic CX is still notable, which suggests the existence of the crystallized CX within the traditionally cured mixture. After being treated with $scCO_2$, no sharp characteristic peaks of CX are observed, which may suggest a decrease in crystallinity of CX in the polymer system. However, this decrease in crystallinity is so small that it can not be detected by DSC analysis, as discussed in the previous section.

6.3.5 Drug Release Studies

Drug release studies were carried out on $scCO_2$ foamed samples using UV-Vis spectrophotometry. A calibration curve was made to calculate the unknown concentration of CX in the solution. In UV-Vis spectrophotometry, an absorbance value is linearly correlated to solution concentration obeying the Beer-Lambert law[12],

$$A = \varepsilon bc \qquad 6\text{-}1$$

where A is the absorbance, ε is the molar absorbtivity ($Lmol^{-1}cm^{-1}$), b is the path length of the sample (cm), and c is the concentration of the compound in solution ($molL^{-1}$). A calibration curve is a plot of absorbance versus solution concentration, which is used to determine the concentration in an unknown solution by measuring its absorbance. The calibration curve of CX with UV-Vis at 255 nm shows a good linearity, $R^2 = 0.999$ over the range 2.5-35.7 mg/L. (Fig. 6.12).

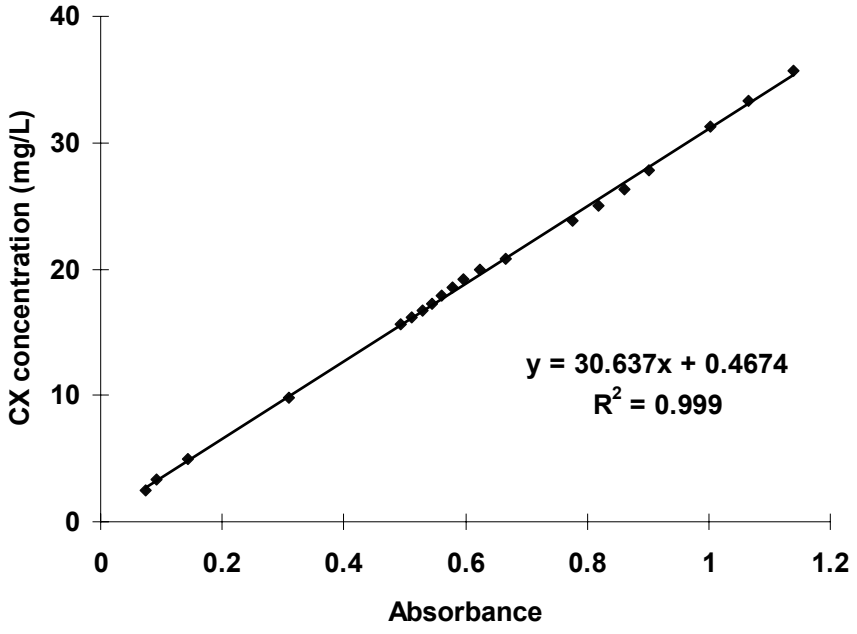

Fig. 6.12 *The calibration curve for CX at 255 nm*

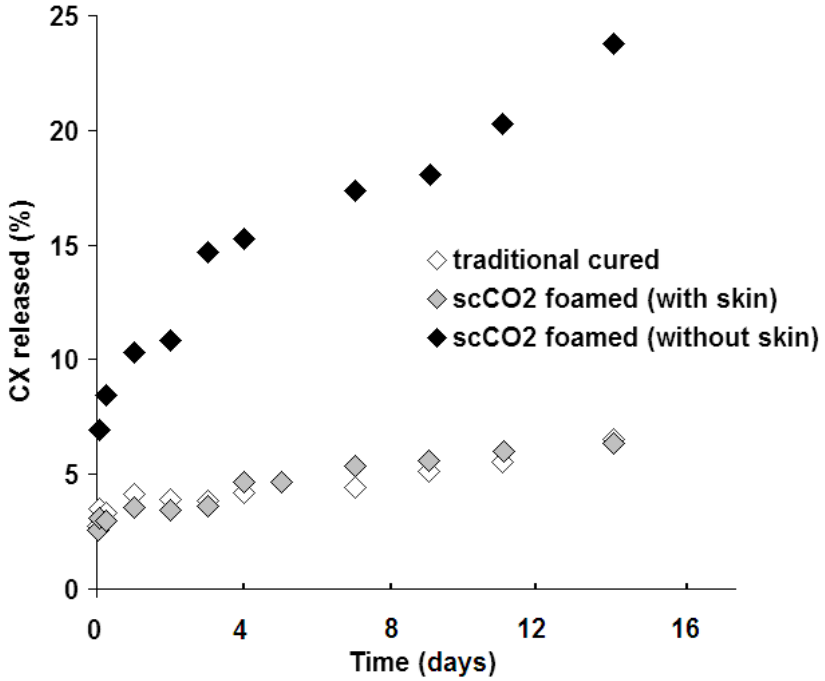

Fig. 6.13 *The release of CX from $scCO_2$ foamed samples containing 12 wt.% CX (40 °C and 1300 psi for 3 hr and 30 min as releasing time)*

Both the traditionally cured and $scCO_2$ foamed samples (with or without non-porous skin) are studied for drug release behaviour. The skin was cut off before testing for samples without skin. Fig. 6.13 shows the typical drug release curve of the percentage of CX released from the samples plotted against time. The release of CX from the traditional cured PEM/THFM system achieved a high initial release followed by a slower diffusion-controlled process and in total 7 % of CX was released in 14 days and 50 % of the total amount of CX released appeared in the first 24 hr. The $scCO_2$ foamed sample with the non-porous skin shows a similar level of drug release to that of traditionally cured samples, while drug release from samples without skin occurred much faster; approximately 4 times as much CX was released from the specimen (up to 25 %) over 14 days. The dense PEM/THFM matrix absorbs up to 30 % water in two stages: a rapid Fickian process followed by the development of discrete clusters of water at, as yet, unidentified osmotically active sites[13,14]. In the

presence of CX, the initial burst reflects surface release. Water diffuses into the matrix and the water cluster forms around CX particles to dissolve the drug upon contact. The drug particles, once dissolved, leave behind pores in the polymer matrix. The drug molecules can then diffuse out through the interconnecting pores. The slow diffusion-controlled release is controlled by the water uptake process of the polymer and the diffusion of the CX molecules. When the sample was foamed by $scCO_2$, the porous structure significantly promoted the water uptake and the diffusion of the CX molecules and therefore, a faster release of CX was achieved. This relative faster release of CX is expected to be related to porosity and the pore size of the sample, which will be discussed in more detail in terms of CX content, CO_2 saturation time and depressurization time. For the foamed sample with skin, the non-porous skin acts as a barrier inhibiting this advantage and controls the whole process when present on the surface of the specimen.

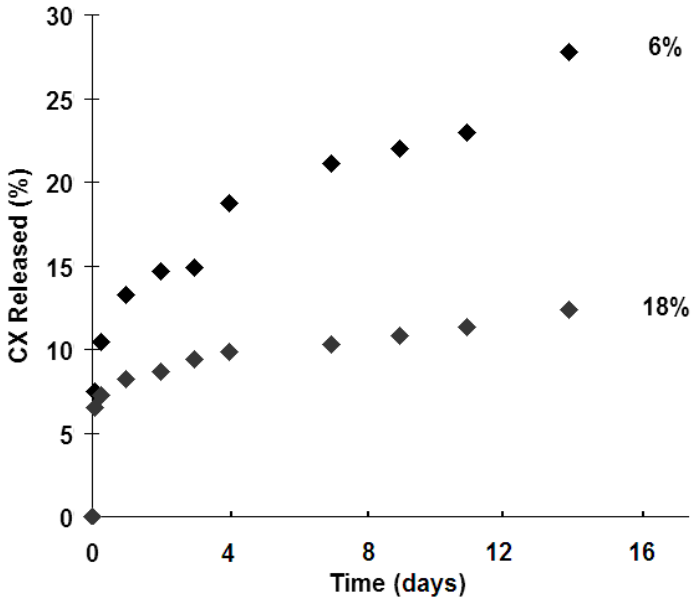

Fig. 6.14 *The release of CX from $scCO_2$ foamed samples containing 6 wt.% and 18 wt.% CX. All the samples were treated under $scCO_2$ at 40 °C and 2200 psi for 3 hr and 30 min as releasing time*

The samples having different CX loadings are compared in Fig. 6.14. An increase in the loading of the drug affecting the release kinetics has been reported earlier. In a study of CX release from traditional PEM/THFM systems, the release percentage of CX was higher with an increased loading of the drug[15]. In this study, although the actual amount of CX released from the 18 wt.% sample is higher than that from the 6 wt.% one, the release in percentage of load terms is lower. The release rates were increased with an increase in the effective pore size. With the increase in drug loading, the pore size became smaller (Fig. 6.6), which retarded the water penetration into the polymer matrix, thus reduced the release rate of the drug.

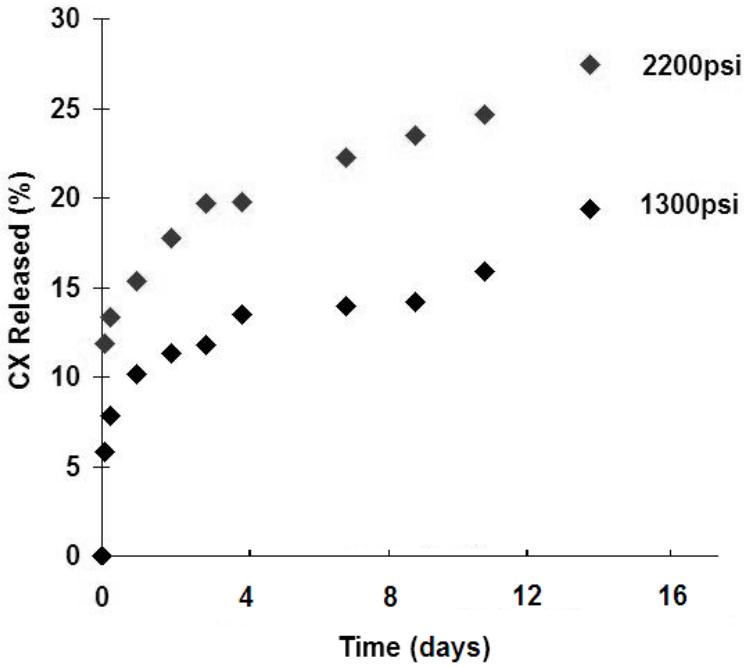

Fig. 6.15 *The release of CX from $scCO_2$ foamed samples containing 12 wt.% CX treated under $scCO_2$ at 40 °C 3 hr and 5 min as releasing time*

Fig. 6.15 compares the CX release for samples processed under different $scCO_2$ holding pressures. The 2200 psi sample gives a higher release rate than the 1300 psi sample. The 2200 psi sample has a lower density indicating a higher porosity of the

sample, which could speed up water uptake by the polymer and diffusion of the CX molecules, thereby causing a higher CX release rate.

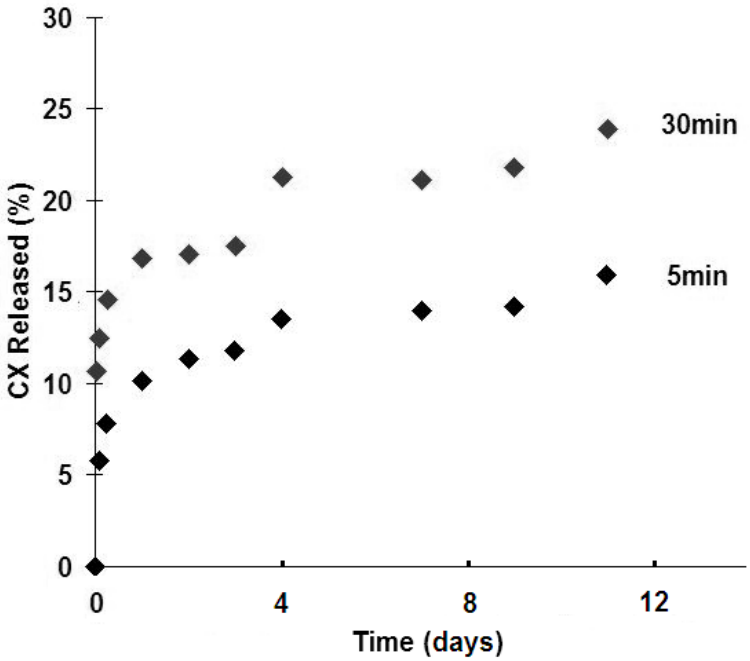

Fig. 6.16 *The release of CX from $scCO_2$ foamed samples containing 12 wt.% CX treated under $scCO_2$ at 40 °C and 1300 psi for 3 hr with a releasing time of 5 min and 30 min*

Fig. 6.16 shows that the release rate of the sample, with 30 min as releasing time, is higher than that of the sample processed using 5 min as the releasing time. The bigger pores in the 30 min release time sample may enhance the water uptake in the polymer and dissolve the CX inside the polymer, while for the 5 min release time sample, the smaller and more even pores may cause higher surface tension and prevent water permeation (Fig. 6.4).

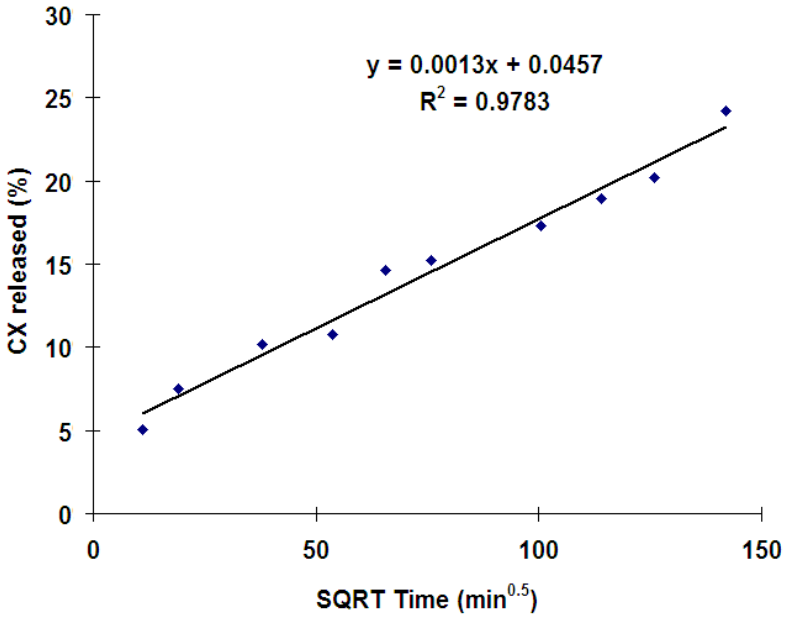

Fig. 6.17 *The cumulative release of CX versus square root time profile (Higuchi's model) for scCO₂ foamed samples containing 12 wt.% CX (40 °C and 1300 psi for 3 hr and 30 min as releasing time)*

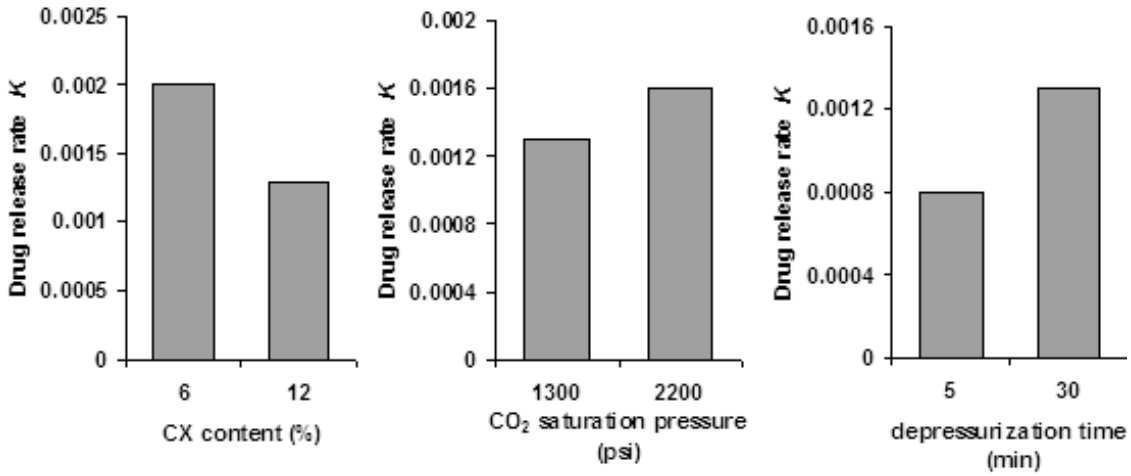

(a) (b) (c)

Fig. 6.18 *Effect of processing conditions on the Higuchi release rate (drug released %/time$^{1/2}$) of (a) CX content (b) CO_2 saturation pressure and (c) CO_2 depressurizaiton time*

Both Higuchi's model and the Korsmeyer-Peppas model were chosen to interpret the drug release mechanism. The parameter used to compare the goodness-of-fit is the coefficient of determination R^2. The linear profile of Fig. 6.17 suggests that CX release from the $scCO_2$ foamed sample is consistent with a Fickian diffusion mechanism. The positive intercept on the Y-axis represents a burst release of the drug prior to the development of the diffusion-controlling mechanism[16]. The rate of drug release was calculated from the slope of the Higuchi curve expressed as % CX released/$min^{0.5}$ (Fig. 6.18). An increase in CX loading and a decrease in CO_2 saturation pressure or CO_2 depressurization time results in a decrease in drug release rate due to a decrease in total porosity of the matrices (initial porosity plus porosity due to the dissolution of the drug). The influence of the pore creation and enlargement by the increased CX particles is so small by comparison.

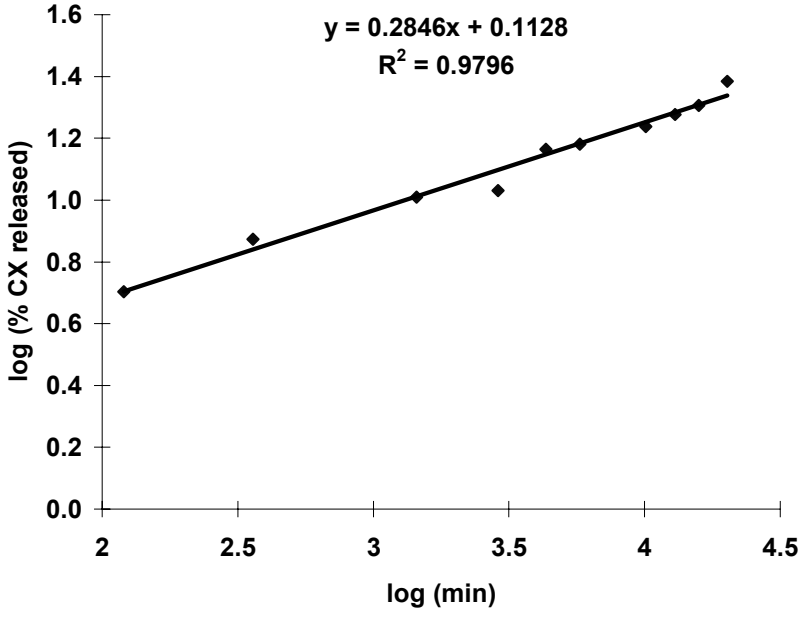

Fig. 6.19 *Linear relations between the log(% CX released) vs. log(time) with the line slope being equal to the exponent n in the Korsmeyer-Peppas model for $scCO_2$ foamed samples containing 12 wt.% CX (40 °C and 1300 psi for 3 hr and 30 min as releasing time)*

The data were also fitted using the Korsemeyer-Peppas model to further evaluate the release mechanism. Accordingly, in Fig. 6.19, log(% of released CX) is plotted as a function of log(time). The resulting linear plots permit the determination of the release exponents *n*, which will give information about the release mechanism. From Fig. 6.19, the release exponents were 0.285 which is beyond the limits of the Korsmeyer-Peppas model. The power law can only give limited insight into the exact release mechanism of the drug. It has been reported that drug release from a porous system may lead to $n < 0.45$. Gong *et al*. has found that for the foamed CX-PEM/THFM system, the drug release rate was found to be in agreement with the 1/3 ($n = 1/3$) power law[11]. This unusual release behaviour is related to the porosity and nature of the matrix, and the rate of water uptake.

6.4 Conclusions

A foamed CX-PEM/THFM drug delivery system was successfully prepared by $scCO_2$ processing. Different experimental conditions have been investigated. $ScCO_2$ efficiently foamed the drug polymer system and produced a highly porous structure, which dramatically increased the release rate of CX by comparison with traditional unfoamed systems. By altering the processing conditions, such as CO_2 saturation time and depressurization time, we can modulate the porosity and pore size of the foamed samples, and drug release rate can be tailored accordingly. There is no evidence of changes in the CX structure or of interaction between the polymer and CX during $scCO_2$ processing. The drug release kinetics of this formulation corresponds well with Higuchi's model which indicates that CX is consistent with a Fickian diffusion mechanism. The *n* value calculated from the Korsmeyer-Peppas equation is beyond the limits of this model and appears to be related to the porosity and nature of the matrix, and the rate of water uptake.

6.5 References

1. Barry JJA, Silva MMCG, Cartmell SH, Guldberg RE, Scotchford CA and Howdle SM. Porous Methacrylate Tissue Engineering Scaffolds: Using Carbon Dioxide to Control Porosity and Interconnectivity. J. Mater. Sci. 2006, 41, 4197.

2. Barry JJA, Gidda HS, Scotchford CA and Howdle SM. Porous Methacrylate Scaffolds: Supercritical Fluid Fabrication and In Vitro Chondrocyte Responses. Biomater.2004, 25, 3559

3. Sheridan MH, Shea LD, Peters MC, Mooney DJ. Bioabsorbable Polymer Scaffolds for Tissue Engineering Capabale of Sustained Growth Factor Delivery. J. Control. Release. 2000, 64, 91

4. Goel K and Beckman EJ. Generation of Microcellular Polymeric Foams using Supercritical Carbon Dioxide. II: Cell Growth and Skin Formation, Polym. Eng. Sci. 1994, 34, 1148

5. Martini-Vvedensky JE, Duh NP, and Waldman FA. Microcellular Close Cell Foams and Their Method of Manufacture. U.S. Patent. 1984, 4473665

6. Stafford CM, Russell TP and McCarthy TJ. Expansion of Polystyrene using Supercritical Carbon Dioxide: Effects of Molecular Weight, Polydispersity and Low Molecular Weight Components. Macromol. 1999, 32, 7610

7. Arora KA, Lesser AJ and McCarthy TJ. Preparation and Characterization of Microcellular Polystyrene Foams Processed in Supercritical Carbon Dioxide, Macromol. 1998, 31, 4614

8. Tai H, Mather ML, Howard D, Wang W, White LJ, Crowe JA, Morgan SP, Chandra A, Williams DJ, Howdle SM and Shakesheff KM. Control of Pore Size and Structure of Tissue Engineering Scaffolds Produced by Supercritical Fluid Processing. Eur. Cell. Mater. 2007, 17, 14, 64

9. Goel SK, Beckman EJ. Generation of Microcellular Polymeric Foams using

Supercritical Carbon Dioxide. 1. Effect of Pressure and Temperature on Nucleation. Polym. Eng. Sci. 1994, 34, 1137

10. Shieh YT, Su JH, Manivannan G, Lee PHC, Sawan SP and Spall WD. Interaction of Supercritical Carbon Dioxide with Polymers. 2. Amorphous Polymers. J. Appl. Polym. Sci. 1996, 59, 707
11. Gong K, Braden M, Patel MP, Rehman IU, Zhang Z and Darr JA. Controlled Release of Chlorhexidine Diacetate from a Porous Methacrylate System: Supercritical Fluid Assisted Foaming and Impregnation. J. Pharm. Sci. 2007, 8, 2048
12. Ingle JDJ and Crouch SR. Spectrochemical Analysis. New Jersey: Prentice Hall; 1988
13. Sawtell RM, Downes S, Patel MP, Clarke R and Braden M. Heterocyclic Methacrylates for Clinical Applications-Further Studies of Water Sorption. J. Mater. Sci. Mater. Med. 1997, 8 , 667
14. Riggs PD, Braden M and Tilbrook DA. The Water Uptake of Poly(tetrahydrofurfuryl methacrylate). Biomater. 1999, 20, 435
15. Patel MP, Cruchley AT, Coleman DC, Swai H, Braden M and Williams DM. A Polymeric System for the Intra-oral Delivery of an Anti-fungal Agent. Biomater. 2001, 22, 2319
16. Ford JL, Rubinstein MH and Hogan JE. Formulation of Sustained Release Promethazine Hydrochloride Tablets using Hydroxypropylmethylcellulose Matrices. Int. J. Pharm. 1985, 24, 327

Chapter 7

Drug Release from Microcapsules in Biodegradable Poly(lactic-co-glycolic acid) Fibres

7.1 Introduction

Drug-loaded fibres have been widely prepared by electrospinning techniques. However, water-soluble drugs are very difficult to incorporate in the process because electrospinning requires a full dissolution of all the components in the polymer solution[1,2]. In this Chapter, a new way of incorporating water-soluble drugs into PLGA fibres was introduced. Rhodamine 6G (R6G) and bovine serum albumin (BSA) were selected as model drugs for the release studies. Trypsin was selected for the enzyme activity test. Initially, either R6G, BSA or trypsin was captured within the porous calcium carbonate ($CaCO_3$) microparticles by coprecipitation. Microcapsules of drug-loaded $CaCO_3$ were also prepared by depositing a layer of poly(sodium

4-styrenesulfonate) (PSS) following the technique of LbL polyelectrolyte assembling[3]. Then, these drug-loaded $CaCO_3$ microparticles were mixed in to the PLGA solution to form a suspension. By electrospinning the suspension, drug-loaded fibres were prepared. The morphology of the fibres produced was studied. The structural integrity of the fibre and the drug release curve were investigated in detail by SEM and fluorescence spectroscopy. The enzyme activity was tested.

7.2 Experimental

7.2.1 Materials

The PSS (M_w ~ 70,000) and R6G (99 %, M_w = 479) were obtained from Aldrich. The BSA (M_w ~ 66,000), trypsin, rhodamine B isothiocyanate (RBITC) and protease fluorescent detection kit were acquired from Sigma. PLGA (Resomer LG 857 S with i.v. of 5.0-7.0 and LA:GA = 85:15) was purchased from Boehringer Ingelheim Pharma GmbH & Co., Germany. All materials were used as supplied without further purification.

The water used in all experiments was prepared in a three-stage Millipore Milli-Q Plus 185 purification system and had a resistivity higher than 18.2 MΩ cm.

7.2.2 Microparticles Preparation

The conjugation of RBITC with BSA was produced as follows: BSA was dissolved in a 0.1 M carbonate buffer, pH 8.5, and RBITC which had been dissolved in methanol, was added drop by drop. After 2 days of incubation in the dark under constant stirring at 4 ºC, the RBITC-BSA conjugates were purified by dialysis to

separate the remaining free RBITC. The RBITC-BSA solution was stored at 4 ºC.

The preparation of all the drug-loaded $CaCO_3$ microparticles was carried out according to the coprecipitation method[3]. Briefly, for BSA-loaded $CaCO_3$ microparticles, for example, 0.33 M solution of $CaCl_2$, were added to an equal volume of a 0.33 M solution of Na_2CO_3 containing 1.2 mg/ml of RBITC-BSA, which were captured by growing $CaCO_3$ microparticles. After intense agitation on a magnetic stirrer for 30 sec, the reaction mixture was left without any further stirring for 5 min. During this time, the formed amorphous primary precipitate of $CaCO_3$ slowly transformed into spherical microparticles. Finally, these microparticles were centrifuged and triple washed and dried in air. Spherical $CaCO_3$ microparticles with an average diameter ranging between 3 to 5 μm were obtained. For the $CaCO_3$ microcapsules with one layer of PSS coating, mild agitation of the suspension of BSA-loaded $CaCO_3$ microparticles in a PSS solution of 2 mg/ml was performed using a microshaker for 15 min. The non-bounded PSS was then removed by centrifugation, and a triple washing of the precipitate was carried out. The particles were stored in the dark at 4 ºC.

For R6G-loaded microparticles, the preparation procedure is the same except 2 mg/ml of R6G solution was used instead of 1.2 mg/ml of RBITC-BSA.

7.2.3 Electrospinning

The procedure of electrospinning was shown in Fig. 7.1. The spinning solution was prepared by dispersing drug-loaded $CaCO_3$ in chloroform first, followed by the gradual addition of the PLGA (2 wt.% of chloroform). The drug-loaded $CaCO_3$ was added at 2 levels, 5 wt.% and 20 wt.% of the PLGA. An ultrasonic bath was used

here to achieve a good dispersion of particles in the solution. The mixture was then kept under constant stirring overnight to achieve a full dissolution of the PLGA. The electrospinning process was carried out in a horizontal spinning configuration using a flat-end needle with a syringe pump producing a steady flow rate of 2 ml/hr at 22 °C and 28 % humidity. A collecting aluminium film was placed on a drum rotating at 100 rpm. The applied voltage was 22 kV. The collected fibre mat was placed in a vacuum oven overnight at room temperature to eliminate residual solvents, and then stored at 4 °C in the dark for the release study and other characterization analysis.

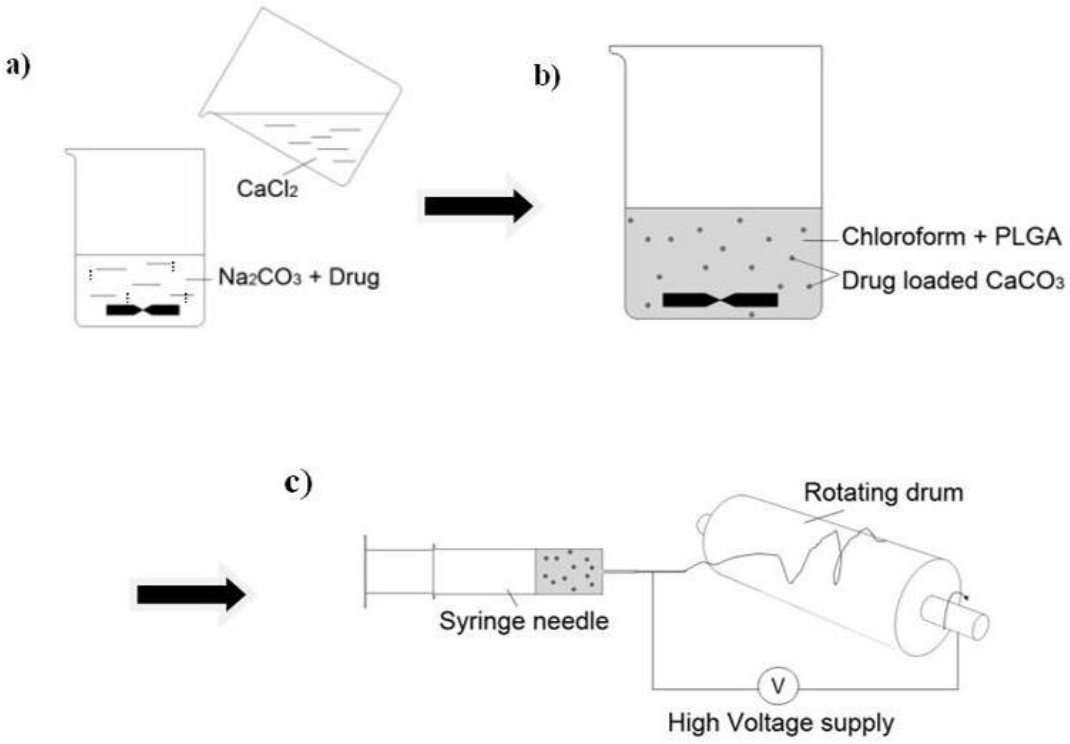

Fig. 7.1 *The major steps of electrospinning: (a) loading the drug in $CaCO_3$ microparticles; (b) the dissolution of PLGA in chloroform with the presence of drug-loaded $CaCO_3$ and (c) electrospinning the well mixed solution*

7.2.4 The Determination of Drug Loading in Fibres

About 2 mg of fibre mat was cut and extracted in 2 ml of 0.1 M NaOH for 12 hr to facilitate its full dissolution, and then neutralized by a 1 N HCl solution. The sample was centrifuged and the concentration of R6G or BSA in the supernatant was determined using a fluorescence spectrometer by the intensity of the peak at 555 nm or 595 nm, respectively. The wt.% of drug entrapped was then deduced. Each batch was tested in triplicate.

Fluorescence calibration curves were built up to define the relationship between the amounts of light absorbed by the solution versus the concentration of the drug solution. The BSA and R6G calibration curves are presented in Fig. 7.2.

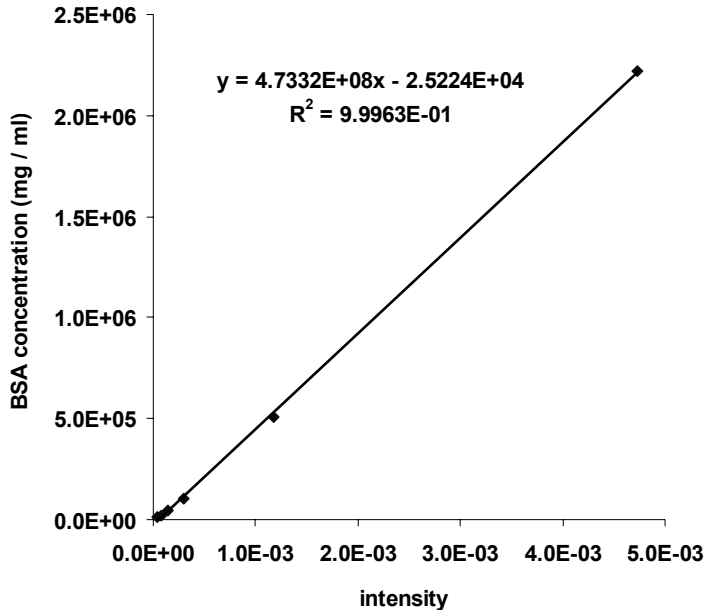

(a)

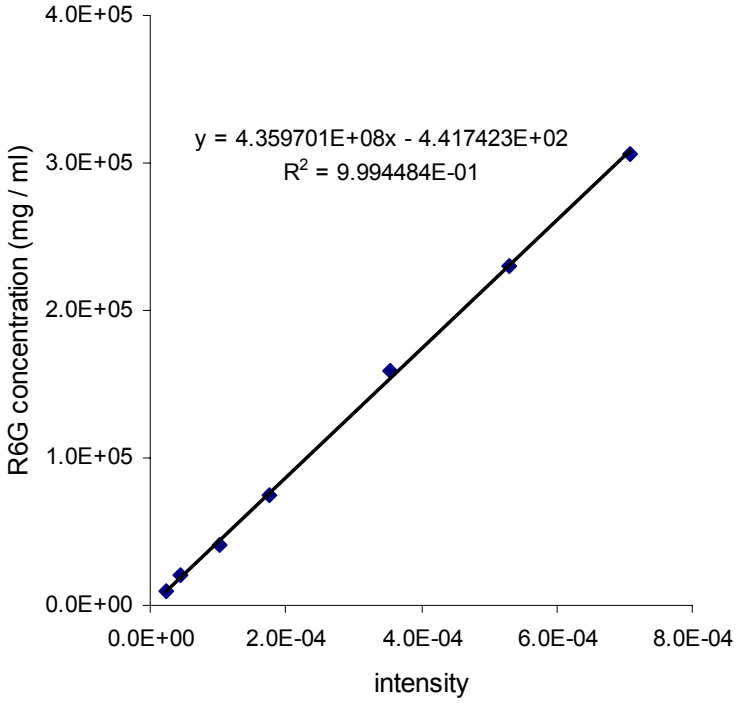

(b)

Fig. 7.2 *(a) RBITC-BSA and (b) R6G fluorescence calibration curves, showing the linear relationship between the drug model concentration and fluorescence intensity*

The drug loading was also indirectly calculated according to the wt.% of the drug in

the $CaCO_3$ microparticles and the wt.% of particles in the fibres. The drug-loaded $CaCO_3$ microparticles were dissolved in 0.1 M HCl and adjusted to pH 7 by NaOH. The results produced by both methods were compared.

7.2.5 Drug Release from Fibres

The drug release study was customized by performing in pH 1, 2, 4, 7 release media adjusted by HCl. The fibre mat was first cut into 2×2 cm^2 squares. Each square sample was accurately weighed and placed separately into a 2 ml release medium. The test was performed on the microshaker at 50 rpm. At appropriate intervals, 1 ml of the supernatant was removed and replenished with an identical volume of fresh medium. The drug concentrations were determined by the fluorescence spectrometer as described above. Each sample was tested in triplicate.

Drug release profiles were curve-fitted to commonly used models, Higuchi's equation and Korsmeyer and Peppas' equation, to characterize and derive the drug release parameters for comparative purposes. These equations are described in detail in Section 5.4.2.

7.2.6 Enzyme Activity Assays

To study the enzyme activity in PLGA fibres, trypsin was coprecipitated with $CaCO_3$ microparticles and impregnated in the PLGA fibre following the same procedure as R6G and BSA. The Bradford reagent was used to determine the concentration of trypsin in the solution. The activity of the trypsin enzyme was tested using a protease fluorescent detection kit. It uses casein labelled with fluorescein isothiocyanate (FITC) as the substrate. Trypsin activity results in the cleavage of FITC-labelled

casein substrate into small fragments, which do not precipitate under acidic conditions. Therefore, when the mixture is centrifuged, the undigested substrates form a pellet and the small, acid soluble fragments remain in the solution. So the activity of trypsin can be measured by taking the supernatant (neutralized) and using the fluorescence to assay the FITC-labelled fragments at 560 nm.

7.2.7 Morphology Characterization

Both drug-loaded $CaCO_3$ and fibres were examined using optical microscopy (Olympus BX-60 using reflected or transmitted light sources with crossed polarizers), scanning electron microscopy (SEM) (JEOL 6300^{TM}) and fluorescence microscopy (Leica, DMI 4000B, DFC 300FX). Specimens were gold-coated and analysed at a voltage of 5 kV for SEM.

7.3 Results and Discussion

7.3.1 Drug-Loaded $CaCO_3$ Microparticles

Drug-loaded $CaCO_3$ microparticles were fabricated by the coprecipitation of $CaCO_3$ with the drug in the solution. The morphology of the BSA-$CaCO_3$ particles is presented in Fig. 7.3.

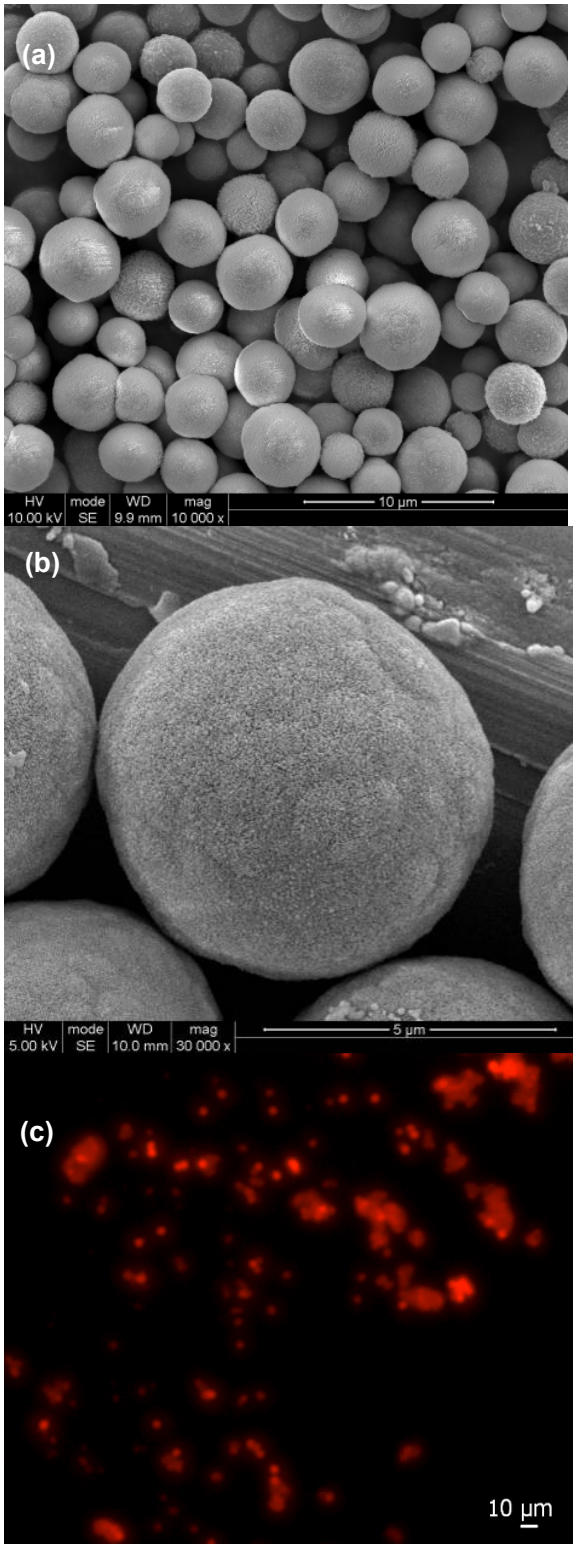

Fig. 7.3 *The morphology of BSA-$CaCO_3$ particles (a) SEM image, 10,000×; (b) SEM image, 30,000× and (c) fluorescence microscopy*

As it shows, the homogeneous size microparticles were successfully prepared with a diameter of around 4 μm (Fig. 7.3a). On closer inspection, highly developed porous structures consisting of smaller spherical nanoparticles can be observed (Fig. 7.3b). There is no substantial difference between these BSA-$CaCO_3$ and the PSS coated BSA-$CaCO_3$ from the observations since the thickness of the PSS layer is only around 5nm[3]. Because the BSA has been labelled with RBITC, the loading of BSA can be confirmed easily using fluorescence microscopy (Fig. 7.3c). A bright red colour indicates the presence of BSA inside the $CaCO_3$ microparticles.

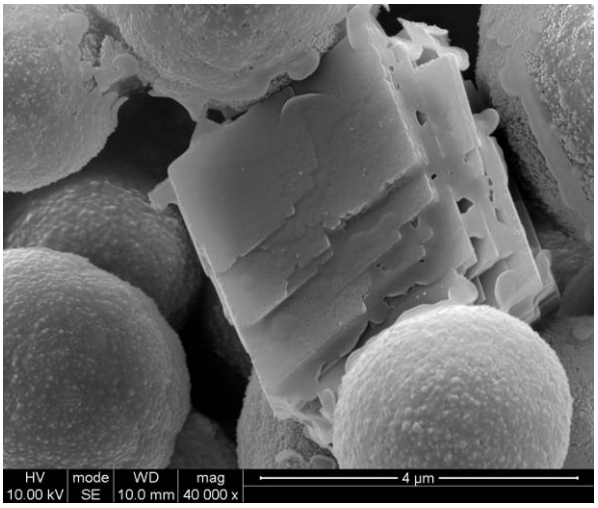

Fig. 7.4 *An SEM image of rhombohedral calcite microcrystals of $CaCO_3$ due to the recrystallization phenomenon happened in the preparation*

The quality of the $CaCO_3$ microparticles strongly depends on the experimental conditions, which affect the rate of the nucleation process of $CaCO_3$. It has been reported that the growth of the $CaCO_3$ microparticles starts with the forming of an amorphous primary precipitate, followed by a colloidal aggregating to form spherical micron-sized microparticles, eventually recrystallizing into rhomobohedral calcite microcrystals[3] (Fig. 7.4). To obtain the homogeneously-sized, non-aggregated, highly porous spheres, the experimental conditions need to be carefully controlled to preserve the $CaCO_3$ microparticles of spherical morphology before the

recrystallization phenomenon occurs.

7.3.2 PLGA Fibres Incorporating Drug-Loaded $CaCO_3$ Microparticles

Drug-loaded $CaCO_3$ microparticles have been successfully incorporated into the PLGA fibres. Optical microscopy images confirmed the presence of $CaCO_3$ microparticles inside the fibres. Rather than single lengths of string, electrospinning of the spinning mixture resulted in the formation of a characteristic morphology; a bead-and-string structure was clearly achieved (Fig. 7.5).

The 5 % drug-loaded fibres have an average diameter of between 2 and 5 μm. For the 20 % drug-loaded samples, more microparticles are present along the fibres and the thickness of the fibres increases. Under cross polarized illumination, because of the refractive index differences between $CaCO_3$ and PLGA, $CaCO_3$ microparticles can be seen clearly along the fibres. (Fig. 7.5c)

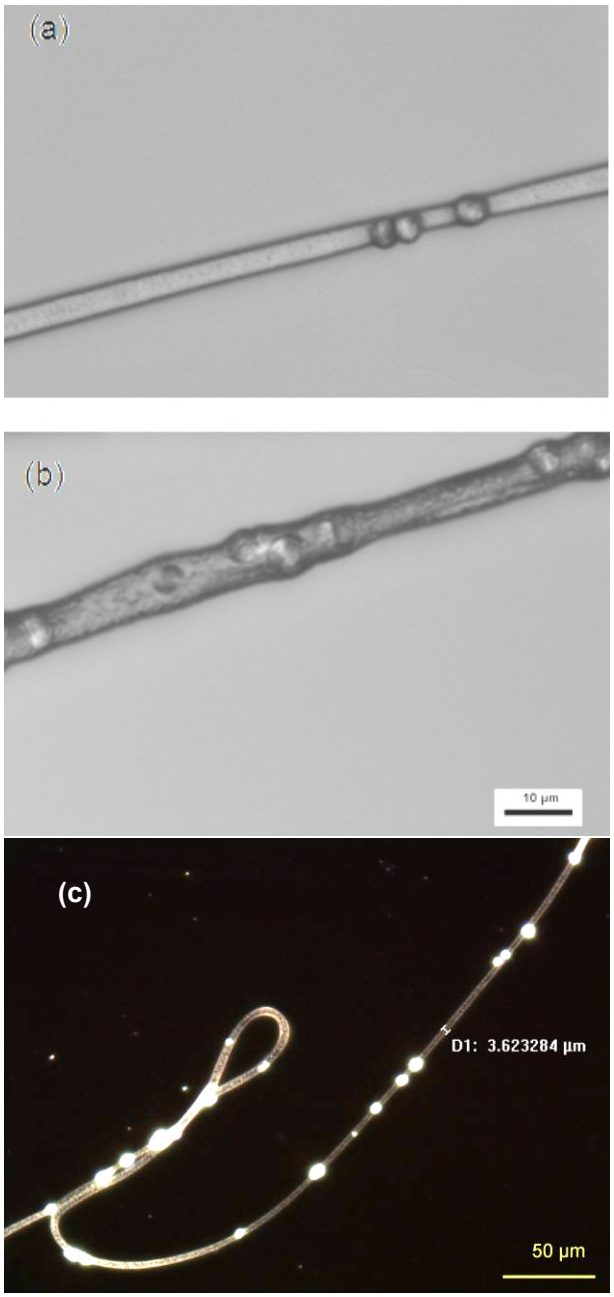

Fig. 7.5 *Optical microscopy images of typical PLGA fibres incorporating drug-loaded $CaCO_3$ microparticles. (a) 5 % PLGA-BSA-$CaCO_3$ fibres (b) 20 % PLGA-BSA-$CaCO_3$ fibres (c) 20 % PLGA-BSA-$CaCO_3$ fibres under cross polarized illumination*

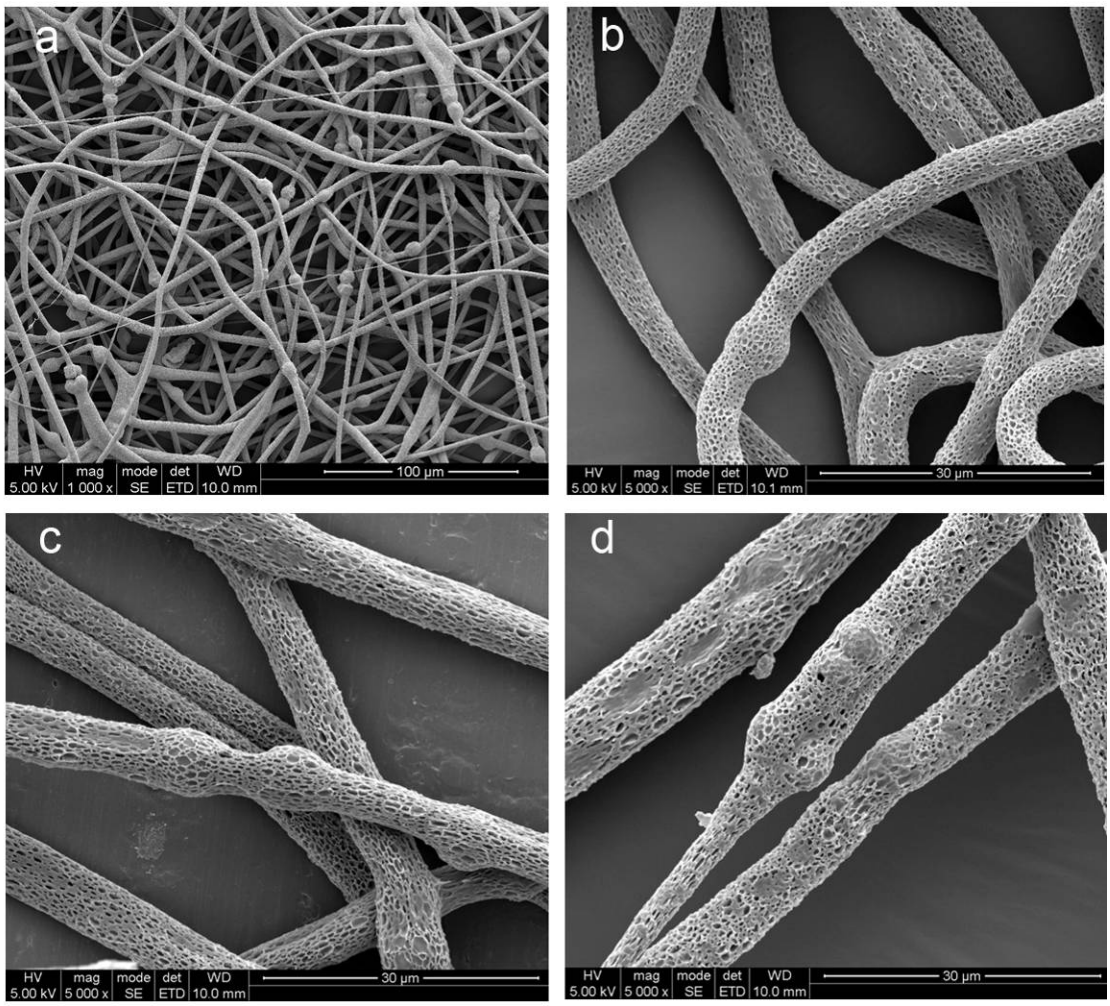

Fig. 7.6 *SEM images of (a) 5 % PLGA-R6G-$CaCO_3$ fibres, 1000× (b) 5 % PLGA-R6G-$CaCO_3$ fibres, 5000× (c) 5 % PLGA-BSA-$CaCO_3$ fibres (d) 20 % PLG-BSA-$CaCO_3$ fibres*

The SEM images show that the composite fibre mat has a 3-D structure with a random fibre orientation which is evenly distributed on the substrate. (Fig. 7.6a) Upon closer inspection, for both R6G-loaded and BSA-loaded fibres, the fibre surfaces appear to be highly porous (Fig. 7.6b, c and d). Compared with the 5 % BSA-loaded fibres, the sample with 20 % BSA loading shows a significant increase of particles along the fibre and an aggregation of the particles was observed. (Fig. 7.6d) Moreover, very large fibre diameter variations from 1 to 9 µm indicate that the

aggregated particles highly influence the stability of the fibre forming process. There are no noticeable differences between the PLGA-BSA-$CaCO_3$-PSS fibres and PLGA-BSA-$CaCO_3$ fibres in this respect.

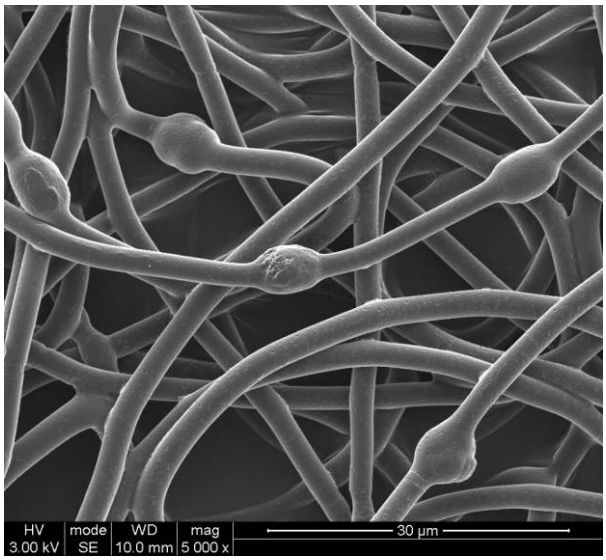

Fig. 7.7 *An SEM image of 5 % PLGA-R6G-$CaCO_3$ fibres produced under 20 % humidity*

The morphology of electrospun fibres can be influenced by many factors. These include the solvent boiling point, surface tension, solution viscosity, solution conductivity, solution concentration, glass transition temperature of the polymer, applied voltage and the tip to collector distance.[4-5] It is believed that the formation of the porous structures is a consequence of breath figure and phase separation mechanisms. The humidity and temperature of the operation conditions strongly influence the porosity of the fibres. One set of 5 % PLGA-R6G-$CaCO_3$ fibres was produced under lower humidity, 20 %, instead of 28% for comparison. The fibre surfaces hardly had any pores on the surfaces and appeared smoother and much denser (Fig. 7.7). Since the morphology of the fibres has a crucial effect on the drug release behaviour, the conditions of the electrospinning process were carefully

monitored and kept constant throughout.

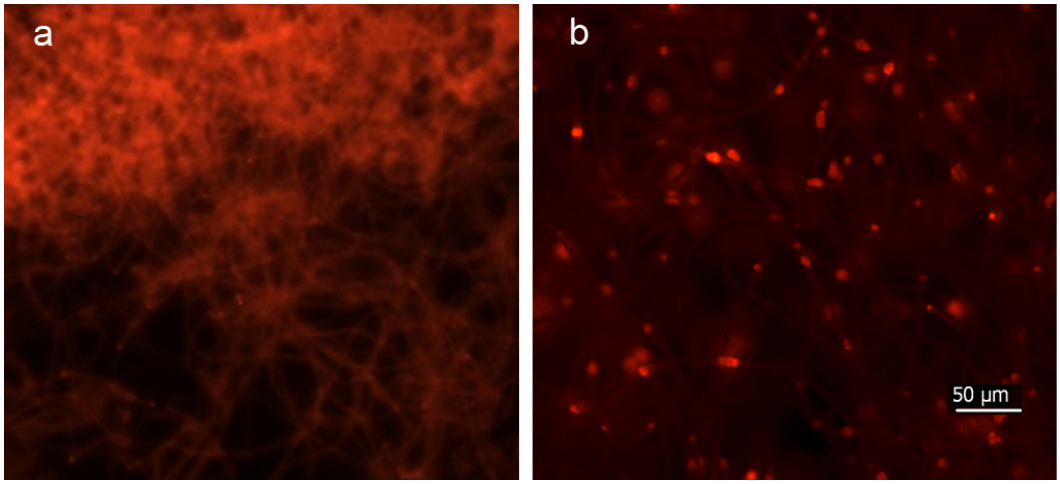

Fig. 7.8 *Fluorescence microscopy of (a) 5 % PLGA-R6G-$CaCO_3$ fibres and (b) 5 % PLGA-BSA-$CaCO_3$ fibres*

Although the differences between R6G-loaded and BSA-loaded fibres are not obvious from SEM study, under the fluorescence microscope, R6G-loaded fibre emits fluorescence from both the particles inside the fibres and the fibres themselves (Fig. 7.8a), whereas the BSA-loaded fibres show much stronger emission from the particles and little emission from the fibres (Fig. 7.8b). For R6G-$CaCO_3$ microparticles, because the R6G molecules are very small (molecular weight ~ 479), although R6G has been captured inside $CaCO_3$ microparticles, some of these R6G molecules would pass through the pores of the $CaCO_3$ spheres and dissolve in the chloroform solvent in the electrospinning process. The presence of R6G in the solvent during the electrospinning process determines the stain of the fibres, therefore both microparticles and fibres show bright red under fluorescence microscopy. On the other hand, RBITC labelled BSA is much bigger (M_w ~ 66,000), which can be easily restrained inside the $CaCO_3$ microparticles, and therefore only the microparticles show under fluorescent light in this case.

7.3.3 In Vitro Degradation of Fibres

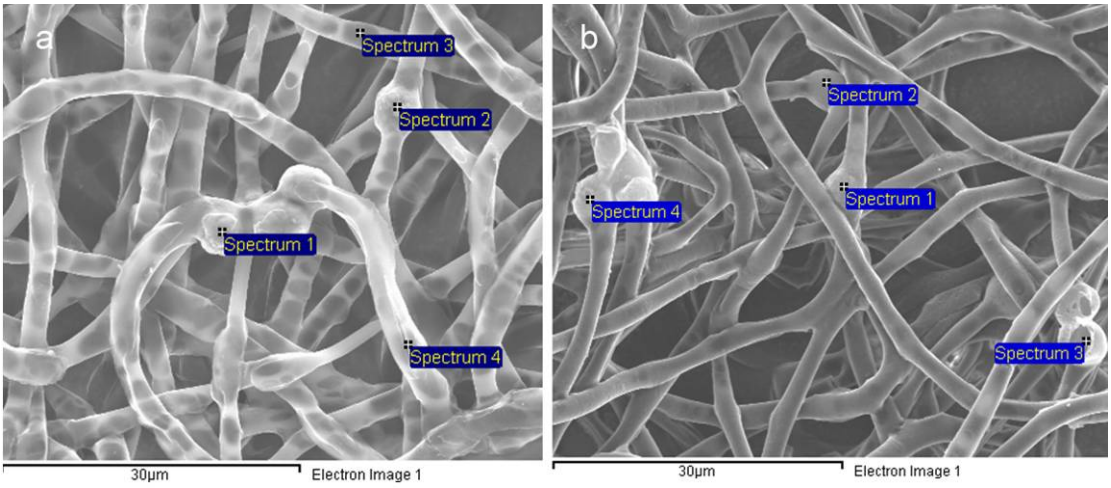

Fig. 7.9 *SEM with EDX analysis of (a) original 20 % PLGA-6G-$CaCO_3$ fibres and (b) PLGA-6G-$CaCO_3$ fibres after release in the pH 1 release medium (3 days)*

The progress of degradation of drug-loaded PLGA fibre mats was studied and the sample was analysed using SEM with EDX. Fig. 7.9a shows a sample of original fibres for comparison. The spectrum on the bead clearly shows the Ca element presence in the original fibres (see Fig. 7.9a spectrum 1 and 2), which is not present in fibres after release (see Fig. 7.9b spectrum 3 and 4). Table 7.1 provides an elemental composition obtained from the EDX analysis. This confirms that drug-loaded $CaCO_3$ particles were released from the fibres, leaving the shells behind.

Table 7.1 *An elemental composition of original 20 % PLGA-6G-$CaCO_3$ fibres and sample after release in the pH 1 medium (3 days) (All results in wt.%)*

Spectrum		C	O	Na	Si	S	Cl	Ca	Total
Original	Spectrum 1	13.94	31.43	0.53	-	-	1.02	53.07	100.00
	Spectrum 2	21.91	50.53	0.44	-	-	0.33	26.80	100.00
	Spectrum 3	85.87	13.20	0.35	-	0.58	-	-	100.00
	Spectrum 4	90.38	9.06	0.16	-	0.19	0.21	-	100.00
After release	Spectrum 1	79.69	8.03	3.26	-	0.81	8.20	-	100.00
	Spectrum 2	90.87	6.14	0.79	0.47	-	1.72	-	100.00
	Spectrum 3	86.46	12.99	-	0.55	-	-	-	100.00
	Spectrum 4	90.69	6.58	0.85	0.57	-	1.30	-	100.00

Fig. 7.10 illustrates the progress of the degradation of PLGA fibres during the drug release test. After being merged in the release medium, the fibres maintained their fibrous structure for several days before the fibres' wall started to look swollen and the sharp edges of the pores become indistinct. The bead-and-string structure has changed into bag-and-string structure (as circled in Fig. 7.10a). With the passing of time, the fibres broke down to smaller segments and these segments broke down to even shorter segments (Fig. 7.10c). The pores on the surfaces became bigger and started connecting with each other as a consequence of the hydrolytic degradation. From the fluorescence microscopy, the decrease in brightness from the fibres and microparticles confirms the release of the drug (Fig. 7.10b and d). However, the presence of red dots in Fig. 7.10d means that only some of the microparticles had been released and that there were still microparticles trapped inside the broken fibre segments.

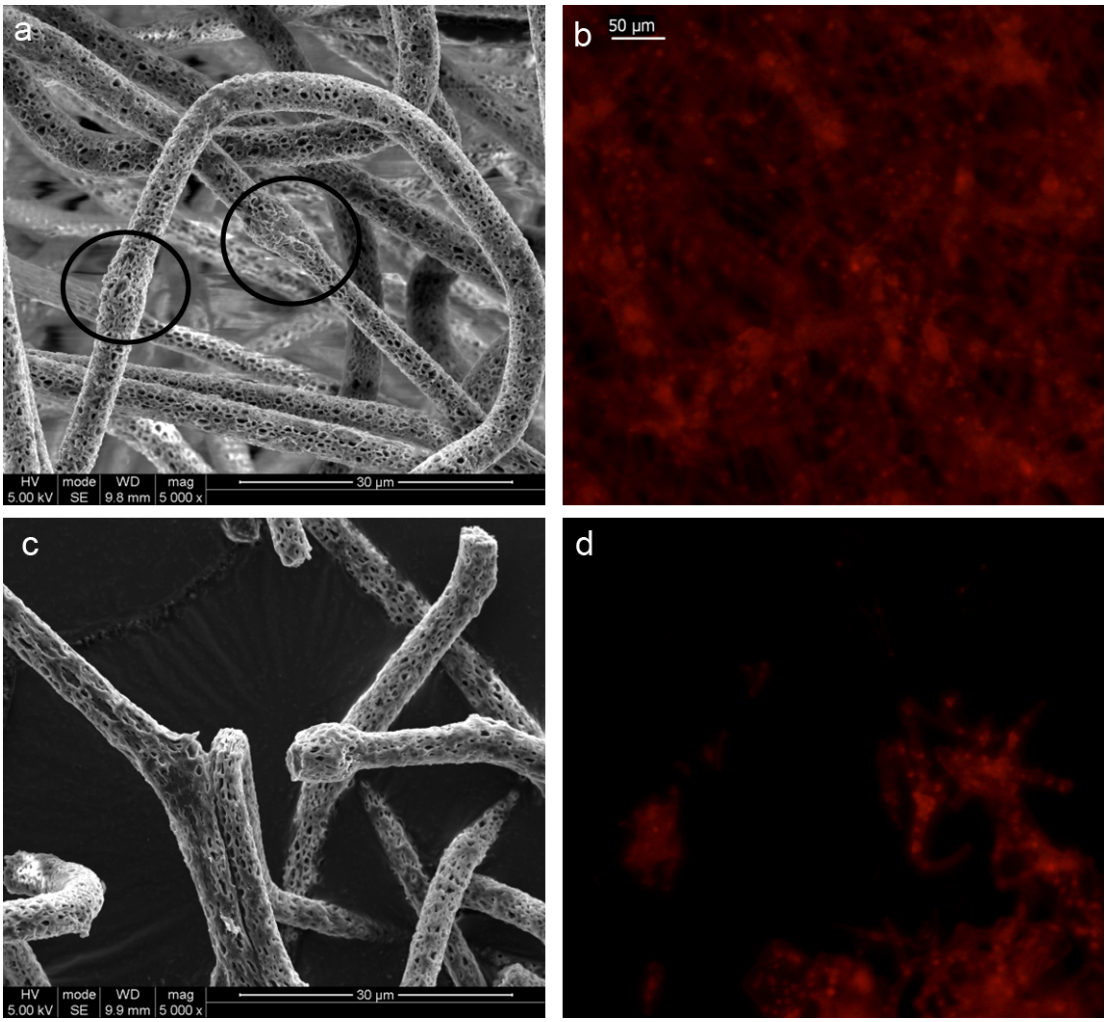

Fig. 7.10 *The progress of degradation of 20 % PLGA-BSA-$CaCO_3$ fibres exposure to pH 4 over time of (a) 9 days, SEM images (b) 9 days, fluorescence microscopy (c) 20 days, SEM images and (d) 20 days, fluorescence microscopy*

The degradation of PLGA has been described as bulk erosion. It has been mentioned in Chapter 5 that the acidic microclimate pH inside the PLGA results in the acceleration of the degradation process of PLGA[6]. However, in the case of the porous ultrafine fibrous structure of the PLGA, diffusion of degradation products are rapid due to the high surface to volume ratio and porosity; therefore, local acidic microclimate pH is not presented. The release of $CaCO_3$ microparticles has a significant effect on the degradation of PLGA fibres. When the fibre diameter is

smaller than the particles, the PLGA fibre wall around the microparticles is believed to be very thin; therefore, particles are able to escape first, long before bulk erosion happens. The holes left behind allow more water to penetrate the polymer creating a new surface area. Moreover, the walls of the holes are the most vulnerable places for water absorption, and it is where the breakage of fibres may first happen. Therefore, polymer degradation will be accelerated. Whereas when the fibre diameter is larger than the incorporated microparticles, these particles are more likely to remain inside the fibres, and may even fail to be released even after the bulk erosion of the PLGA occurs. The presence of $CaCO_3$ particles has also been reported, acting as pH modifiers to buffer the pH of the PLGA matrix, thereby reducing autocatalysis and retarding degradation[7].

7.3.4 In Vitro Drug Release

To determine the drug loading in the PLGA fibres, two methods were used and data are compared in Table 7.2.

Table 7.2 *Drug loading in $CaCO_3$ particles and PLGA fibres*

Drug	Drug-loaded $CaCO_3$ wt.% in PLGA	Drug wt.% in $CaCO_3$	Deduced drug wt.% in PLGA	Measured drug wt.% in PLGA
R6G	5	0.132	0.0063	0.0018
BSA	20	2.97	0.50	0.48

For PLGA-R6G-$CaCO_3$ fibres, by the direct extraction of fibres in an NaOH solution, the amount of R6G released from these fibres is less than half the amount obtained

from the wt.% calculation. It indicates that 70 % of R6G in the $CaCO_3$ microparticles were released into the solvent during the electrospinning process and trapped inside fibre. Therefore, very little R6G is subsequently released later during the drug release test. For BSA-loaded fibres, results from both methods are comparable. Considering the M_w of BSA used is as high as 66,000, it is no surprise that almost all the BSA molecules are retained inside the $CaCO_3$ microparticles during electrospinning. The data from the direct extraction method were used to calculate the drug release, because the drug release percentage is proportional to the amount of drug that could be released rather than the amount of drug used during the fibre preparation.

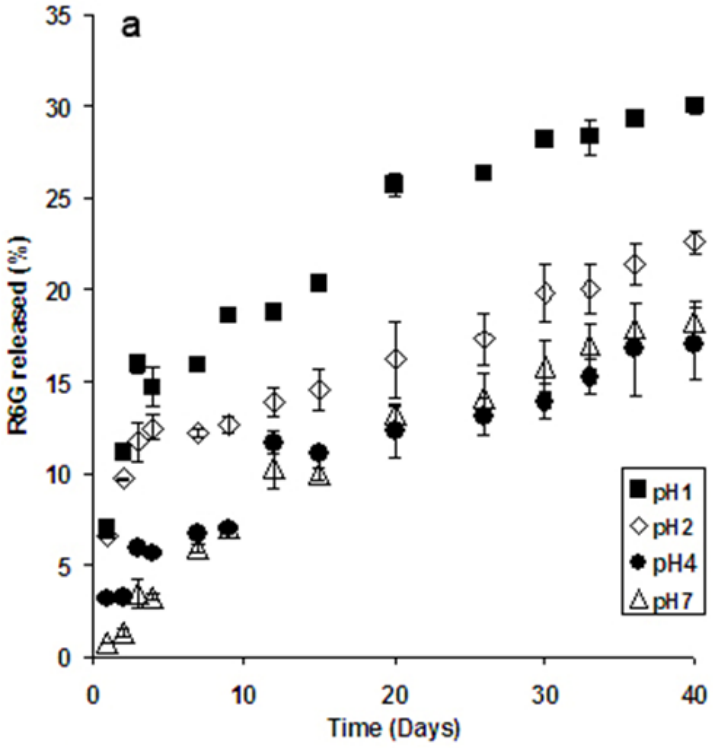

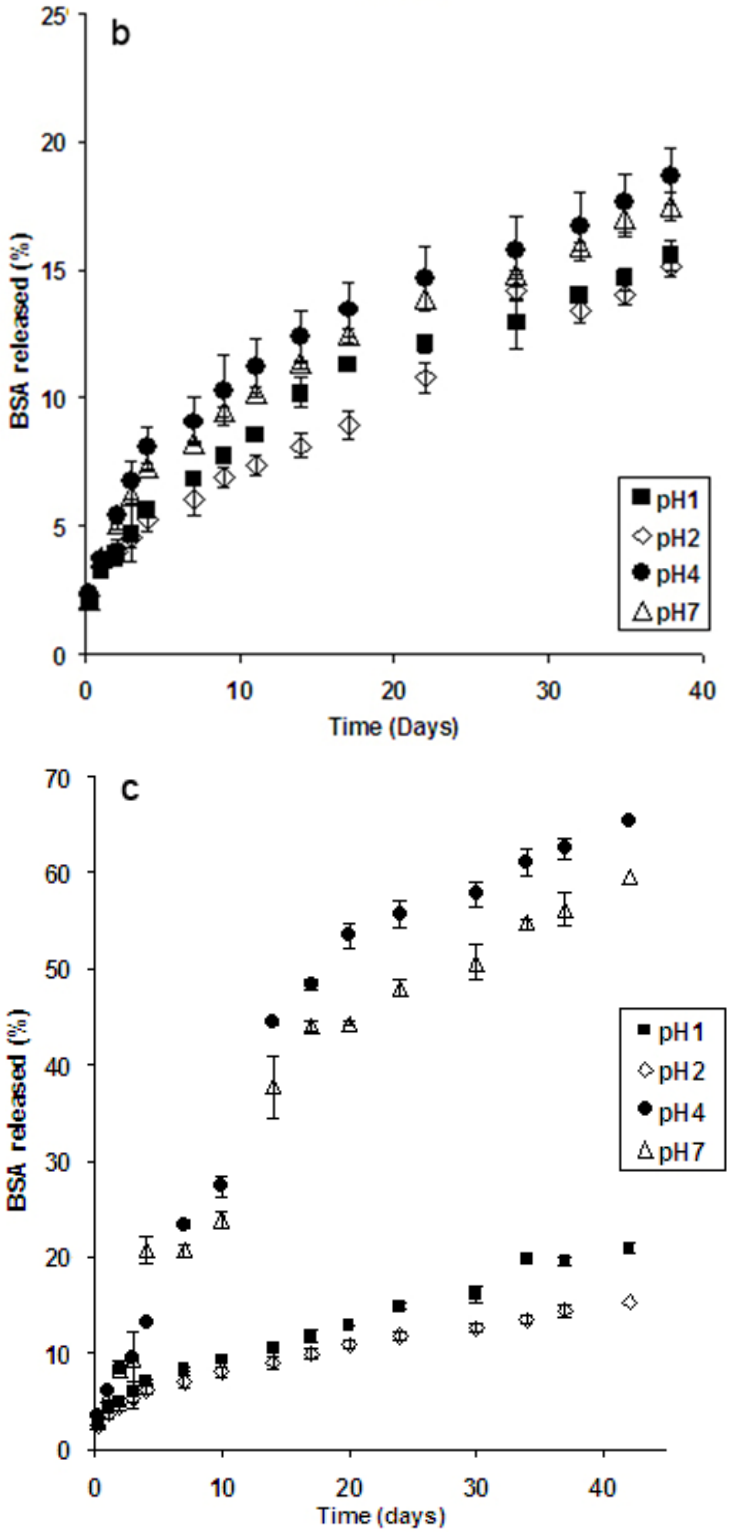

Fig. 7.11 *Drug released in different pH release media (pH=1, 2, 4, 7) (a) PLGA-R6G-$CaCO_3$ fibres (b) PLGA-BSA-$CaCO_3$ and (c) PLGA-BSA-$CaCO_3$-PSS fibres*

The release profiles shown in Fig. 7.11 suggest that both the R6G release and the BSA release were sustained for 40 days for all the dosage forms. However, a complete release of the drug was not achieved by the end of the tests. The initial burst was suppressed by encapsulating the drug-loaded $CaCO_3$ microparticles in the PLGA fibres. There is no obvious trend for the release curves. The typical biphasic phenomena, in which a drug release from the PLGA has been described as an initial bursting followed by a late bursting caused by the bulk erosion of PLGA[8] is not present here. The drug released gradually over time until the test was over. The detailed effects of drug type, drug loading and pH of the release medium will be discussed below.

7.3.4.1 The Influence of Drug Types

For R6G-loaded fibres, the initial bursting release is dependent on the pH of the release medium used and was found to increase with a decrease in pH (Fig. 7.11a). For BSA-loaded fibres, little initial bursting was observed from the drug release curves (Fig. 7.11b). The initial burst release of R6G is due to the dissolution of R6G molecules on the fibre surface, which were deposited during the electrospinning process. While BSA molecules were captured inside $CaCO_3$ microparticles, there was hardly any leakage thereof. The total amounts of drug released are different for R6G- and BSA-loaded samples. Up to 30 % was achieved for R6G-loaded fibres. For BSA loaded samples, 17 % is for PLGA-BSA-$CaCO_3$ fibres and 62 % for PLGA-BSA-$CaCO_3$-PSS fibres (sample in pH 4 release medium). The smaller size of R6G molecules makes it easier for diffusion by comparison with the BSA molecules. However, with a PSS coating around the BSA-loaded $CaCO_3$ microparticles, the release behaviour becomes complicated.

7.3.4.2 The Influence of a PSS Coating of the Microparticles

The PSS coated and uncoated drug releasing systems showed different release behaviours. It is not so obvious for the R6G-loaded samples (Figures not shown); however, the BSA-loaded samples show a significant increase of BSA release in the pH 4 and pH 7 release media (62 % and 56 % respectively in 40 days). Due to the hydrophobic nature of PSS and PLGA, during the fibre preparation procedure, the interaction between the PSS and PLGA may be strengthened by the outward diffusion of PSS into PLGA. PSS is a negatively charged polyelectrolyte. It has been considered that BSA is a polyampholyte having the isoelectric point (iep) of 4.5[9]. When pH > iep, the net charge of BSA is negative, and for pH < iep, it has a net positive charge. There may be interaction between PSS, PLGA and BSA in the pH 4 and pH 7 release media, which may somehow weaken the structure of $CaCO_3$ microparticles and facilitate the release of BSA.

7.3.4.3 The Influence of Drug Loadings

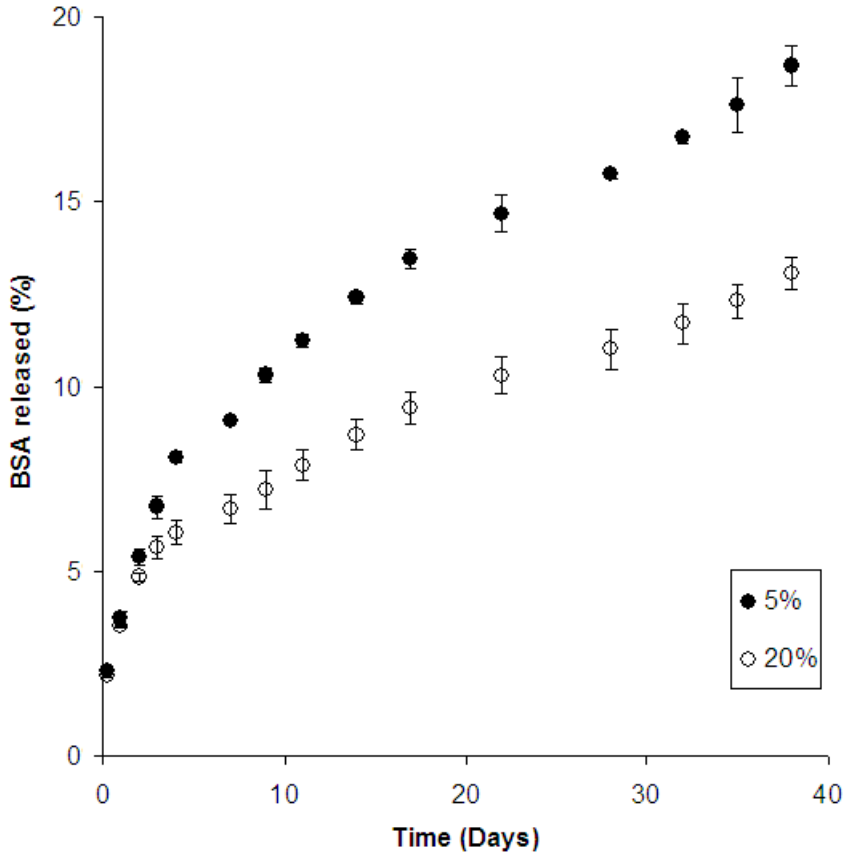

Fig. 7.12 *Drug released for PLGA-BSA-$CaCO_3$ fibres in the pH 4 release medium*

Drug loading has a considerable effect on the drug release rate. In the case of 20 % BSA-loaded samples, the release reached 13 % in 40 days. This is in contrast to 17 % for 5 % loading (Fig. 7.12). The increase of the drug loading will increase the number of aqueous channels formed by the dissolution of the hydrophilic drug, which will act as pathways for further aqueous penetration[10]. However, the dimension of the fibre with 20 % drug loading was much thicker than that of 5 % loading, (Fig. 7.6c and d) which could indicate that 20 % drug-loaded fibres entrap the incorporated $CaCO_3$ microparticles more deeply inside the fibre, leading to a slower release process. In the case here, the slower release received from higher

drug-loaded samples indicates that the second factor is dominant.

7.3.4.4 The Influence of the pH of Release Media

For PLGA-R6G-$CaCO_3$ fibres, the release rate increases with the decrease of pH with a release of up to 30 % achieved in pH 1. In the case of PLGA-BSA-$CaCO_3$, the total amount of BSA released in 40 days is very similar in each release medium. For PLGA-BSA-$CaCO_3$-PSS fibres, the BSA release was much more rapid in the pH 4 and pH 7 media and the total release was as high as 62 % and 56 % respectively in 40 days.

The pH value plays a significant role in release behaviour, because it is acting on the PLGA degradation rate, the dissolution of $CaCO_3$ microparticles and protein stability. The strong acidic medium can accelerate the PLGA degradation, as it enhances the hydrolysis of the polymer's ester bond linkages[11]. It also accelerates the dissolution of the $CaCO_3$ microparticles. However, a strong acidic solution can cause the aggregation of the BSA[12]. Therefore, R6G-loaded samples showed an increase in release in lower pH media due to a faster degradation of the PLGA and the dissolution of $CaCO_3$. While for BSA-loaded samples, the effect from aggregation of the BSA is so strong that the release of the BSA was heavily suppressed. Lu *et al.*[13] reported the same phenomenon with growth factor-beta1(TGF-β1) release in different pH buffers. For PLGA-BSA-$CaCO_3$-PSS fibres in pH 4 and pH 7, without the negative effect from aggregation of the BSA, the releases of BSA were promoted by the PSS coating.

7.3.4.5 Kinetics of Drug Release

To study the release kinetics, data obtained from the drug release studies were plotted against Higuchi's model and the Korsmeyer and Peppas equation. Data fitted to the Higuchi model (Fig. 7.13) showed that R6G-loaded samples had a R^2 value of 0.949-0.977. PLGA-BSA-$CaCO_3$ samples had a higher R^2 value of 0.996 and follow Higuchi diffusion kinetics. PLGA-BSA-$CaCO_3$-PSS samples in higher pH media (pH 4 and pH 7) show slightly lower R^2 value of 0.951 and 0.963.

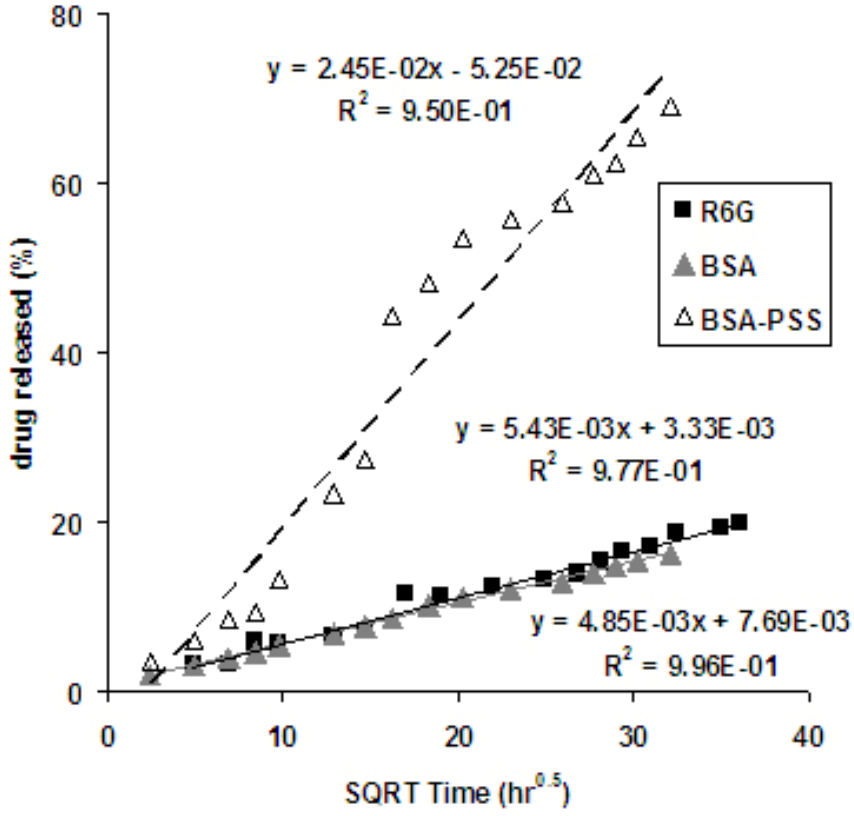

Fig. 7.13 *Drug release fitted to Higuchi's model for drug-loaded samples in the pH 4 release medium*

Release data were also fitted using the equation of Korsmeyer and Peppas (Fig. 7.14). The slope of the line gives the value of *n*, which indicated the release mechanism.

For R6G samples, the *n* value was between 0.33 and 0.48 depending on the pH of the release medium. For PLGA-BSA-$CaCO_3$ samples, the *n* value was around 0.41. Both values of *n* are beyond the range of the model ($0.5 \leq n \leq 1$). It has been mentioned in Chapter 6 that drug release from a porous system may lead to $n < 0.45$. PLGA-BSA-$CaCO_3$-PSS samples in higher pH media (pH 4 and pH 7) show an *n* value of 0.64 and 0.62.

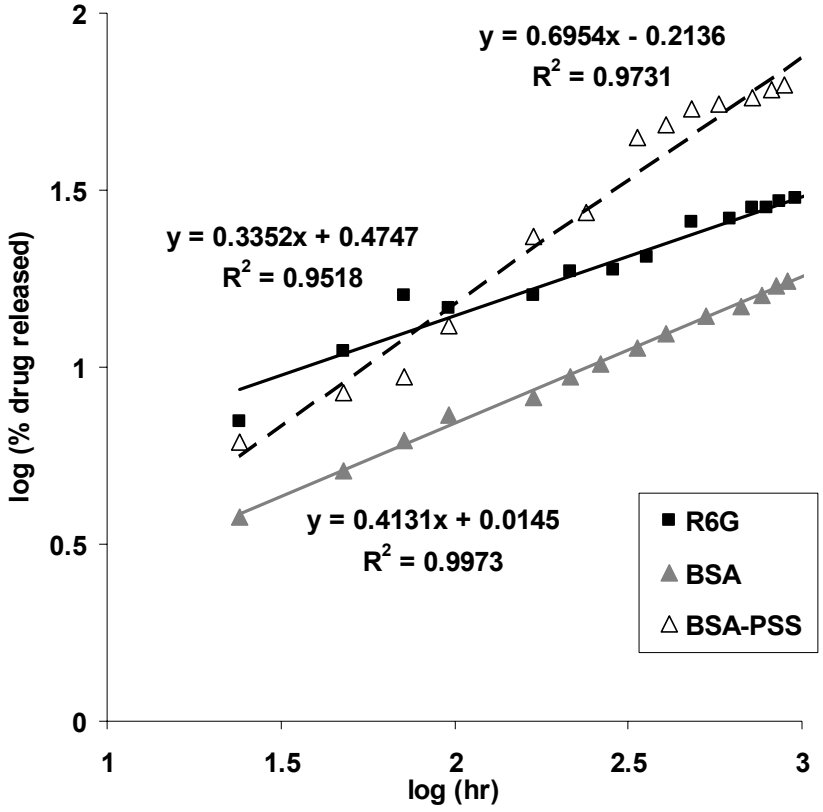

Fig. 7.14 *Drug release fitted to Korsmeyer-Peppas' model for drug-loaded samples in the pH 4 release medium*

The R^2 values of different models indicate the goodness-of-fit to the type of model to which the release data are being fitted. PLGA-BSA-$CaCO_3$ samples follow both models well. Other samples do not follow either of the models so well by comparison. The complexity of this double incorporated drug system reduces the accuracy of

these models. The mechanism of the drug release is complex because it involves the diffusion of the drug from the matrices, diffusion of the drug from $CaCO_3$ particles, release of the $CaCO_3$ particles, as well as the PLGA degradation. The alterations in the polymer phase properties during degradation also bring changes in drug diffusivity and permeability with time. Nevertheless, both diffusion and degradation are believed to participate in establishing the release pattern.

7.3.5 Enzyme Activity Assays

To study the enzyme activity in PLGA fibres, trypsin was encapsulated in $CaCO_3$ microparticles and then impregnated into the PLGA fibre following the same procedure as R6G and BSA. The results show that the enzyme preserves 70 % of its activity after the $CaCO_3$ encapsulation process (Fig. 7.15). However, the fibre samples do not show any activity that can be attributed to the trypsin. It may be due to the harsh alkaline solution (0.1 M NaOH) used in the dissolution of trypsin-loaded fibres, which causes the denaturation of the trypsin. A better enzyme activity test needs to be established.

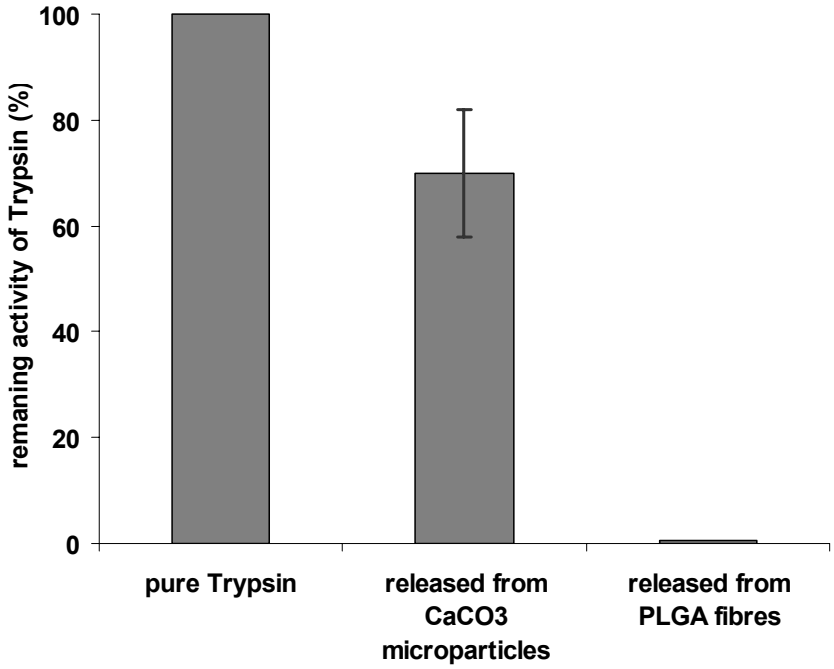

Fig. 7.15 *The activity of trypsin through the process*

7.4 Conclusions

Water-soluble drugs, R6G and BSA, loaded $CaCO_3$ microparticles were successfully incorporated in PLGA fibres by a combined coprecipitation and electrospinning technique. A bead and string structure of the composite fibre was achieved. The initial burst release was restrained because of the presence of $CaCO_3$ microparticles as a second barrier. The drug release profile is affected greatly by the drug properties, drug loading and pH of the release medium. For R6G-loaded fibres, a release of up to 30 % was achieved in 40 days and the release rate increased with the decrease of pH. For BSA-loaded fibres, a release of up to 19 % was achieved in 40 days. Although a strong acidic medium accelerates the degradation of PLGA and dissolution of $CaCO_3$, it causes the aggregation of the BSA which suppresses the BSA release. The PSS coating of microparticles resulted in a complex release mechanism, resulting in a rapid release up to 62 % in the pH 4 medium for the PLGA-BSA-$CaCO_3$-PSS sample.

This double barrier drug release system is too complex for the Korsmeyer and Peppas model to interpret the drug release mechanisms. Nevertheless, the preparation of drug-loaded $CaCO_3$ incorporated fibre structures provides an alternative strategy for incorporating water-soluble drugs and proteins in the electrospinning process.

7.5 References

1. Jiang H, Fang D, Hsiao B, Chu B. and Chen W. Preparation and characterization of ibuprofen-loaded poly(lactide-co-glycolide)/poly(ethylene glycol)-g-chitosan electrospun membranes. J. Biomater. Sci., Polym. Ed. 2004, 15, 279
2. Kim K, Luu YK, Chang C, Fang DF, Hsiao BS, Chu B and Hadjiargyrou M. Two-Phase Electrospinning from a Single Electrified Jet: Microencapsulation of Aqueous Reservoirs in Poly(ethylene-co-vinyl acetate) Fibers. J. Control. Release. 2004, 98, 47
3. Petrov AI, Volodkin DV and Sukhorukov GB. Protein-Calcium Carbonate Coprecipitation: A Tool for Protein Encapsulation. Biotechnol. Prog. 2005, 21, 918
4. Lee KH, Kim HY, La YM, Lee DR and Sung NH. Influence of a Mixing Solvent with Tetrahydrofuran and N,N-Dimethylformamide on Electrospun Poly(vinyl chloride) Nonwoven Mats. J. Polym. Sci. Part B: Polym. Phys. 2002, 40, 2259
5. Bognitzki M, Hou H, Ishaque M, Frese T, Hellwig M, Schwarte C, Schaper A, Wendorff JH and Greiner A. Polymer, Metal, and Hybrid Nano- and Mesotubes by Coating Degradable Polymer Template Fibers (TUFT Process). Adv. Mater. 2000, 12, 637
6. Göpferich A. Polymer bulk erosion. Macromol. 1997, 9, 2598
7. Ara M, Watanabe M, Imai Y. Effect of Blending Calcium Compounds on Hydrolytic Degradation of Poly(DL-lactic acid-co-glycolic acid). Biomater. 2002, 23, 2479
8. Heller J and Baker RW. Theory and Practice of Controlled Drug Delivery from Bioerodible Polymer. In: Controlled Release of Bioactive Materials. New York: Academic Press; 1980

9. Shimabayashi S, Hirao K, Bando, J and Shinohara C. Formation of a Polymer Complex between Bovine Serum Albumin and Sodium Chondroitin-6-Sulphate in an Aqueous Phase and on a Solid / Water Interface of Kaolin. J. Mater. Sci. Pure Appl. Chem. 1994, A31, 65
10. Alexis F. Factors Affecting the Degradation and Drug-Release Mechanism of Poly(lactic acid) and Poly[(lactic acid)-co-(glycolic acid)]. Polym. Int. 2005, 1, 36
11. Makino K, Ohshima H and Kondo T. Mechanism of Hydrolytic Degradation of Poly(L-lactide) Microcapsules: Effects of pH, Ionic Strength and Buffer Concentration. J. Microencapsulation. 1986, 3, 203
12. Schwendeman SP. Recent Advances in the Stabilization of Protein Encapsulated in Injectable PLGA Delivery Systems. Crit. Rev. Ther. Drug Carr. Syst. 2002, 19, 1
13. Lu L, Yaszemski MJ and Mikos AG. TGF-Beta1 Release from Biodegradable Polymer Microparticles: Its Effects on Marrow Stromal Osteoblast Function, J. Bone Joint Surg-Ser. 2001, A83, part2

Chapter 8

Conclusions and Future Work

8.1 Conclusions

This thesis investigated potential improvements in the processing of polymer-based systems for enhanced mechanical properties of nanocomposites and for controlled drug release in polymer delivery systems.

In Part A, $scCO_2$ assisted mixing was used to process PP/sepiolite or MWNT nanocomposites for improved mechanical properties. By comparison with nanocomposites processed by traditional melt compounding methods, relatively homogeneous dispersed and well separated sepiolite nanoclays were obtained throughout the PP matrix for nanocomposites processed in $scCO_2$ even without the

aid of PP-g-MA as a compatibilizer. Also, the sepiolite retained its fibre length better than in melt compounding. Consequently, the mechanical properties of PP nanocomposites prepared in $scCO_2$ were significantly improved, especially without the need of PP-g-MA which is a commonly used compatibilizer to aid the dispersion of clay in melt compounding. Also for PP/MWNT nanocomposites, a better preservation of nanotube lengths in the $scCO_2$ assisted mixing was observed. Good dispersions and mechanical properties were achieved with pristine MWNTs, which is unlike melt compounding in which improved dispersion and properties can only be achieved through the use of HDPE coated MWNTs. For both clays and MWNTs nanocomposites, the addition of these nanofillers enhanced the PP nucleation process. Apart from the benefits of a lower viscosity of the polymer melt in $scCO_2$ assisted mixing, more interestingly, techniques designed to achieve high quality PP nanocomposites, such as the use of masterbatches, PP-g-MA compatibilizer or polymer coated nanofillers were not needed when using $scCO_2$ assisted mixing. This is very encouraging from a technological and economical point of view.

Part B focused on the development of polymer sustained release devices for controlled drug release. The traditional cured non-degradable polymer system, CX-PEM/THFM, was modified by the $ScCO_2$ foaming technique for an optimum CX release. Highly porous structures were successfully produced and the level of CX released from $scCO_2$ foamed samples was 3 times higher by comparison with the traditionally cured sample. Moreover, the drug release rate was tailored by altering the processing conditions, such as the CO_2 saturation time and the depressurization time. A significant improvement was also made for a biodegradable polymer PLGA fibre system. Here, the layer by layer encapsulation technique was used to trap water-soluble drugs inside $CaCO_3$ microparticles before carrying out the electrospinning process. The water-soluble drugs, R6G or BSA, loaded $CaCO_3$

microparticles were successfully incorporated into the PLGA fibres. A bead and string structure of the composite fibre was achieved. The initial burst release due to the dissolution of the drug present on the surface was clearly restrained. The drug release from this system is complicated and is affected greatly by the drug's properties, drug loading and pH of the release medium. The mechanisms of the drug release involved both diffusion and degradation. However, common kinetic models, Higuchi's equation and Korsmeyer and Peppas' equation, did not give a clear insight into the drug release mechanisms.

8.2 Future Work

The viscosity of a polymer melt is a crucial factor in the polymer/filler mixing process. In $scCO_2$ assisted mixing, CO_2 dissolved in the polymer will cause a reduction of viscosity as mentioned in Chapter 2. It affects the productivity, operating conditions and the properties of the final products. It will be interesting to investigate the relationship between the reduction in viscosity of the PP melt and the final dispersion results. However, it is very difficult to measure the viscosity of a polymer/$scCO_2$ solution using conventional rheometers such as a capillary rheometer or a rotational rheometer because of the vaporization of CO_2. In literature, some equipments have been successfully designed for the measurement. A special loading assembly and a back pressure assembly into a plunger type capillary rheometer have been introduced by Mendelson[1] and Gerhardet *et al*.[2]. An online measurement of polymer/gas solution viscosities was also designed using capillary dies and a wedge die attached to a single screw or twin screw extrusion systems[3].

From an industrial point of view, to achieve the continuous production of polymer nanocomposites, it is essential to apply a $scCO_2$ assisted extrusion process. CO_2

needs to be fed continuously into the molten polymer stream in a modified extruder. In order to ensure a single-phase polymer/$scCO_2$ solution, a special extruder setup incorporating a CO_2 injection device needs to be designed for generating the high pressures involved. Also, the extruder requires modifications in its screw configuration to avoid the leakage of CO_2. An example of a modified extruder is suggested in Fig. 8.1. There have been various attempts to incorporate $scCO_2$ into continuous processing systeme. Garcia-Leiner[4] reported using a modified single screw extruder with a $scCO_2$ injection near the feed hopper for processing PE/montmorillonite nanocomposites. Treece and Oberhauser[5] modified a single screw extrusion with direct $scCO_2$ feed to the extruder barrel. A twin screw extruder has been investigated by Hwang *et al*.[6] with $scCO_2$ being injected directly into the mid-stream to produce the PP/clay nanocomposites.

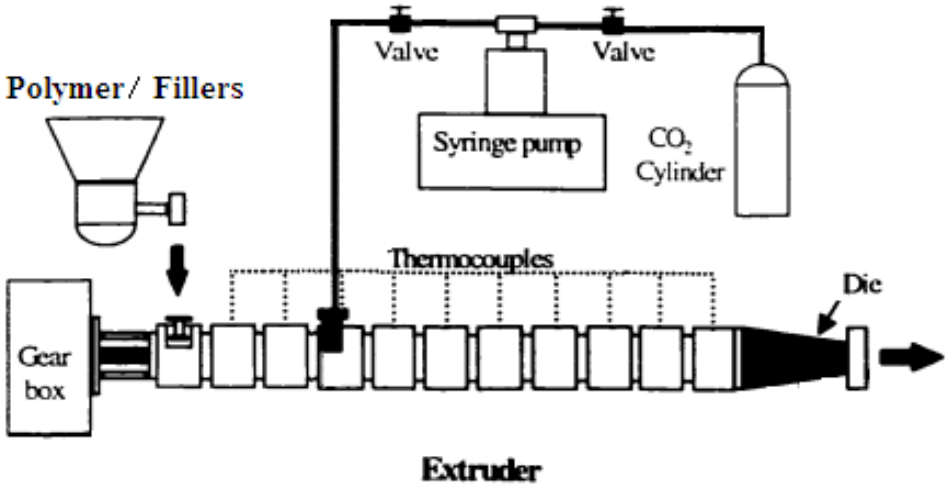

Fig. 8.1 *A schematic setup of a $scCO_2$ assisted extruder process system*

For the CX-PEM/THFM drug system, the great potential of enhanced drug release has been shown with the $scCO_2$ foamed systems. In terms of future work, it would be interesting to investigate the water uptake of the samples during drug release. It has been mentioned in Chapter 5 that THFM has an unusual water uptake behaviour.

Poly(THFM) absorbs 50 % water when the polymer is immersed in water per se.[7]. Because the drug release begins with the absorption of water into the polymer matrix and the water uptake can also cause a change in mass and/or volume of the polymer/drug system, the drug release behaviour may be influenced by its water uptake. Water uptake of the traditional cured CX-PEM/THFM has been measured by Patel *et al*.[7]. The results showed that the PEM/THFM absorbed 12 % water whilst a CX-PEM/THFM (12 wt.% CX) system absorbed 22 % water in 6 months. It indicated that CX promotes the water uptake of the system. It will be of research interest to compare these data with that of the $scCO_2$ foamed CX-PEM/THFM system and to investigate the contribution of the water uptake to the final drug release behaviour. In terms of the applications of this porous system, it is likely to be commercialized as a drug-loaded denture for antifungal and anti-infection purposes. Apart from CX, antifungal agents such as Amphotricin B, fluconazole, nystatin can also be applied in the system[8].

Regarding the PLGA fibres that incorporate drug-loaded $CaCO_3$ microparticles, the measurement of the bioactivity of the drugs after being incorporated inside the fibre is a major issue. Since the optimum pH of trypsin is 8, the conformation of trypsin is well ordered between pH 7 and 8, but is considerably less well ordered at more acidic or alkaline pH values[9]. It may be possible to use different dissolution agents instead of 0.1 M NaOH which are mild to trypsin. Alternatively, some organic solvents may be used to dissolve the PLGA as long as it is not reactive with trypsin. Organic solvents have been employed to dissolve PLGA including ethyl acetate, NMP, benzyl alcohol, triacetin, benzyl benzoate, 2-pyrrolidone, PEG, dichloromethane, DMSO, chloroform, etc. The efficiency of the dissolution depends on the ratio of PGA and PLA, and the solubility parameter of the solvent. On the other hand, instead of trypsin, other enzymes which have a wider range of pH

stability maybe used.

Moreover, a single layer of PSS was coated outside the drug loaded $CaCO_3$ microparticles to study the drug release behavior. It makes sense to deposit multiple layers using the common electrolyte combination of PSS and PAH in order to study the influence of a different number of layers on the final drug release.

8.3 References

1. Mendelson RA. A method for viscosity measurements of concentrated polymer solutions in volatile solvent at elevated temperatures. J. Rheol. 1979, 23, 545
2. Gerhardt LJ, Garg A, Manke CW and Gulari E. Supercritical fluids as polymer processing aids. Proc. 3rd int. symp. Supercrit. Fluids. 1994, 3, 265
3. Lee M, Park CB and Tzoganakis C. Measurements and modeling of PS/supercritical CO_2 solution viscosities. Polym. Eng. Sci. 1999, 39, 1, 99.
4. Garcia-Leiner MA. Solid and melt state processing of polymers and their composites in supercritical carbon dioxide. Dissertation. 2004
5. Treece MA and Oberhauser JP. Processing of polypropylene-clay nanocomposites: Single-screw extrusion with inline supercritical carbon dioxide feed versus twin-screw extrusion, J. Appl. Polym. Sci. 2007, 103, 884
6. Hwang TY, Lee SM, Ahn1 Y and Lee JW. Development of polypropylene-clay nanocomposite with supercritical CO_2 assisted twin screw extrusion. Korea-Australia Rheol. J. 2008, 4, 235
7. Patel MP, Cruchley AT, Coleman DC, Swai H, Braden M and Williams DM. A polymeric system for the intra-oral delivery of an anti-fungal agent. Biomater. 2001, 17, 2319
8. Dar-Odeh NS and Shehabi AA. Oral candidosis in patients with removable dentures.

Mycoses. 2003, 46, 187

9. Simon ML, László K, Kotormán M and Szajáni B. A comparative study of the conformational stabilities of trypsin and chymotrypsin. Acta Biol. Szegediensis. 2001, 45, 43

List of Publications

Ma J, Deng H and Peijs T. Processing of Polypropylene/Carbon Nanotube Composites Using $ScCO_2$-Assisted Mixing. Macromolecular Materials and Engineering. 2010, 295, 566

Ma J, Bilotti E, Peijs T and Darr JA. Preparation of Polypropylene/Sepiolite Nanocomposites Using Supercritical CO_2 Assisted Mixing. European Polymer Journal.2007, 43, 4931

Ma J, Meng J, Simonet M, Stingelin N, Peijs T and Sukhorukov GB. Biodegradable Fibre Scaffolds Incorporating Water-Soluble Drugs and Proteins. Submitted to Journal of Materials Chemistry.

Bilotti E, Ma J, Peijs T. Polyolefin/needle-like Nanoclays Composites. Mittal V. Advances in Polyolefin Nanocomposites. CRC Press, 2010